Title
Surround integration during active sensation in the mouse barrel cortex

Author
Lyall, Evan Harrison

Publication Date
2018

Peer reviewed|Thesis/dissertation

Surround integration during active sensation in the mouse barrel cortex

by

Evan Harrison Lyall

A dissertation submitted in partial satisfaction of the

requirements for the degree of

Doctor of Philosophy

in

Biophysics

in the

Graduate Division

of the

University of California, Berkeley

Committee in Charge:

Dr. Hillel Adesnik, Chair
Dr. Bruno A. Olshausen
Dr. Daniel E. Feldman
Dr. Yang Dan

Fall 2018

ABSTRACT

Surround integration during active sensation in the mouse barrel cortex

by

Evan Harrison Lyall

Doctor of Philosophy in Biophysics

University of California, Berkeley

Professor Hillel Adesnik, Chair

Organisms scan their sensors around their environment to build an internal representation of that environment in a process known as active sensation. The integration of information across time and space is critical to providing context as to what is the organism is perceiving. However, the neural circuits that encode and underlie the integration of incoming sensory information have predominantly been studied in the context of passive sensation. Studying these circuits in the context of active sensation is imperative to generating a better understanding of how the brain naturally encodes sensation. This would have profound impacts on understanding the mechanisms of a number of neural disorders, including autism and attention-deficit/hyperactivity disorder, as well as how to improve the acuity of artificial sensation implanted into disabled individuals.

To better understand how the mammalian brain encodes and integrates information during active sensation, my collaborators and I developed several novel paradigms to study surround integration in the mouse barrel cortex during active whisking. In Chapter 1 I establish why this is an important problem, and briefly summarize what is already known about sensory coding in the mouse whisker system. In Chapter 2 my collaborators and I probe how mice represent the location of an object within its whisking field, and how the integration of information across surround whiskers affects this representation. In doing so we discover a novel thalamocortical transformation where surround integration in the cortex suppresses activity in layer 4 of the cortex, ultimately generating a smooth map of scanned space in cortical layer 2/3. In Chapter 3 I utilize a novel tactile display to better understand the logic of multi-whisker integration in two cortical layers. In this unpublished work, I show that contrary to the previous literature in anesthetized mice, cortical neurons in awake, whisking mice powerfully summate specific whisker combinations supralinearly, generating a sparse code representing the entire combinatoric space of whisker touch. In Chapter 4, I conclude with some closing thoughts and propose some future lines of inquiry to further this research.

DEDICATION

This work is dedicated to the mice that gave their lives in our pursuit to discover more about ourselves. May the findings herein be worthy of their sacrifice.

ACKNOWLEDGEMENTS

This work would not be possible without the hard work and support of countless people and institutions. First and most importantly I must thank Professor Hillel Adesnik for his tireless dedication, brilliant mind, and profound elocution. None of this would have been remotely possible without his brain and the skill set he has honed over a tremendously successful, young career. Secondly, I must thank my parents, Robin and Jeff Lyall, for providing nearly everything I have in my life. They are rock star parents that deserve all the recognition in the world, moreso than I can possibly put in writing. Third, I must thank Claire Lee for being the first person to help me up when I fall, discuss what went wrong, and push me back in. I must thank my siblings, Chase Lyall, Hunter Lyall, and Heather Hallman, for putting up with my annoyances and yet supporting me despite them. I must thank Alex Naka, whose brilliant mind and amazing ability to absorb all information was extremely important for helping me discover doors when I thought there were none. As well I must thank Dan Mossing for being a very accommodating rig mate and for his extreme eagerness to discuss and ponder all scientific problems, true or imagined.

Additionally, I need to thank all members of the Adesnik Lab, including Scott Pluta, whom I tried to emulate but could never replicate; Lucy Yao, for not being the worst; Alan Mardinly, for asking the right questions; Julia Veit, for her constant companionship and constant smile; Greg Telian, for his many talents and nerdy brain; Elena Ryapolova-Webb, for her friendship and ability to keep us all grounded; Nico Pegard, for his much needed optics help and brilliant emails; Ian Oldenburg, for always providing competition even when none was necessary; Jenny Brown, for her cheerfulness and ability to brighten every conversation; Ming-Chi Tsai, for his constant support; Ben Shababo, for lending his exquisite brain; Savitha Sridharan for her compassion and amazing skillset; Silvio Temprana, for being a great friend; Nikhil Bhatla, for his unabashed questions and support; Hayley Bounds, for her intellect and tirelessness; David Taylor, Rich Hakim, Desi Chu, Kiarash Shamardani, and Janine Beyer, for their much needed support and completion of so many painful and boring tasks; and anyone else in the lab I might have missed, including undergrads and rotons of which there are too many to name here. Every member of the lab deserves a great deal of thanks for their helpful comments, well-poised questions, and the escape they provided from the monotony of long, repetitive experiments. Outside of our lab, I must thank Dr. Dan Feldman, Dr. Bruno Olshausen, Dr. Yang Dan, Dr. Laura Waller, and Dr. Frederic Theunissen, for the time they spent pondering my projects, as well as the well informed and very helpful feedback they provided.

Next, I would like to thank the people in my past that have been important to my development as a scientist and capable adult. This includes previous teachers that have had a profound impact on my life, including Dr. Lydia Sohn, Dr. Brandon Lujan, Mr. Paul Hunt, Mrs. Mattson, Mr. James Lynch, Mr. David Pearl, Prof. Robert Reich, Prof. Alan Ross, and Mrs. Jan. Lastly, my Scoutmaster Mr. Carl Gorsuch deserves a great deal of praise for the many life lessons he helped convey.

Finally, I need to thank the institutions whose existence and persistence made my research possible. This includes the US Government, the NIH, the Government of California, the University of California, Berkeley, and a multitude of divisions and support people at UC Berkeley, including Research IT, OLAC, Kate Chase, Barbara Duncan, Krishna Muriki, Maurice Manning, the purchasing staff, the delivery staff, and, arguably, the most important of all, the janitorial staff.

TABLE OF CONTENTS

CHAPTER 1

INTRODUCTION

SENSATION IS AN ACTIVE PROCESS

Individuals scan their sensors across their sensory environment

An animal's ability to perceive the world around it is critical for navigating obstacles, finding food, and avoiding predators, all key facets of survival. The act of perception could be accomplished in a completely passive manner, observing changes in the environment while remaining absolutely still. However, in practice all animals scan their sensors across their local environment in a process known as active sensation. This process not only allows the organism to sample from a larger area of their sensory environment, but by integrating information over space and time they can build a more complete cognitive representation of that environment. This integration of information across the sensor array is known as surround integration, and is key to providing context as to what it is they are perceiving.

A great example of active sensation is that of primate visual perception. When a primate perceives a visual scene, the primate does not park its eyes in one spot, rather it scans its foveas around the scene in order to integrate information across space and time. This concept is well documented in Alfred Yarbus's book "Eye Movements and Vision". He writes, "Records of eye movements show that the observer's attention is usually held only by certain elements of the picture. […] study of these elements shows that they give information allowing the meaning of the picture to be obtained" (Yarbus 1967). An example of eye movement traces recorded from a subject perceiving a photo of a woman's face can be seen in Figure 1.1 from Alfred Yarbus's 1967 book ". Here the subject spends a great deal of time focusing on the woman's eyes and lips as they "are the most mobile and expressive elements of the face" and therefore provide the most context to the observer as to the woman's mood and current situation.

A second great example of active sensation is that of a blind man trying to perceive the world around him using active touch. To perceive his environment, the blind man will move his hands or walking cane across his environment to probe the location, texture, and identity of objects. One of the earliest reflections on active sensation in the literature is by James Gibson in his 1962 editorial entitled "Observations on Active Touch". Gibson writes, "[Active touch] ought to be distinguished from passive touch, or being touched. In one case the impression on the skin is brought about by the perceiver himself and in the other case by some outside agency. The difference is very important for the

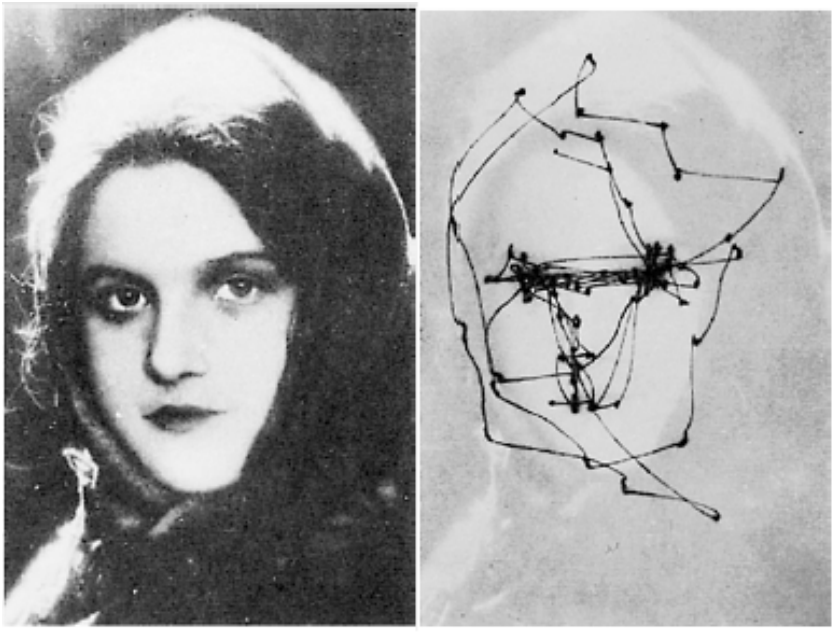

Figure 0.1 Example human eye movements when observing a complex scene
Adapted from Yarbus 1967.

individual but it has not been emphasized in […] the experimental literature" (Gibson 1962). Gibson was writing from the viewpoint of a sensory psychologist, however the same statements apply today, over a half century later, in regards to the field of sensory systems neuroscience.

Sensory systems neuroscience is the study of how neural circuits encode information about the world around us and ultimately generate perception. Understanding how the healthy brain encodes and processes information is an important first step in discovering what causes many mental diseases, including but not limited to, autism, sensory processing disorder, and attention-deficit/hyperactivity disorder. Furthermore, such an understanding would allow for the artificial encoding of high-acuity sensation in handicapped patients, such as those suffering from paralysis, as well as allow for the enhancement of the natural senses in all humans. But, to this point most sensory systems neuroscience research has been performed in the context of passive sensation, generally in anesthetized or fixating animals. To provide a full understanding of how sensory circuits function, and ultimately lead to the generation of perception in behaving organisms, more research needs to be performed in the context of active sensation.

RECORDING AND ANALYZING NEURAL ACTIVITY *IN VIVO*

Electrophysiology vs imaging

There are numerous techniques available to record from individual neurons in the brain, but for the most part they can be broken down into two main categories: electrophysiology and imaging. Most *in vivo* experiments are performed in head-fixed animals such that their brains are held still. However, both electrophysiology and imaging approaches do exist for freely moving animals with some caveats that I won't get into as freely moving paradigms do not allow the sensory stimulus to be finely controlled.

The main techniques available when performing electrophysiology with single neuron resolution in a head-fixed preparation are: whole-cell patch clamp, cell-attached patch, and multicellular electrophysiology. The first two allow a user to unambiguously record from single neurons as well as separate individual currents via a combination of voltage clamping and pharmacology. However, the single-cell nature of these techniques make them very low throughput, and additionally they can be extremely difficult to perform if there is any sort of brain motion, which is particularly prevalent when the organism is awake. Multicellular electrophysiology involves sticking an array of electrodes, generally laid out on a grid on a thin silicon wafer, into the brain and measuring local voltage fluctuations within an approximately 50-micron radius around each electrode. When a neuron within that radius spikes, it creates a very distinctive waveform within the voltage trace measured by that electrode. Neurons close enough to multiple electrode contacts will produce a unique spike waveform on each contact. Software will use these coincident spiking events and the known positions of the electrodes to identify that each of those measured spikes came from the same cell. Additionally, the software will use the shape of those waveforms to track that cell's spiking over time, and to identify whether the cell is a fast-spiking (FS) neuron, putatively a parvalbumin-positive (PV) inhibitory neuron, or a regular-spiking (RS) neuron, most commonly an excitatory neuron. This type of electrophysiology has the beneficial advantage of being able to record from many neurons at one time, however it does not grant access to the underlying currents driving the cell to spike. All electrophysiology techniques have high temporal resolution (on the order of tens of kilohertz)

because they rely on standard electrical measurements being performed in silico with no moving parts.

Imaging techniques on the other hand rely on a sensor that changes its fluorescence in response to a change in membrane voltage or a correlate of neural spiking, such as a change in the concentration of calcium ions. Imaging approaches have worse temporal resolution than electrophysiological approaches as they have an exposure time on the order of nanoseconds to milliseconds. As well to achieve cellular resolution in dense tissue *in vivo* the researcher either needs to express the sensor in a very sparse or localized subset of neurons, or utilize the phenomenon of two-photon absorption to greatly decrease out of focus fluorescence. Two-photon imaging requires sending in photons of nearly twice the wavelength, and therefore half the energy, of photons in the one-photon absorption spectrum of the sensor. This results in an exponential falloff in fluorescence away from the focal plane. The added benefit is that longer wavelength photons scatter less in brain tissue and as a result travel deeper in the brain. This rule holds up until approximately 1400nm where light starts to reach the absorption spectrum of water and instead of travelling deep, gets converted into heat. To reduce cross-talk due to the light scattering properties of tissue, and to mitigate the amount of heating resulting from light absorption, two-photon imaging is almost always paired with a scanning system that scans a single focused spot of light across the brain. This scanning process results in a tradeoff between the number of neurons imaged, and the temporal resolution of the recording. However, imaging provides the ability to record from large regions of the brain, especially with newly developed large field of view, high numerical aperture objectives that provide field of view diameters on the order of millimeters (Sofroniew et al. 2016; Stirman et al. 2016; Tsai et al. 2015). One major benefit of imaging is that you can multiplex information by using multiple wavelengths and fluorophores, and can use today's genetic toolbox to only record from specific types of neurons. For example, a researcher can express GCaMP, a green calcium-indicator, in only neurons while also targeting RFP, a red fluorophore, to all inhibitory neurons, and thereby identify which neurons are excitatory and which are inhibitory. In summary, imaging is the technique of choice when one wants to record from a large population of neurons or a specific population of neurons, and only needs temporal sampling on the order of one to tens of hertz. While electrophysiology is preferred when a researcher requires high temporal resolution, or recordings from neurons deeper than one millimeter in the brain (though with certain tradeoffs imaging can still be used for deep recordings, see Horton et al. 2013 and Jung et al. 2004).

Correlative measurements (e.g. receptive fields and feature tuning)

The easiest approach to understand what a neuron is encoding is to correlate its spiking with controlled changes in its environment. Pivotal work performed by Sherrington in 1906 showed that stimulating localized regions of a dog's skin elicits specific scratch reflexes via circuits localized to a relative part of the spine (Sherrington 1906). Here Sherrington coined the term "receptive field" to describe the localized region of sensory space that needed to be stimulated to initiate a specific reaction. Later work by Hartline extended this term to individual neurons by showing that individual optic fibers only respond to stimuli localized to unique regions of the retina (Hartline 1938). Two decades later, further pivotal work by Hubel and Wiesel would show that neurons in cat primary visual cortex are tuned to specific features within its receptive field, such as the orientation of an edge (Hubel & Wiesel 1959). To measure a neuron's receptive field and tuning, a researcher will present a series of different stimuli to the

subject multiple times, and then average the neuron's responses with respect to each stimulus. Averaging across multiple trials is critical to reduce the effect of any noise in the neuron's firing patterns. Then the researcher will plot out the neuron's average response as a function of the stimulus presented, generating what is referred to as a tuning curve, or a stimulus-triggered average. The major caveat of this approach is that the dimensionality of the stimulus space generally needs to be limited so that all the stimuli can be presented in a reasonable amount of time.

An alternate approach is to continuously present stimuli to the subject, generally with well-defined, specific statistical properties, and then to perform what is known as a spike-triggered average. Here the researcher identifies when each spike occurred for an isolated neuron, and then averages together the stimulus that was presented right before and up to the start of the spike. This technique addresses the major caveat of a stimulus-triggered average by greatly increasing the dimensionality of the stimulus space sampled from, however it also comes with its own caveat that its samples are limited to lying within the predefined statistical distribution being sampled. For instance, a relatively simple visual stimulus where the screen is half black and half white will never be presented if the subject is viewing white noise, a stimulus where each pixel value is randomly sampled from a Gaussian distribution.

Performing a stimulus-triggered average or spike-triggered average are great tools for understanding what features individual neurons are extracting, but these techniques fail to quantify how much information each neuron, or a collection of neurons encodes. Researchers have relied on recent advances in computing power, open-source code banks, and statistics to address these types of questions.

Decoding what stimulus was presented

Classification problems have become ubiquitous in the field of data science; here they are used to simplify a high dimensional dataset into a mixture of labeled groups. Supervised classification is the most common approach, where a classifier is trained on some ground truth, generally hand labeled, data, and then used to label the entire dataset. Alternatively, there exists unsupervised classification, also known as clustering, which looks for natural groupings in the data. There are dozens of commonly used classification models, each with their own advantages and disadvantages.

In sensory neuroscience, supervised classification is commonly used to perform neural decoding. This is where a researcher decodes what stimulus was presented based solely on the neural data. To do this a researcher first divides the trials into a training set and a testing set. Then the researcher trains the model on the training set, supplying the stimulus that was presented and the simultaneously recorded neural activity. Then the researcher applies the classifier to the testing set, and calculates how often the classifier, or decoder, guessed the correct stimulus that was presented. This decoding approach can be used to analyze how well a single neuron, or a population of neurons encodes the stimulus space. The most commonly used technique for neural decoding is logistic regression. Logistic regression places a linear weight on each neuron for each outcome making it easy to interpret, while also applying a nonlinearity that provides the classifier flexibility and makes it easier to fit. However, any arbitrarily fit-able classification model can be used (e.g. random forest, support vector machine, artificial neural network, etc.).

Regardless, a neuron's spiking in response to an external stimulus is often noisy and influenced by internal cognitive mechanisms such as brain state and attention, especially neurons higher in the processing steam. These sources of variance in the neural response pattern can easily confuse the decoder unless they are measured in the data, and are present in the training set. Therefore, the major caveat of decoding is that it requires a great deal of data when there is any noise in the neural responses.

Predicting spikes via an encoding model

Where a decoding model tries to predict the stimulus based off the neural activity, an encoding model tries to predict the neural activity based off the stimulus. Encoding models can be arbitrarily complex, accounting for many sources of variance. However they are generally hard to fit to *in vivo* data as neurons are both noisy, and influenced by internal cognitive processes that often cannot be measured. Nonetheless, producing a well-fit encoding model that predicts most, if not all of a neuron's spikes is truly necessary before a researcher is able to say that a circuit is fully understood. When building an encoding model, most researchers start with a linear-nonlinear model (i.e. a generalized linear model) as the linear part is easy to understand, while the nonlinearity provides flexibility when fitting the model. From there encoding models can get arbitrarily complex. Because of this, encoding models have two major caveats: they can easily be over-fit to the data, and their structure might be vastly different from the underlying neural architecture, making interpreting their function difficult. Both caveats can be addressed, but in general an encoding model is avoided unless you have a ton of data from a single circuit, with the goal being that the data encompasses the entire activity space naturally reached by the circuit. In well-stereotyped circuits this can be addressed through many replicates across many animals, however in variable circuits, like those found in the cortex, a researcher would need to acquire data from the same circuit in a single individual across many days. Such experiments are now within reach due to the latest advances in surgery and recording technologies, but will not be addressed in this dissertation.

INTRODUCTION TO THE MURINE WHISKER SYSTEM

The mouse whisker system as a model system

Mice, and many other rodents, have evolved to be mostly nocturnal creatures that reside in subterranean burrows. In doing so they have developed to heavily rely on their tactile whisker system for navigating their immediate environment, and generally have relatively poor visual acuity. To perceive its immediate environment, the mouse will move its whiskers in a back and forth, rhythmic motion known as whisking. Whisking its whiskers back and forth allows the mouse to palpate objects in its vicinity, and build up a representation of the location, shape, and texture of those objects. This active whisking behavior, as well as how relatively easy it is to record from populations of neurons in the mouse brain, makes the mouse whisker system a great model system for studying the neural correlates of active sensation.

Whisker array and somatosensory pathway is stereotyped across mice

Every mouse has the exact same configuration of whiskers, also known as vibrissae, on each side of its snout, in an area known as the mystacial pad (Figure 1.2; Schubert et al. 2007; Petersen 2007). The whisker array is broken down into two parts, the more posterior macrovibrissae, which contain larger, very prominent hairs positioned in a well-stereotyped grid, and the more anterior microvibrissae, which are smaller and harder to identify by eye. It is believed that the macrovibrissae are more important for object localization, while the microvibrissae are especially tuned to object discrimination, however all vibrissae move together in each whisk cycle (Brecht et al. 1997).

Each vibrissa is a specially evolved hair, that has a follicle innervated by hundreds of primary sensory neurons whose cell bodies lie in the trigeminal ganglion. When a vibrissa comes into contact with an object and is deflected, it opens mechanosensitive, excitatory ion channels in a specific subset of the innervating neurons, dependent upon the direction and force of the deflection. The opening of these channels generates a positive electrical potential that is carried down the body of the neuron to its axonal boutons, where it synapses on neurons in the trigeminal nucleus of the midbrain. The excitatory potential causes the release of excitatory neurotransmitter at the synapse, causing the firing of the downstream neuron. Neurons in the trigeminal nucleus primarily synapse on neurons in the ventral posteromedial thalamus (VPM) in the forebrain. The canonical pathway model of cortical connectivity, established over decades of research, says that VPM neurons primarily synapse on neurons in layer 4 (L4) of the primary somatosensory cortex (S1), who then synapse on neurons in L2/3 above them, who themselves primarily synapse on projection neurons in L5 directly below the L4 barrel. However many recent studies have shown that the canonical model is not complete (Pluta et al. 2015; Naka et al. 2018) and that plenty of exceptions to the rule exist (e.g. VPM synapsing on neurons in L2, etc.).

At each of the first three stages of sensory processing, the trigeminal nucleus, VPM, and cortical L4, there exists a one-to-one mapping of clusters of neurons to individual vibrissae on the mouse's face. At each stage this cluster has a different name: in the trigeminal nucleus they are called barrelettes, in the VPM there exists barreloids, and in L4 they are known as barrels. These barrels are so prominent in histology, that this part of the brain is known as the barrel cortex. These barrel-like structures are created by the concentration of cell bodies in their center, and the concentration of vertical fibers of passage in the areas between barrels, known as the septa. As a result of this anatomy, there is little to no connectivity between barrels. L2/3, on the other hand, has no barrel-like structures and rather exhibits a plethora of horizontal connectivity. Thus, it is believed that L2/3 is the first principal site of the integration of information across the whisker array. However, some feed-forward integration of information across whiskers has been observed at every step of the pathway.

Whisker tuning during anesthetized deflections

To examine how neurons respond to deflections of different whiskers, a series of recordings have been performed in anesthetized rat and mouse while deflecting individual whiskers one at a time. Whole-cell recordings from rat L4 barrel neurons revealed that they exhibit subthreshold responses to many whiskers, but that the strongest response was almost always to the principle whisker (Brecht & Sakmann 2002). As well it was shown that spike threshold sharpens this tuning. Repeating the same experiments while patching neurons in L2/3

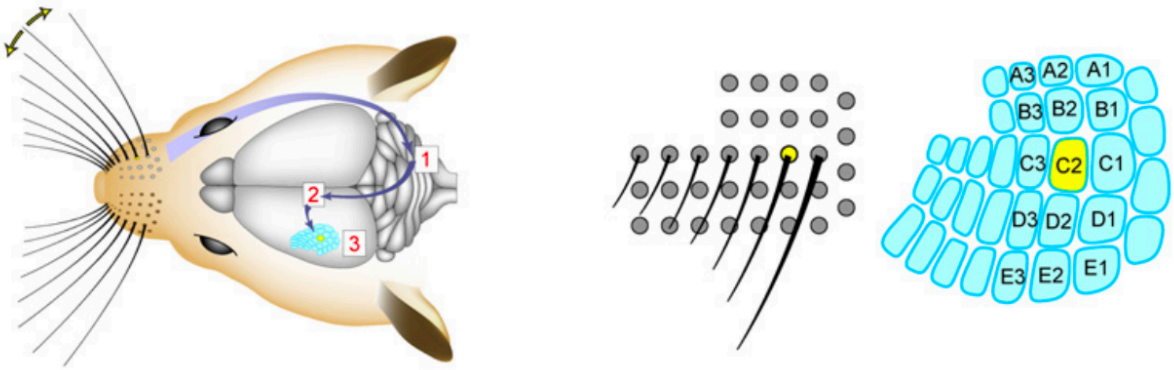

Figure 0.2 Diagram of the mouse whisker system
Left: An example of a mouse head, whiskers, and brain with the primary sensory pathway overlaid. Information from the follicles travels along the trigeminal nerve to the trigeminal nucleus in the brainstem, then to VPM, and then to L4 of S1. Right: diagram showing the one-to-one mapping of whiskers on one side of the mouse's snout to barrels in the contralateral hemisphere. Adapted from Petersen 2007.

revealed that neurons in L2/3 have even broader tuning than neurons in L4 (Brecht et al. 2003), however calcium imaging experiments in mice have shown that their preferred whisker often differs from their anatomical principal whisker, though the largest plurality of neurons in a barrel column do prefer the principal whisker (Clancy et al. 2015).

Beyond being tuned for which whisker was deflected, neurons at every level of the somatosensory pathway also exhibit tuning for the direction in which the whisker was deflected, referred to as angular tuning (Simons 1978). However despite a large number of neurons exhibiting angular tuning to deflections of multiple whiskers individually, only a very small number of neurons share the same angular tuning across whiskers (Hemelt et al. 2010).

Differences in brain state between anesthesia and active whisking

During most neural recordings, researchers will anesthetize an animal to keep it completely still (save cardiac and pulmonary movements). Different forms of anesthesia will have different mechanisms of action, but all will have some effect on neural activity to produce an unconscious state. Most anesthetics result in reduced neural activity (Berg-Johnsen & Langmoen 1992; Cariani 2000). Even worse anesthesia can create increased variability in the neural responses by producing what are known as up-states, or waves of correlated neural spiking (Constantinople & Bruno 2011; Luczak & Barthó 2012). As well, several studies have shown that anesthesia can abolish or alter several forms of neural dynamics (Lamme et al. 1998; Major & Tank 2004). Lastly, an animal that is anesthetized or fixating is not moving its sensors as it does when performing active sensation. This motion results in increased firing in the sensory processing pathway that produces adaptation at synapses at every stage, reducing the probability of producing a spike in the downstream neuron. This adaptation has been shown to move a mouse from a brain state that favors detection to one that favors discrimination, as well it sharpens the tuning of neurons at multiple steps in the sensory hierarchy (Ganmor et al. 2010; Whitmire et al. 2018; Waiblinger et al. 2018; Whitmire & Stanley 2016; Zheng et al. 2015). Consequently, researchers need to present stimuli in an awake, ethological setting in order to gain a complete picture as to what it is neurons are encoding, particularly when observing

neurons far from the periphery and putatively more susceptible to top-down, cognitive influences.

Neural tuning during active whisking

Several experiments have analyzed neural coding in rats and mice during active whisking. As well, a number of studies have been performed in rodents whose motor nerve is stimulated to produce artificial whisking (e.g. Brown & Waite 1974; Szwed et al. 2003), however this has fallen out of favor in the field for more ethological paradigms.

A recent study in a head-fixed mouse tried to understand what causes primary sensory neurons innervating the whisker follicle to fire. They did so by presenting a vertical pole at one of many positions within the mouse's whisking field while the mouse was running of its own volition and recording from the trigeminal ganglion. They found that primary sensory neurons innervating the whisker follicle responded both to self-motion and active touch. Responses to self-motion encoded the whisker's phase within the whisk cycle, and with spikes reflecting whisker inertia and activity of mystacial pad muscles. Responses to active touch were best accounted for by models that used the bending moment (torque) at the base of the whisker and its rate of change as inputs (Severson et al. 2017).

A series of studies were performed in mice trained to discriminate the location of a vertical pole between anterior and posterior positions with one to three whiskers (O'Connor, Clack, et al. 2010; O'Connor, Peron, et al. 2010; O'Connor et al. 2013). In one study where they recorded from VPM and L4 of the barrel cortex, they found that VPM neurons and FS neurons in L4 encoded both self-motion and active touch, while RS neurons in L4 primarily encoded touch (Yu et al. 2016). This proposes that PV neurons in L4 are filtering out the self-motion signals entering the L4 excitatory neurons. A separate study showed that there are populations of neurons throughout the cortex that are tuned for touch, whisking, or both, as well as overlapping populations that encode task-related activity (Peron et al. 2015).

A different study from the same lab presented mice on a floating ball with walls on each side of its body, creating a virtual hallway. Here they showed that neurons in S1 exhibit radial tuning for the wall's distance from the face (Sofroniew et al. 2015). A study from 2009 showed that neurons in S1 were tuned to the phase in the whisk cycle at which touch occurred (Curtis & Kleinfeld 2009). A recent study from our lab showed that neurons in L5 of S1 are tuned for the location of an object in rostral-caudal space (Pluta et al. 2015).

A series of studies have looked at how neurons in S1 differentially encode textures. They show that whiskers moving along a texture undergo transient, high velocity slip-stick events that produce time-locked spikes in S1 neurons (Jadhav et al. 2009; Jadhav & Feldman 2010; Wolfe et al. 2008). A very recent study from their lab shows that temporally precise spikes encode local edges, while the population's overall firing rate is modulated by the surface's roughness (Isett et al. 2018).

Integration across whiskers is critical for contextual perception

It's clear neurons respond to the deflections of multiple whiskers, but are multiple whiskers important ethologically? Rodents putatively could've evolved on a single whisker on each side, and yet they evolved with an array of whiskers. Beyond allowing the rodent to probe a larger region of sensory space at any given time, having multiple whiskers allows a rodent to integrate information across its sensors to generate a better understanding as to what each

individual whisker is touching. This has been shown in numerous behavioral studies but is best exemplified in one study where rats were trained to discriminate the width of an aperture (Krupa et al. 2001). After being trained on the task, the rats were tested while their whiskers were progressively trimmed off. The researchers found that the rats' performance fell off nearly linearly as a function of their trimming regime (Figure 1.3), proving that the rat was relying on the integration of information across whiskers to perform the task.

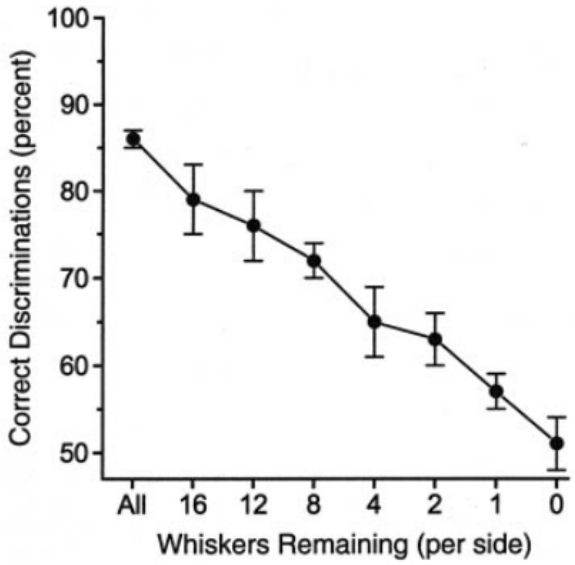

Figure 0.3 Performance on a discrimination task decreases as a function of the number of remaining whiskers
Adapted from Krupa et al. 2001.

Surround integration effects on neural coding in the whisker system

To better understand how neurons integrate information across whiskers, a series of experiments have been performed in anesthetized rats and mice where multiple whiskers are deflected either at the same time or at specific interdeflection intervals. Early experiments in this realm established that surround whisker deflections were mostly suppressive to responses to the principal whisker (Simons & Carvell 1989; Moore et al. 1999), while a more recent study showed that specific whisker combinations at specific interdeflection intervals, unique to each neuron, can actually be facilitory (Ego-Stengel et al. 2005). Additionally, neurons responses can be influenced by deflections of whiskers on the ipsilateral whisker pad (Shuler et al. 2001).

To address the limitations of a stimulus-triggered average approach, some very recent studies have presented constant stimuli and performed spike-triggered averaging or reverse correlation. One set of studies out of the Shulz lab performed multicellular electrophysiology recordings in multiple cortical regions while deflecting up to 24 whiskers in the rostral-caudal direction (Estebanez et al. 2012; Estebanez et al. 2016; Goldin et al. 2018). They then calculated the spike-triggered covariance of all the sorted units, and performed principal component analysis on the population of filters. They found that the top two filters (i.e. principal components) accounted for approximately eighty percent of the spiking variance in primary and secondary somatosensory cortex, with the filters produced from the units in secondary somatosensory cortex being slightly longer in time. The filters are on the order of twenty to forty milliseconds, roughly similar to the duration of a slip-stick event (Wolfe et al. 2008; Isett et al. 2018; Jadhav et al. 2009). Additionally in one study, the researchers performed calcium imaging and found that neurons that preferred stimuli uncorrelated across whiskers, clustered toward the center of barrel columns, while neurons that preferred correlated global motion clustered in septa (Estebanez et al. 2016).

Another such study presented multi-directional Gaussian noise to the whisker pad of an anesthetized rat while recording from individual neurons in multiple layers of primary somatosensory cortex (Ramirez et al. 2014). Rather than utilizing a spike-triggered analysis, which requires a great deal of spikes per neuron, the researchers performed whole-cell patch

clamp recordings and computed a voltage-weighted average stimulus (i.e. reverse correlation) from the entire voltage trace, greatly speeding up their experiments. First the researchers presented a simple stimulus that deflected whiskers in isolation and were able to capitulate that neurons across all layers exhibited broad whisker tuning. However, when the researchers presented their complex, white noise stimulus, they found that neurons exhibited drastically sharper whisker tuning, and almost always preferred their anatomically aligned whisker. Using their technique, they were also able to show that neurons' whisker and angular tuning exhibited complex temporal dynamics unique to each neuron. But when neurons within each layer were averaged together, they found that neurons' maximal responses generally occur when a principal whisker deflection lags a surround whisker deflection by only a few milliseconds.

Nonetheless, despite the rigor and elegance of these approaches, one major caveat is that they were performed in anesthetized rats and mice, where the brain state has been shown to be very different. But one 1999 awake, behaving study did look at how surround whiskers affect firing rates in VPM and S1. They did so by training rats to explore a mesh screen while recording multicellular activity in VPM and S1. During this task, the researchers acutely trimmed off all surround whiskers and compared the firing rates pre-trimming to those post-trimming. They found that activity in thalamus decreased by 37% while, conversely, activity in cortex increased by 20% (Kelly et al. 1999). However, this study could not analyze how surround integration effects the underlying neural code as the stimulus was not stereotyped.

THE ROLE OF SURROUND INTEGRATION DURING ACTIVE SENSATION

For decades neuroscientists have studied how the nervous system encodes the features of a sensory stimulus. However, in the vast majority of the literature this has been accomplished in reduced preparations where the animal is anesthetized, trained to fixate, or not had its full sensor array intact. In these paradigms, not only is the brain state very different from that of a behaving animal, but it also means that the recorded neural tuning functions are in response to passive sensation, rather than active sensation. With passive sensation and active sensation being completely different phenomena to the animal, it is unclear how different these stimuli would be encoded in the brain.

Some recent research has begun to study how the brain encodes sensory stimuli during active sensation. And yet, the effects of surround integration, which is key to generating the representations produced by active sensation, has not been studied in the context of active sensation. This dissertation attempts to address this deficiency by collecting and analyzing cerebral neural activity in the mouse whisker system, during several relatively ethological, active sensing paradigms. All the while using some sophisticated approaches to probe the role surround integration plays in generating the neural representation.

CHAPTER 2

SURROUND INTEGRATION CRITICAL FOR GENERATING CORTICAL REPRESENTATION OF SCANNED SPACE

FOREWORD

In this chapter I present work from the first half of my doctorate research in which we examine how the cortex encodes the location of an object within the space scanned by the whiskers, and how this encoding is affected by the integration of information across multiple whiskers. I was responsible for all two photon calcium imaging experiments and analysis in the paper, including the key findings that anterior whiskers suppress activity in posterior L4 barrels, and that multi-whisker integration generates a smooth map of scanned space in L2/3. I had the honor of collaborating closely with Dr. Scott Pluta on this project, who performed all electrophysiology experiments in L5 and analyzed all the electrophysiology data. Key contributions were also made by Elena Ryapolova-Webb, who recorded all the electrophysiology data in the thalamus, and Greg Telian, who collected and analyzed all high-speed whisker tracking data.

Pluta, S. R.*, Lyall, E. H.*, Telian, G. I., Ryapolova-Webb, E., & Adesnik, H. (2017). Surround Integration Organizes a Spatial Map during Active Sensation. *Neuron*, *94*(6), 1220–1233.e5. https://doi.org/10.1016/j.neuron.2017.04.026 *Contributed equally

SUMMARY

During active sensation, sensors scan space in order to generate a representation of the outside world. However, since spatial coding in sensory systems is typically addressed by measuring receptive fields in a fixed, sensor-based coordinate frame, the cortical representation of scanned space is poorly understood. To address this question, we probed spatial coding in the rodent whisker system using a combination of two-photon imaging and electrophysiology during active touch. We found that surround whiskers powerfully transform the cortical representation of scanned space. On the single neuron level, surround input profoundly alters response amplitude and modulates spatial preference in the cortex. On the population level, surround input organizes the spatial preference of neurons into a continuous map of the space swept out by the whiskers. These data demonstrate how spatial summation over a moving sensor array is critical to generating population codes of sensory space.

INTRODUCTION

Cortical neurons represent sensory space through topographic projections of the peripheral sense organs, creating maps of the physical world in the brain. Sensory coding through maps is thought to make both the structure and function of neural circuits more efficient (Knudsen et al. 1987) In passive systems, maps can be probed by systematically stimulating different parts of the sensor array and measuring the receptive fields of individual neurons. In many sensory systems, such as the retina, integration over the sensor array is critical for receptive field formation (Hartline et al. 1956; Kuffler 1953). During active sensation, however, the sensors themselves move – scanning space to provide greater coverage of the outside world (Kleinfeld et al. 2006). How neurons in the cortex encode scanned space, and whether integration across the sensor array is involved, is not known. Furthermore, sensor scanning has the potential to create its own spatial map in the cortex, not of the sensor array itself, but of the

space swept out by the sensors. Such a map of scanned space could provide a basis for fine object localization and identification needed for behaviors such as prey capture, predator avoidance, and navigation.

The rodent whisker system is an advantageous system to address this question (Brecht 2007; Feldmeyer et al. 2013; Petersen 2007). On one hand, the topographic and discretized representation of the rodent's whiskers along the sensory hierarchy facilitates detailed analysis for how sensory neurons perform multi-whisker integration (Woolsey & van der Loos 1970). On the other, the stereotyped pattern of whisking during spatial exploration facilitates investigation into the sensorimotor processes underlying active sensation (Diamond et al. 2008; Hartmann 2011). Decades of physiological analysis have quantified how spatial summation across the whisker array influences the cortical representation of touch (Armstrong-James et al. 1992; Boloori & Stanley 2006; Brecht et al. 2003; Brecht & Sakmann 2002; Brumberg et al. 1996; Brumberg et al. 1999; Chen-Bee et al. 2012; Ego-Stengel et al. 2005; Estebanez et al. 2012; Ghazanfar & Nicolelis 1999; Goldreich et al. 1999; Higley & Contreras 2003; Hirata & Castro-Alamancos 2008; Kwegyir-Afful et al. 2005; Mirabella et al. 2001; Moore & Nelson 1992; Moore et al. 1999; Petersen et al. 2001; Ramirez et al. 2014; Shimegi et al. 2000; Zhu & Connors 1999). Yet nearly all these investigations have utilized passive whisker stimulation, which can only probe receptive fields in discretized whisker space, and not in the continuous space scanned by the whiskers. An artificial whisking paradigm in anesthetized animals has allowed investigators to probe spatial coding during active touch, albeit in a reduced brain state (Brown & Waite 1974; Castro-Alamancos & Bezdudnaya 2015; Szwed et al. 2003; Wallach et al. 2016; Yu et al. 2015). These studies have revealed how spatial summation and the vibrissotopic map evolve across the sensory hierarchy or change dynamically with experience (Feldman & Brecht 2005; Fox 2002; Oberlaender et al. 2012).

Surprisingly, despite the well-ordered anatomical topography of the barrels in L4 (Woolsey & van der Loos 1970), two-photon imaging in layer 2/3 (L2/3) has revealed that on the cellular scale, the whisker map breaks down, exhibiting a salt and pepper tuning for whisker preference (Clancy et al. 2015) with some spatial correlation on the more global level (Sato et al. 2007). Similar receptive field studies in other rodent cortical areas, such as the auditory and visual cortices, have also found local breakdowns in maps of sensory space (Bandyopadhyay et al. 2010; Rothschild et al. 2010; Smith & Häusser 2010), despite some evidence of an underlying organization (Ringach et al. 2016). Nonetheless, these works analyzed maps of a fixed sensor array and not of scanned space. It remains uncertain whether an orderly map of scanned space exists in the barrel cortex or elsewhere.

During active touch, barrel cortex neurons are often well tuned to the horizontal location of an object (Pluta et al. 2015; Yu et al. 2015). Multiple mechanisms potentially contribute to their tuning. These include selectivity for the phase (Curtis & Kleinfeld 2009), deflection angle (Knutsen et al. 2008), inter-contact interval (Crochet et al. 2011), or contact forces (Bagdasarian et al. 2013; Yang & Hartmann 2016) at the moment of touch. These schemes can all operate at the single whisker level, and do not require multi-whisker integration, which is likely to occur in most natural contexts. Several studies have found that rodents perform better on whisker-guided behaviors when using multiple whiskers, suggesting that multi-whisker integration is critical for perceptual acuity (Knutsen et al. 2006; Krupa et al. 2001; O'Connor, Clack, et al. 2010). Although spatial summation is not required for spatial tuning *per se*, multi-whisker integration could powerfully transform the cortical representation of space. This might be particularly true during active sensing, where neighboring sensors probe overlapping regions of space. This raises

the possibility that multi-whisker integration during active sensing might transform a discretized vibrissotopic map into a continuous map of scanned space that could be highly advantageous for object localization and discrimination.

Whether such a map exists in the barrel cortex, and, more specifically, how multi-whisker integration could shape its organization, is unknown. Most prior studies of the barrel cortex during active sensation have either been done in unrestrained animals, when controlling the stimulus is challenging, or in head-fixed mice where only a single whisker is left intact. One study in unrestrained animals quantified tactile responses before and after removing select whiskers surrounding the principal whisker (PW) column and found opposing effects in the cortex and the thalamus (Kelly et al. 1999). Yet in these freely behaving conditions, precise measurements of neuronal receptive fields could not be obtained.

We used two photon imaging and multi-electrode array physiology to address spatial summation and map organization in the somatosensory thalamocortical system. First, we tracked how spatial summation evolves across four stages of the sensory hierarchy, from the thalamus through three cortical layers. We found that neurons in the cortex, but not in the thalamus, exhibited an asymmetric, rostro-caudal gradient of summation over surround whiskers. Surround modulation not only had dramatic impacts on firing rates, but also generated a heterogeneous and substantial shift in the spatial preference of most neurons. On the population level, our data reveal a highly ordered and continuous map of scanned space in L2/3 of the barrel cortex. This map was nearly absent when only a single whisker was intact, indicating that summation over surrounding whiskers is critical to map organization. These data demonstrate that multi-whisker integration in the cortex organizes the spatial preference of neurons to create a continuous map of scanned space. Maps of scanned space may contribute to high fidelity encoding of the location and shape of objects during natural exploration.

RESULTS

Quantifying spatial coding and summation during active sensation

To address how barrel cortex neurons encode scanned space and summate over whiskers in naturally whisking mice, we employed a head-fixed preparation in which mice ran on a free-spinning circular treadmill while we presented a vertical bar to the whiskers at fixed locations for 1.5 seconds (Fig. 2.1A). Mice were habituated to run for extended periods, a condition in which they move their whiskers in a highly rhythmic fashion (Pluta et al. 2015; Sofroniew et al. 2014) (Fig 2.1G). Under these conditions we could measure and quantify spatial representations with high precision. Neural activity was recorded with two-photon calcium imaging in the upper cortical layers or multi-electrode arrays in the lower cortical layers and the ventro-posterior medial nucleus of the thalamus (VPM). Neural data was analyzed in the final 500 ms of stimulus presentation, during which neural activity and whisking kinematics had returned to a stable state after abrupt positioning of the stimulus bar (Fig. S2.1). Experimental trials were selected based on the velocity and consistency of treadmill running to minimize variation in whisking behavior (Fig. S2.1E, and see Methods). This strict sampling of running behavior ensured consistent, repetitive touches with the stimulus throughout the object presentation period (Fig. S2.1F). Prior to each experiment, we first identified the location of the C2 whisker's representation in each mouse using intrinsic optical imaging. In both imaging and electrophysiology experiments, we found neurons across all layers of the barrel cortex whose tactile-evoked responses were tuned to

the horizontal location of the vertical pole (Fig. 2.1B-D). By labeling a single 'principal whisker' (PW) in a subset of mice with reflective paint we could track this whisker reliably in the presence of all other whiskers (Fig. 2.1E-H, Fig. S2.1). Using high-speed whisker tracking we found that across the full 'whisking field' the PW made rhythmic contact with the stimulus bar throughout the stimulus period at central but not lateral locations, where only adjacent whiskers (AWs) contacted the bar, defining a principal whisker contact zone (PWCZ) and an adjacent whisker contact zone (AWCZ, Fig. 2.1E,F).

To explore spatial summation during active sensation, we sought to quantify the contribution of the PW and the AWs to each neuron's spatial representation. We reasoned that we could measure this by comparing a neuron's spatial tuning function before and after acutely trimming off all the surround whiskers. The difference in these two measurements would reveal the parallel contributions of the AWs and PW to each neuron's spatial receptive field. Towards this aim, we collected spatial tuning curves both before and after trimming all but the principal whisker in a single experimental session (< 1 hour), so that after trimming, only the PW could contact the stimulus bar. Importantly, whisker trimming on such an acute time-scale is much shorter than required for the induction of sensory-deprivation induced plasticity (Bender et al. 2006; Glazewski & Fox 1996; Wen et al. 2013). The dataset consisted of 1016 neurons in L4 (340±120 ROIs/mouse; 3 mice), 2572 neurons in L2/3 (640±120 ROIs/mouse; 4 mice), 172 regular spiking (RS) units in L5 (10±2 units/mouse; 16 mice), and 90 units in VPM (11±2/mouse; 8 mice). Since acute whisker trimming might alter an animal's pattern of whisking during active sensation, in a subset of mice we tracked the PW both before and after surround whisker trimming and found that trimming did not significantly alter the kinematics of the animals' whisking patterns, except for a minute difference in amplitude (Fig. S2.1, mean ± s.e.m: 0.90 ± 0.20 degrees, far smaller than the 10–15 degrees between presented stimuli). This indicates that any changes we observed in neuronal response functions were due to changes in neural computation and not to changes in whisking behavior.

Spatial summation in L4

First we addressed spatial coding and summation in excitatory neurons in L4 of the barrel cortex. To record from a large population of L4 excitatory neurons across the spatial map in S1 we expressed GCaMP6s (Chen et al. 2013) in excitatory neurons in L4 using a Cre-dependent AAV and a L4-specific Cre line (Madisen et al. 2010; Pluta et al. 2015) (Fig. 2.2A). Prior to whisker trimming we observed contact-evoked responses across the entire imaging field. Following removal of the surround whiskers, sensory evoked responses were essentially abolished outside of the PW 'column' (68 ± 9% decrease in number of significantly driven units, n = 3 mice, for column identification see Methods and Fig. S2.2), demonstrating that the PW preferentially drives touch responses within its anatomically aligned column, consistent with prior observations under both passive and active conditions (Goldreich et al. 1999; Hires et al. 2015) Strikingly, in the rostral position of the PWCZ the majority (56 ± 8%, n = 3 mice) of L4 neurons within the PW column exhibited significant enhancements in their contact-evoked activity following surround whisker trimming (4.0 ± 1.3 fold increase in population mean, n = 231, Wilcoxon sign rank, $p < 0.001$, Fig. 2.2B-E). We computed a 'trimming index' as a metric for how surround whiskers influenced the evoked firing rate of each given neuron, defined as the difference over the sum of evoked activity between pre and post-trimming conditions. In the rostral PWCZ position, nearly all neurons had a positive trimming index, indicating pronounced

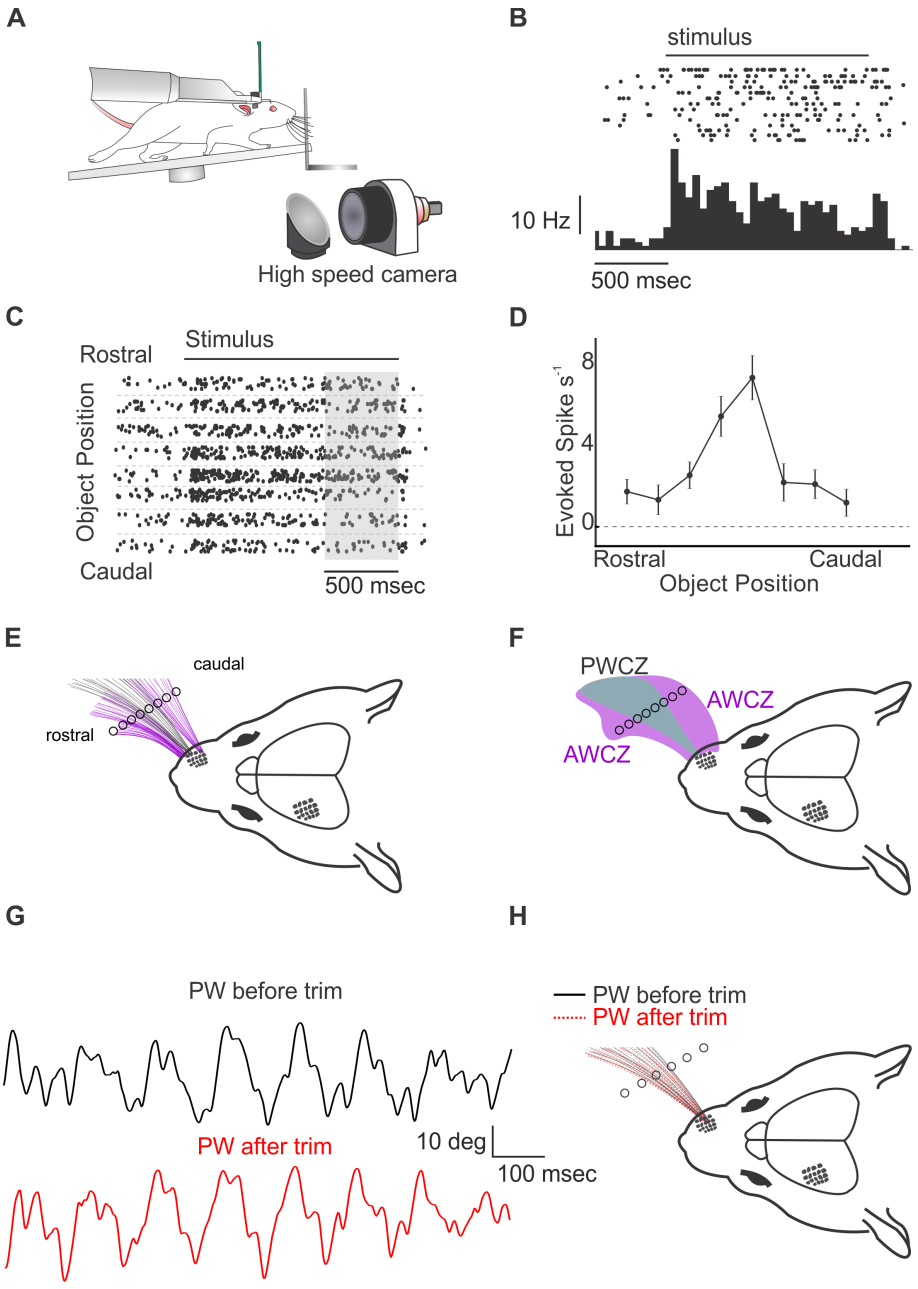

Figure 0.1 Probing the cortical representation of scanned space in the whisker system
A) Experimental schematic: a head-fixed mouse runs on a circular treadmill, while a vertical bar is moved to different locations along the horizontal whisking axis. A high speed camera captures movements of the whiskers. B) An example raster plot (top) and PSTH (bottom) of a cortical L5 unit in response to touch with the stimulus bar at its preferred location. C) Raster plot for the same unit for several trials across each of the 8 positions probed. The grey rectangle indicates the time window for analysis of neural data. D) Tuning curve (mean ± s.e.m.) for this example unit. E) Plot of the whisker positions across the full range of protraction for four tracked whiskers (during free whisking) overlaid on a schematic of the animal's head. Grey: the selected principal whisker (C2). Purple: the adjacent whiskers of the C row. F) Diagram of the zone swept out by the principal whisker (PWCZ, red) and the adjacent whiskers of the same row (AWCZ, purple). G) Example traces of the principal whisker's (C2) movement along the horizontal axis before (black) and after (red) trimming all but the C2 whisker. H) Example plot of the PW's movement before (black) and after (red) trimming all but the C2 whisker. Red and black traced whisker positions are overlaid.

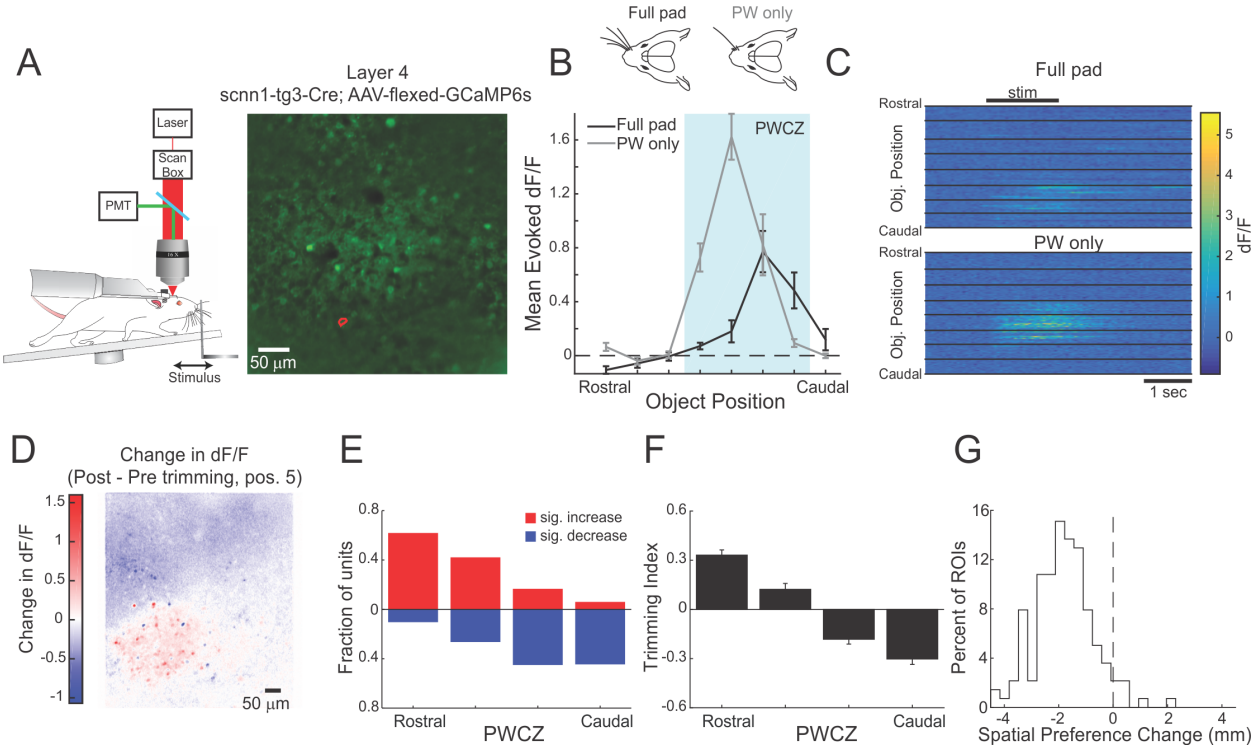

Figure 0.2 Surround whisker input powerfully modulates spatial representations in L4 excitatory neurons

A) Left: experimental schematic of a head-fixed mouse under a two photon microscope. Right: Example image of GCaMP6s-expressing L4 excitatory neurons. The C2 barrel is at center. The red outline indicates the position of the example neuron in B,C. B) Top: schematic of the pre- and post-surround whisker trimming conditions. Bottom: Example tuning curve (mean ± s.e.m.) of a single L4 neuron before (black) and after (grey) trimming all but the C2 whisker. C) Example 'raster' plot of calcium responses of the neuron from B). Top: before trimming. Bottom: after trimming. Responses from all eight stimulus positions are presented in both cases. D) Example image of the mean change in dF/F for each neuron in the field of view in L4 between post and pre trimming conditions for stimulus position five. Red indicates an increase in mean evoked responses, blue indicates a decrease. A Gaussian blur was applied. E) Plot of the fraction of cells in the C2 barrel that show significant increases (red) or decreases (blue) across each of the four stimulus positions within the PWCZ (n = 231 cells in 3 mice). F) Plot of the average trimming index for the same cells across the same stimulus conditions. G) Histogram of the change in spatial preference for all imaged neurons in the C2 barrel that exhibited significant spatial tuning both before and after surround whisker trimming (n = 139 cells across 3 mice, $p < 0.001$, t-test).

disinhibition following surround whisker trimming (trimming index = 0.33 ± 0.03, n = 231, $p < 0.001$, Wilcoxon sign rank, Fig. 2.2F). In contrast, in the caudal PWCZ position, most neurons showed a reduction in tactile evoked response (0.8 ± 0.1 fold decrease in population mean, trimming index = -0.30 ± 0.03, n = 231, $p < 0.001$, Wilcoxon sign rank, Fig. 2.2F). These data indicate that surround input from more caudal whiskers provides facilitation, whereas input from the more rostral whiskers primarily provides suppression. To address how surround whisker input influences spatial coding, we computed an index of spatial preference (the center of mass of the spatial tuning curve in the PWCZ). We found that for nearly all L4 neurons that exhibited spatial tuning (1-way ANOVA), spatial preference shifted forwards (1.77 ± 0.09 mm mean shift, n = 139, $p < 0.001$, t-test, Fig. 2.2G).

Spatial summation in cortical projection layers

Next we addressed spatial coding and summation in L2/3 and L5, the two major output layers of the barrel cortex. In L2/3 we used two-photon imaging (110-195 microns deep) to sample a large number of L2/3 neurons across the spatial map in S1. In L5 we employed laminar multi-channel electrodes that spanned the complete depth of L5. The laminar position of the electrode in each experiment was confirmed with a combination of depth readings off a precise micromanipulator, current source density analysis of the touch-induced local field potential (LFP), and post-hoc histology of the electrode track (Fig. S2.2). Prior to any trimming, we observed that L2/3 and L5 neurons in the PW column very often exhibited substantial evoked activity in the AWCZ, the region where the PW makes no contact (Fig S2.2), consistent with prior imaging studies showing that a single whisker could evoke broad activity across multiple barrel columns in L2/3 (Clancy et al. 2015; Peron et al. 2015)(Clancy et al., 2015; Peron et al., 2015). This is in contrast to neurons in L4 and in VPM which responded more specifically (but not exclusively) to stimuli within the PWCZ (see Fig. S2.2). This suggests that surround whisker input in L2/3 and L5 might be particularly important for spatial representations in these cortical projection layers.

To address this hypothesis, we recorded tactile evoked responses in both layers prior and subsequent to trimming all but a single whisker, as above. L2/3 exhibited suppression in the anterior PWCZ, but nearly exclusive facilitation in the caudal PWCZ (rostral position trimming index = 0.14 ± 0.02, $n = 631$, $p < 0.001$, Wilcoxon sign rank; caudal position trimming index = -0.37 ± 0.02, $n = 631$, $p < 0.001$, Wilcoxon sign rank, Fig. 2.3B-F). As a consequence, surround input altered the spatial preference of L2/3 neurons, but did so somewhat more heterogeneously than L4, with most neurons shifting rostrally, but some shifting caudally in their preference (1.42 ± 0.07 mm mean shift, $n = 413$, $p < 0.001$, Wilcoxon sign rank, Fig. 2.3G). In L5, similar to L2/3, the predominant impact of surround input was to facilitate responses at the caudal PWCZ position ($37 \pm 7\%$ mean decrease in spike rate, mean trimming index = -0.29 ± 0.06, $n = 48$, $p < 0.001$, Wilcoxon sign rank, Fig. 2.4A-D), which likewise had the net effect of altering spatial preference in most neurons (0.6 ± 0.2 mm mean shift forward, $n = 39$, $p = 0.001$, Wilcoxon sign rank, Fig. 2.4E).

As a control for these changes, we performed a separate set of experiments where we sham trimmed the whiskers (total experimental time equal to trimming experiments), and observed no significant effects on the population, demonstrating that the neural responses were stable over the recording session (Fig. S2.3). In addition, to assess the stability of spatial preference in each neuron in the trimming datasets, we analyzed the first and second halves of the control and trimmed whisker trials separately. We found that the spatial preference of neurons within each condition were stationary over time (Fig. S2.3), further indicating that slow changes in neuronal response properties independent of surround whisker trimming cannot explain our results. To determine how spatial preference evolves over the time course of object presentation, we analyzed each neuron's activity during eleven different time windows during object presentation. We found that the trimming-induced forward shift in spatial preference plateaued for analysis periods starting more than 600 ms after object presentation (Fig. S2.4). This result agrees with our behavioral analysis of whisking set-point, which stabilized approximately 600 ms after object presentation (Fig. S2.1C), also emphasizing the importance of analyzing the neural data in a time window of high behavioral consistency. It should also be noted that the temporal resolution of GCaMP6s as a reporter of neural activity is substantially

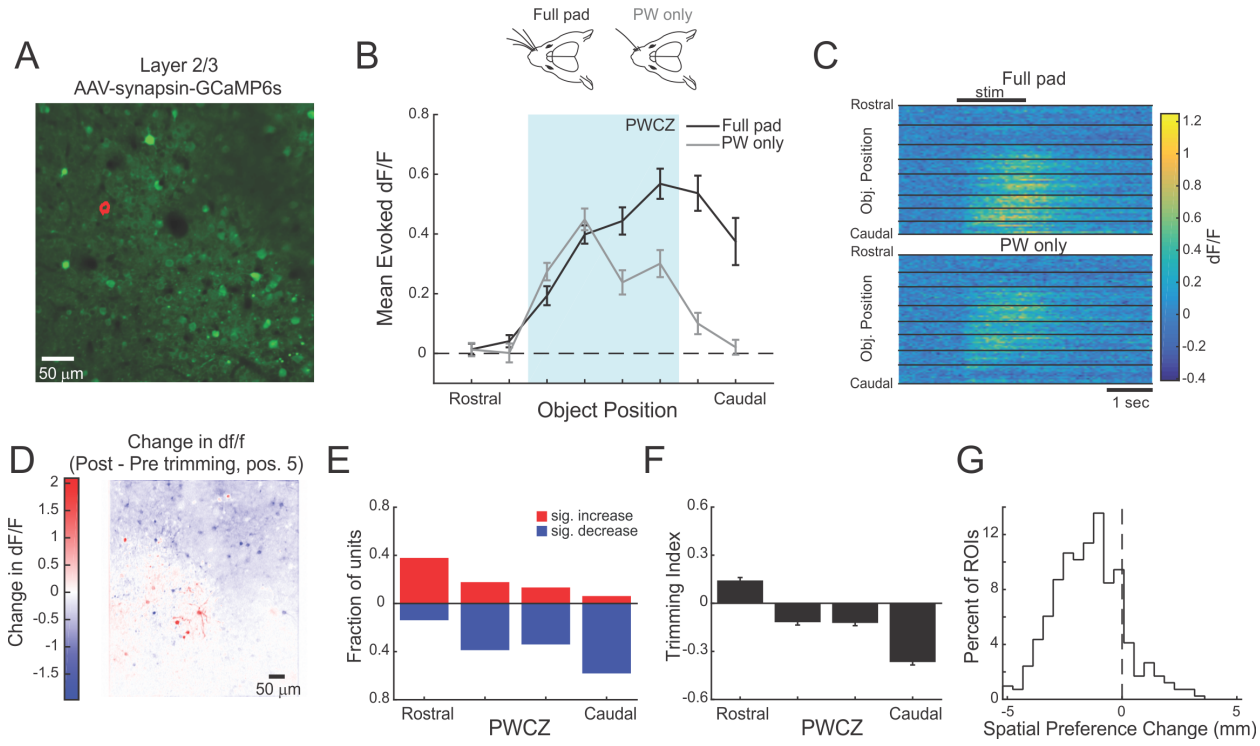

Figure 0.3 Spatial summation in L2/3 neurons
A) Example image of GCaMP6s-expressing L2/3 neurons. The anatomic aligned C2 column is at center. The red outline indicates the position of the example neuron in B, C. B) Top: schematic of the pre- and post-surround whisker trimming conditions. Bottom: Example tuning curve (mean ± s.e.m.) of a single L2/3 neuron before (black) and after (grey) trimming all but the C2 whisker. C) Example 'raster' plot of calcium responses of the cell from B). Top: before trimming. Bottom: after trimming. Responses from all 8 stimulus positions are presented in both cases. D) Example image of the mean change in dF/F for each neuron in the field of view in L2/3 between post and pre trimming conditions for stimulus position 5. Red indicates an increase in mean evoked responses, blue indicates a decrease. A Gaussian blur was applied. E) Plot of the fraction of cells in the C2 barrel that show significant increases (red) or decreases (blue) across each of the four stimulus positions within the PWCZ (n = 631 cells in 4 mice). F) Plot of the average trimming index for the same cells across the same stimulus conditions. G) Histogram of the change in spatial preference for all imaged neurons in the C2 column that exhibited significant spatial tuning both before and after surround whisker trimming (n = 413 cells across 4 mice, $p < 0.001$, Wilcoxon sign rank).

lower than that of electrophysiology. Nevertheless, GCaMP6s activity during our analysis period displayed temporal dynamics not too dissimilar from electrophysiology (Fig. S2.4 E&F).

Spatial summation in the somatosensory thalamus

The data described above demonstrate that surround whisker input powerfully influences how cortical neurons represent scanned space. Which of these surround effects emerge in the cortex, and which are inherited upstream via the thalamus? Whisker pathways converge even at the brainstem level, and can contribute to multi-whisker receptive fields in the thalamus (Timofeeva et al. 2004). To answer this question, we recorded from thalamic neurons in the ventro-posterior medial nucleus (VPM, dorsomedial portion) and compared the impact of surround whisker input

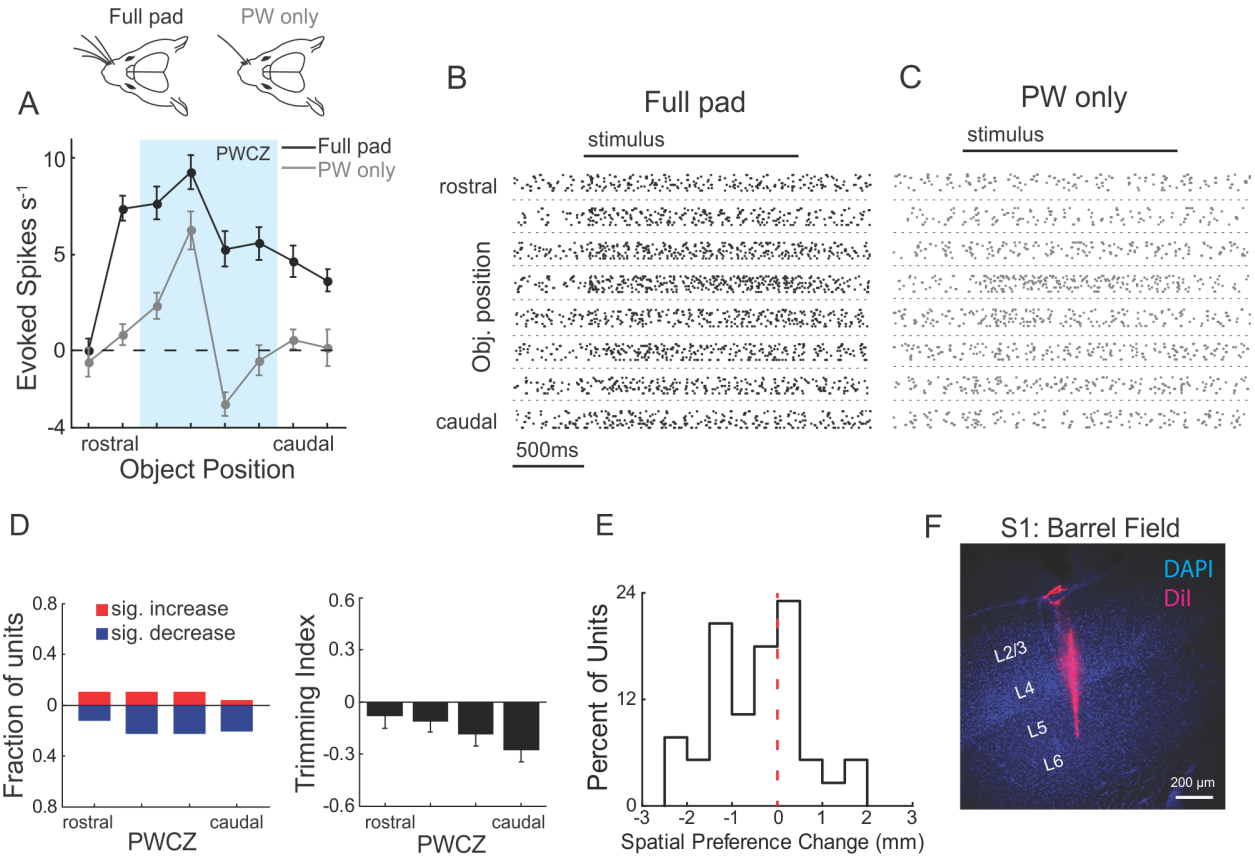

Figure 0.4 Spatial summation in touch responsive regular spiking units of L5
A) Top: schematic of the pre- and post-surround whisker trimming conditions. Bottom: Example tuning curve (mean ± s.e.m.) of a single L5 RS unit before (black) and after (grey) trimming all but the principal whisker. B) Example raster of the unit from A) before trimming to the principal whisker. C) As in B) but for after trimming. Responses from all 8 stimulus positions are presented in both cases. D) Left: Plot of the fraction of L5 RS units in the spared whisker column that show significant increases (red) or decreases (blue) across each of the four stimulus positions within the PWCZ. Right: Plot of the average trimming index for the same cells across the same stimulus conditions (n = 48 units in 8 mice). E) Histogram of the change in spatial preference for all recorded L5 RS units in the spared column with significant spatial tuning both before and after surround whisker trimming (n = 39 units across 8 mice, p = 0.001, Wilcoxon). F) Example image from a recorded animal showing the DiI track (red) of the multi-electrode array extending into L5.

on VPM neurons to our observations in cortical neurons. We found that thalamic neurons showed robust spatial tuning like their cortical counterparts (fraction of neurons tuned, VPM: 83%, L4: 86%, L2/3: 89%, L5: 67%, 1-way ANOVA), demonstrating that tuning, *per se*, is likely to be generated sub-cortically, perhaps as early as the primary mechanoreceptors, according to previous reports (Szwed et al. 2003; Yu et al. 2015) (Fig. 2.5A-C). Nevertheless, trimming the surround whiskers demonstrated that surround input modified thalamic responses, but weakly compared to L4 (Fig. 2.5D-E). A minority of VPM neurons exhibited a significant change in their evoked activity across the center of their spatial receptive field (within the 'PWCZ', Fig. 2.5D). As a population, VPM neurons displayed a reduction in their evoked firing rate at the rostral PWCZ position (trimming index = -0.13 ± 0.06, p = 0.047, n = 54, paired t-test, Fig. 2.5E). This distinctly contrasts to the robust enhancement we observed in L4 neurons at the.

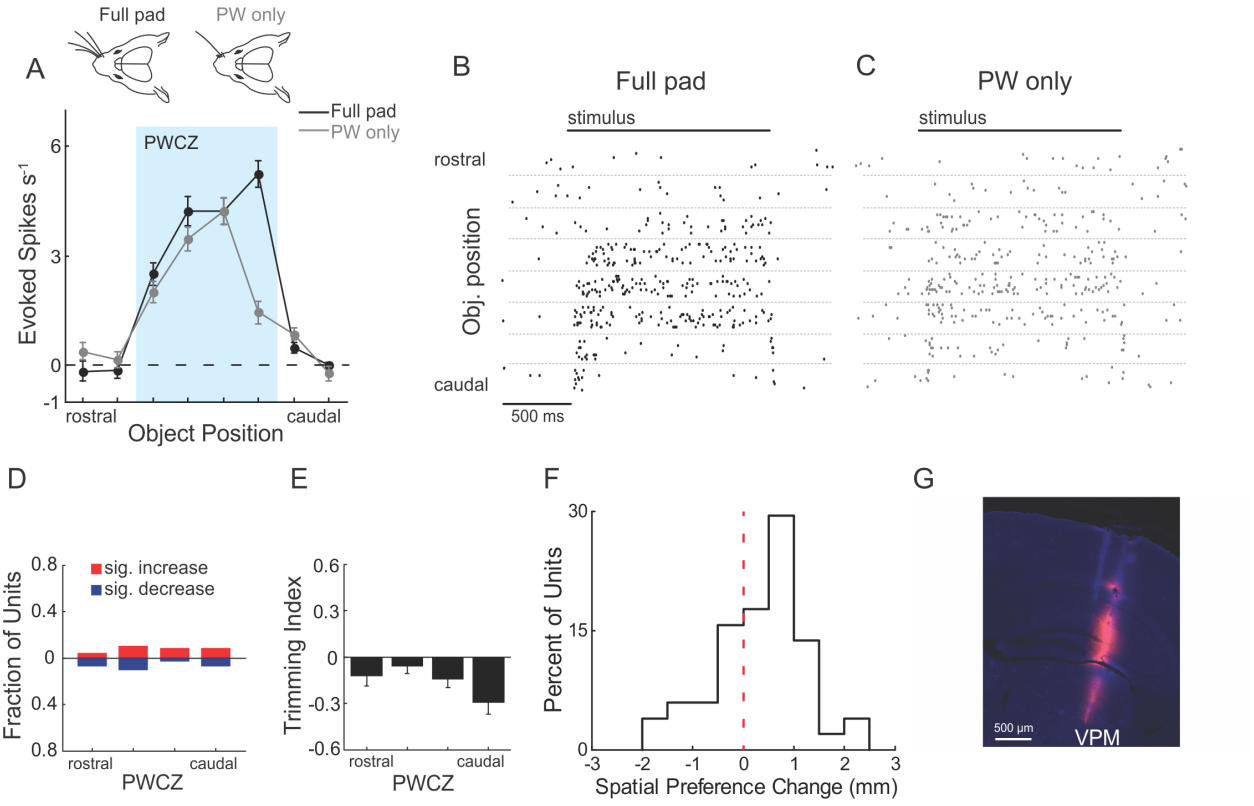

Figure 0.5 Weak surround modulation in thalamic neurons in VPM

A) Top: schematic of the pre- and post-surround whisker trimming conditions. Bottom: Example tuning curve (mean ± s.e.m.) of a single VPM unit before (black) and after (grey) trimming all but the C2 whisker. B) Example raster of the unit from A) before trimming to the C2 whisker. C) As in B) but for after trimming. Responses from all 8 stimulus positions are presented in both cases. D) Plot of the fraction of units in the C2 barreloid that show significant increases (blue) or decreases (red) across each of the four stimulus positions within the PWCZ (n = 54 units across 8 mice). E) Plot of the average trimming index for the same cells across the same stimulus conditions. F) Histogram of the change in spatial preference for all recorded units in the C2 barreloid with significant spatial tuning both before and after surround whisker trimming (n = 51 units across 8 mice, p = 0.23, paired t-test). G) Example image form a recorded animal showing the DiI track (red) of the multi-electrode array extending into VPM.

rostral PWCZ position. Furthermore, unlike for cortical neurons, surround input did not change the spatial preference of VPM neurons (0.16 ± 0.14mm mean shift, n = 51, p = 0.23, t-test, Fig 2.5F). These results imply that surround modulation of the spatial preference of cortical neurons emerges primarily in the cortex.

As a whole, the data above demonstrate that surround input uniquely transforms the cortical representation of space. Conversely, we sought to determine the importance of principal whisker (PW) input to spatial tuning in an output layer of the cortex, L5. Towards this end, in a separate set of mice, we measured spatial tuning functions before and after trimming off only the PW, leaving all the surround whiskers intact (Fig. S2.5). Following removal of the PW, we observed a pronounced reduction in the evoked firing rates of neurons that were facilitated by touch, consistent with the expected function of the principal whisker (-28 ± 5% change, trimming index: -0.20 ± 0.03, Fig. S2.5a, n = 36, p < 0.001, paired t-test). Even though almost all (95%)

L5 units retained significant touch-evoked firing after removal of their PW, they exhibited no change in spatial preference (Fig. S2.5C, n = 20, p = 0.53, Wilcoxon sign rank), in notable contrast to the effect of removing surround whiskers. However, the spatial selectivity of the population was significantly reduced, typified by flatter tuning curves (n = 50, p = 0.003, Wilcoxon sign rank, Fig. S2.5D). These data indicate that the PW is the primary, but not sole, contributor to the amplitude of a given neuron's tactile response, while surround whiskers potently influence its spatial preference.

Surround input organizes a map of scanned space in the barrel cortex

The data above indicate that surround whisker input powerfully influences how individual neurons in the barrel cortex encode scanned space. How might spatial coding be organized on the more global level? On one hand, the spatial preference of nearby neurons might show little correlation, similar to the salt and pepper distribution of orientation tuning in rodent visual cortex (Ohki et al. 2005). Alternatively, the spatial preference of neurons might gradually shift across the rostro-caudal axis of cortex, constituting a continuous map of scanned space. To address this question in L2/3, we plotted spatial preference for each neuron across the entire field of view (1.06 ± 0.30 mm^2), encompassing the region above several adjacent barrels (Fig. S2.6). Strikingly, we observed a topographic representation in the positional preference of neurons across the rostro-caudal axis of stimulus space, arranged approximately across the row axis of the barrel cortex (Fig. 2.6A, see Methods and Fig. S2.6 for a description of how the map axis was determined). The spatial resolution of the aggregated maps was 6.7 μm of physical space per micron of cortical tissue, as quantified by the slope of the linear regression of spatial preferences across all mice (Fig. 2.6D).

Since we did not observe clear discretization in any of the individual maps (see Fig. S2.7), it is possible that summation over surround whiskers help generate this continuous map. To test this idea, we asked how the spatial map changed following removal of all but one whisker. While many neurons across the entire field of view retained significantly evoked responses and spatial tuning, the spatial map all but disappeared (Fig. 2.6B, Fig. S2.7). We quantified this change in several ways. First we compared the correlation of neurons' spatial preference across the axis of best fit before and after trimming (see Methods). Before trimming, the spatial preference of the imaged neurons exhibited a clear correlation along the rostro-caudal axis (Pearson's R = 0.70, $p < 0.001$), implying the presence of a map; however, after trimming, this correlation disappeared (Pearson's R = 0.00, p = 0.9, Fig. 2.6D-E). This relationship held true both across the entire field of view and within a restricted zone that retained strong activity following trimming (Pearson's R pre-trim = 0.48, $p < 0.001$, vs. Pearson's R post-trim = 0.08, p = 0.063), most likely corresponding to the region directly above the spared L4 barrel (486 ± 70 microns along axis of best fit, n = 4 mice). Second, we computed correlations between the spatial preferences of all pairs of neurons within a given map as a function of cortical distance along the axis of best fit. For a map to exist, nearby neurons should display similar spatial preferences, while distant neurons should diverge. Consistent with this notion, before trimming, an analysis of pairwise correlations show that nearby neurons have much greater similarity in spatial preference than distant neurons (Fig. 2.6F). However, after trimming to a single whisker, the relationship between pair-wise cortical distance and spatial preference similarity dramatically decreased (Fig. 2.6F). As a third means to quantify this map, we constructed cumulative distribution functions of spatial preference along the axis of best fit before and after trimming. With surround input intact,

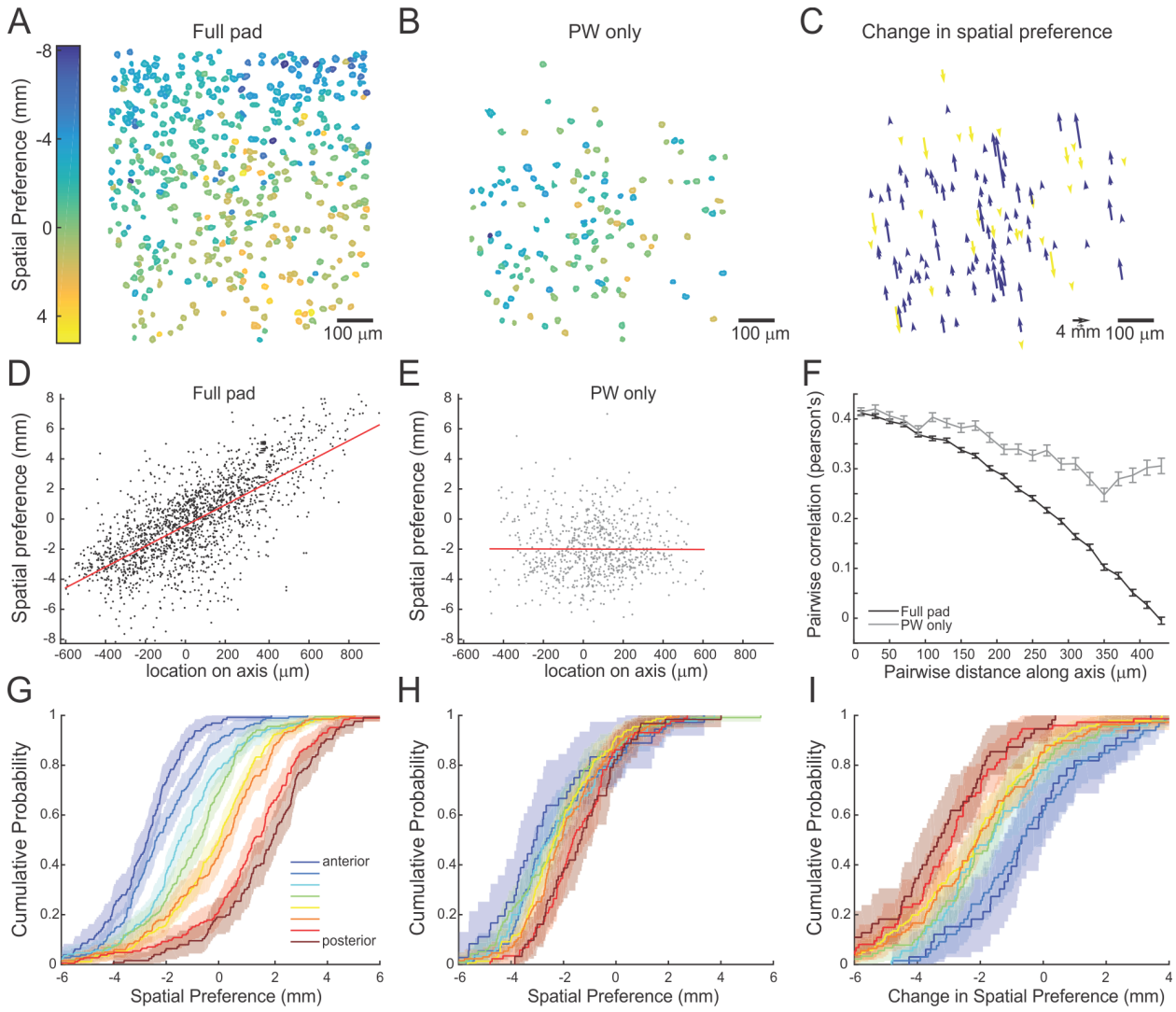

Figure 0.6 Surround whiskers organize a spatial map in L2/3 of the barrel cortex
A) Example spatial preference map in a mouse with all the whiskers intact of a field of view in L2/3 imaged with two photon microscopy. The color indicates the spatial preference of the stimulus bar's position. Only neurons that exhibited significant activity and spatial tuning are shown. B) Same field of view as in A) but collected immediately after removing all but the C2 whisker. Again, only neurons that exhibited significant activity and spatial tuning are shown. C) Plot of the magnitude and direction of change in spatial preference for all imaged neurons within A) and B) that exhibited significant spatial tuning both before and after surround whisker trimming. Yellow: rostral shift, purples: caudal shift. The length of each arrow corresponds to the magnitude of change in spatial preference, and its direction indicates the sign of the change. The arrows are all aligned to the axis of best fit for preferred position calculated prior to trimming. D) Plot of the spatial preference of all significantly tuned L2/3 cells versus their position along the axis of best fit (1789 neurons, 4 mice). The red line is a linear regression to the data. E) As in D) but for after trimming to the C2 whisker (796 neurons, 4 mice). F) Binned plot of the pairwise correlation of spatial tuning curves for all pairs of significantly tuned L2/3 neurons within each mouse as a function of distance in cortical space. G) Cumulative distribution plots of spatial preference of significantly driven and tuned neurons before trimming as a function of cortical position along the axis of best fit. H) As in G) but for after trimming to the C2 whisker. I) Cumulative distribution plot of the change in spatial preference for all the recorded neurons.

there was a gradual and systematic tiling of spatial preference along the entire axis of cortical space ($p < 0.001$, ANOVA, $n = 1486$, Fig. 2.6G). Following trimming to the C2 whisker, these spatial preference distributions coalesced (Fig. 2.6H), due to an increasingly greater forward shift in caudal neurons (Fig. 2.6I), demonstrating that multi-whisker integration is critical for an organized map of the scanned region. The apparent disorganization of the map was not simply due to noisier responses in the cortex after trimming, since our analysis is restricted to neurons significantly tuned for space and significantly driven by the stimuli. Nor is it due to analyzing different total numbers of responsive and tuned neurons between the two conditions, since the results held true even when we restricted our analysis to the population of neurons that were significantly tuned both before and after trimming (Fig. S2.8). Lastly, we addressed whether behavioral variation, such as minute trial-to-trial differences in whisker set-point, could have affected the smoothness (Pearson's R) of the sensory map in L2/3. However, in our L2/3 dataset, the faster the mouse ran on the treadmill (the narrower the range of whisker set-points, Fig. S2.1), the smoother the map became (Fig. S2.8). Therefore, behavioral variation is in fact detrimental to map smoothness.

Finally, we probed this spatial map electrophysiologically using multi-shank laminar electrodes (Fig. 2.7A, B). We inserted three 8-electrode shanks across the C-row axis of the barrel cortex (identified with intrinsic optical imaging and electrophysiologically verified, Fig. S2.2) and measured spatial tuning functions of cortical units across 3 barrel columns both before and after trimming to the C2 whisker (Fig. 2.7C, D). Across the electrode shanks, the rostro-caudal distributions of spatial preference could be quantified by plotting cumulative distribution functions. Before trimming, neurons in different cortical columns had significantly different spatial preferences that corresponded to their relative location in the cortex ($p < 0.001$, ANOVA, $n = 70$, Fig. 2.7C, E). After trimming, the spatial preference of the neurons that retained significant tuning coalesced onto a narrow region of space ($p = 0.32$, ANOVA, $n = 45$, Fig. 2.7D, F). Furthermore, the magnitude of the change in spatial preference varied with cortical location; neurons in the caudal cortical column shifted further forward than neurons in the rostral column ($p = 0.03$, ANOVA, $n = 31$). These results are not simply due to inferior measurements of spatial preference caused by a uniform reduction in response strength, because the spatial selectivity of neurons outside of the spared column did not systematically decrease after trimming ($p = 0.73$, $n = 24$, Wilcoxon sign rank). Although these electrophysiological recordings cannot reveal the same degree of continuity we observed with two photon imaging, they nevertheless further support the notion that surround whisker input distributes the spatial preference of neurons to generate a map of scanned space in the barrel cortex. Lastly, we asked if the map was centered on the head, rather than on the set point of the whisking envelope. If so, the spatial preference of neurons should stay the same, despite a shift in whisker set-point. However, we observed that spatial preference follows the set-point of whisking, implying that the map is not head-centered (Fig. S2.9).

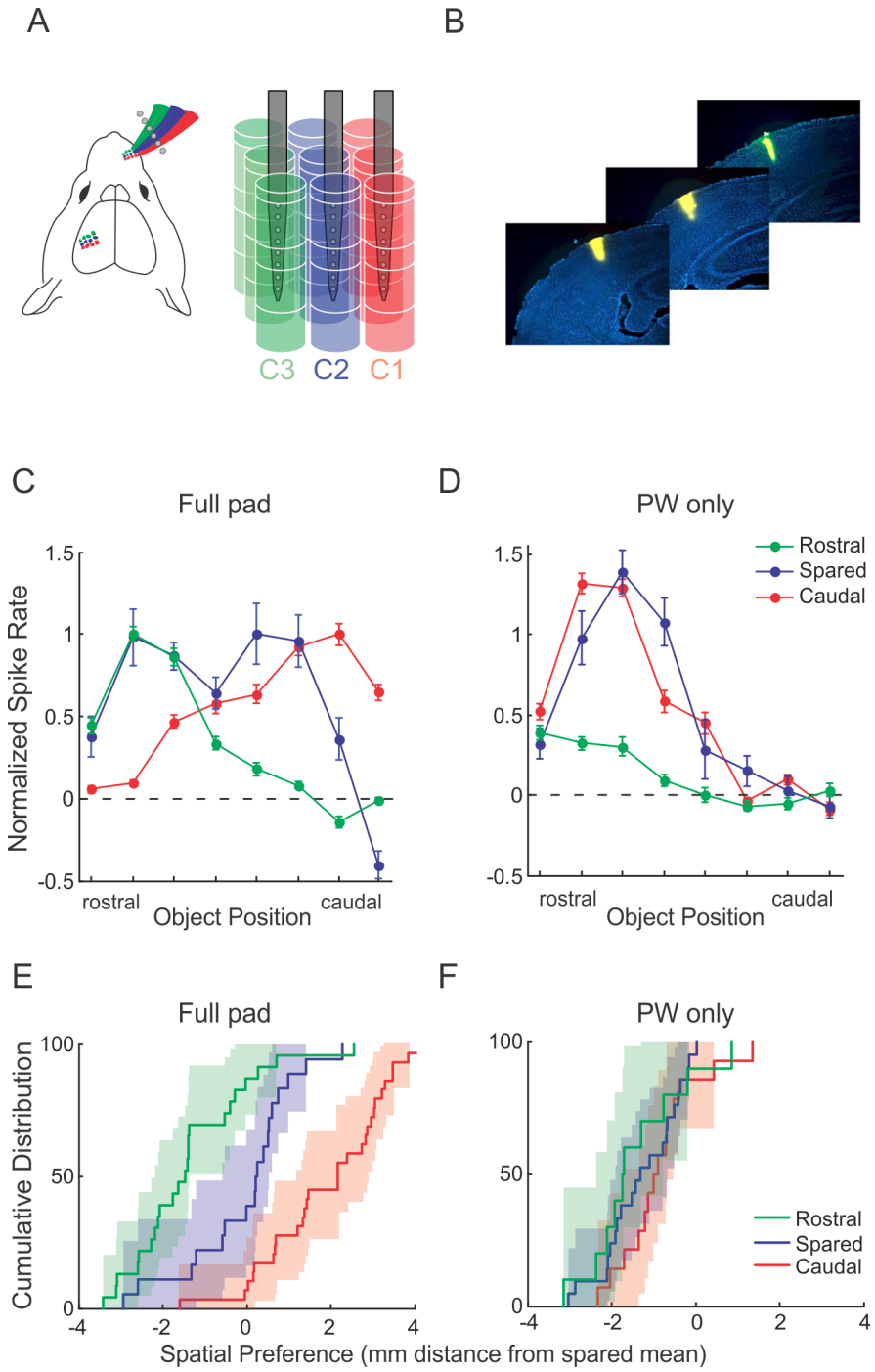

Figure 0.7 Surround whiskers distribute spatial representations in L5
A) Schematic of multi-shank laminar recordings in L5. B) Example histological images of the electrode of three adjacent shanks in S1. C) Example spatial tuning curves from three units on three adjacent electrode shanks. D) As in C) but following trimming off the surround whiskers. E) Cumulative distribution plots of spatial preference of significantly tuned units on each electrode shank before trimming. F) As in E) but following trimming off the surround whiskers.

DISCUSSION

This study examines how neurons across four sequential stages of the thalamocortical system integrate across a sensor array during active sensation to encode the space scanned by the sensors, in this case, the rodent's whiskers. While many previous studies have addressed spatial summation in anesthetized, paralyzed, or fixating animals, how summation influences sensory coding when the sensors are actively and volitionally moving has remained largely unexplored. Several previous studies have compared neural responses between active and passive conditions and reported significant differences, including reduced response amplitudes and more restricted spatial or temporal spread of activity (Fanselow & Nicolelis 1999; Ferezou et al. 2007; Hentschke et al. 2006; Lee et al. 2008). Yet spatial summation, *per se*, has not been rigorously characterized in awake, volitionally whisking mice. In this study, we found that surround whisker input potently transformed barrel cortex neurons' spatial tuning, strongly impacting firing rates, and shifting their spatial preference. In L2/3, these shifts acted to organize a sensory map of scanned space. Such a map – referenced not to the sensors, but instead to the space probed by the moving sensor array, has not been previously demonstrated in any sensory system to our knowledge. Although the whisker system bears many unique qualities that distinguish it from other sensory systems, this spatial map of scanned space in the barrel cortex raises the possibility that similar maps might exist in other cortical areas in rodents, and in other mammalian species. Primates move their hands across surfaces to localize and identify objects (Chapman & Ageranioti-Belanger 1991), similar to how rodents use their whiskers, and a continuous map of scanned space in the primate somatosensory cortex might also exist.

The map we observed was not an ego-centric map – i.e., a head-centered map – but rather a map centered on the set-point of the scanned region (Fig. S2.9). Nonetheless, a map of scanned space, as was observed here, may contribute to the generation of an egocentric (head-centered) map of space downstream that is independent of the scanned region (or 'field of view'). Based on prior evidence in non-human primates, the posterior parietal cortex is a brain area that may be involved in this transformation (Andersen et al. 1985), but likely builds on cues present even at the mechanoreceptors themselves (Yang & Hartmann 2016).

How might a map of scanned space be generated? First, it is important to note that while the map depends on summation over multiple whiskers, spatial tuning for individual cortical neurons persists even with only a single whisker intact. This is largely consistent with prior reports that horizontal location can be computed by cortical neurons even with information from a single whisker (Curtis & Kleinfeld 2009; O'Connor, Peron, et al. 2010), or even by neurons at very early stages of the somatosensory system (Szwed et al. 2003; Yu et al. 2015), a fact consistent with the strong tuning we observed in thalamic neurons. Thus horizontal tuning *per se* does not appear to depend on cortical computation. Instead, we propose that summation over the underlying whisker map, specifically in the cortex, is what helps create the map of scanned space. This computation might be analogous to local smoothing, and could be implemented by the broad dendritic trees and horizontal projections of L2/3 pyramidal neurons that cross cortical column boundaries, as well as the divergence of ascending L4 axons (Bender et al. 2003). Nevertheless, many other possibilities exist, including computations involving efferent or re-afferent signals of whisker motion. While future experiments can address the underlying mechanisms that generate the map of scanned space in L2/3, we propose that the role of surround input in the cortex is not to generate spatial coding *de novo*, but rather to act on the global level to organize spatial preference across the horizontal axis of the cortex in such a way so as to

generate a continuous map of space. Whether other maps that exist in the barrel cortex, such as for contact angle or for correlation selectivity, contribute to the generation of this spatial map, remains to be seen (Andermann & Moore 2006; Estebanez et al. 2016; Kremer et al. 2011; Peron et al. 2015).

In this study, owing to the highly stereotyped pattern of whisking that mice exhibit during head-fixed locomotion, we were also able to reliably quantify single neuron's spatial tuning curves during active sensation. Although this preparation resembles in some respects anesthetized conditions where the whiskers are made to move artificially by electrical stimulation of the facial motor nerves (Brown & Waite 1974; Castro-Alamancos & Bezdudnaya 2015; Szwed et al. 2003), all of our data were collected in the awake, alert state. Since several studies have highlighted how brain state and the level of alertness can dramatically influence sensory processing and the firing of specific cortical subtypes (Adesnik et al. 2012; Castro-Alamancos 2004a; Castro-Alamancos 2004b; Castro-Alamancos & Oldford 2002; Greenberg et al. 2008; Lee et al. 2013; Niell & Stryker 2010; Poulet & Petersen 2008; Reimer et al. 2014; Vinck et al. 2015), we consider it essential that we performed all of our experiments in the awake state while mice ran and whisked of their own volition.

The second key finding of this study with respect to spatial summation is the presence of an asymmetric rostro-caudal gradient of response modulation that emerges in the cortex. This modulation is most pronounced in L4, where contact with anterior whiskers powerfully suppresses responses to the PW, while contact with more posterior whiskers generate substantial facilitation. This effect is very likely to be related to the well-known impact of the temporal sequence of whisker-object contacts revealed in anesthetized recordings (Civillico & Contreras 2006; Drew & Feldman 2007; Higley & Contreras 2003; Shimegi et al. 2000). What is the utility of such across-whisker modulation? One possibility is that the combined action of anterior suppression and posterior facilitation strongly enhances spatiotemporal contrast in the population response in L4 during whisker contact. In other words, as an animal sweeps its whiskers forwards into an object, the largest neural responses will be in the barrel representing the first whisker to contact the stimulus, both because it gets no suppression from any anterior whisker and because it gets facilitation from the more posterior whisker that contacts the object second. However, at the same time, the L4 barrel representing the second whisker to touch will be suppressed by touch with the first whisker. The net effect of this scheme is to generate a high spatial gradient of evoked responses in L4 barrels that could sharpen the population representation of touch in the barrel cortex (Brumberg et al. 1996; Drew & Feldman 2007). This contrast-enhancing, asymmetric integration appears to be involved in generating the continuous map of scanned space we observed in L2/3, although it could be important on its own for other spatial computations. Additional factors unrelated to timing, such as asymmetry in forces on the PW across different object positions, likely shape the properties of surround integration.
Taken together, the results of this study reveal fundamental modes of cortical computation during active sensation, and shed light on key underlying neural mechanisms. Previous studies, primarily in anesthetized or sedated animals, have highlighted how summation across whiskers depends critically on the timing and spatial patterns of surround whisker stimulation (Brumberg et al. 1996; Shimegi et al. 2000). In at least two studies, coordinated waves of surround input, mimicking that which occurs naturally, can profoundly alter the response properties of cortical neurons (Drew & Feldman 2007; Jacob et al. 2008). In this study, since the animals whisked freely, the timing and pattern were not under experimental control, but our results are nevertheless consistent with prior experiments under anesthesia. A previous study, in

anesthetized animals, demonstrated that the degree of correlated whisker movement across the array could profoundly influence single unit responses – with some units enhanced and other suppressed by global correlations (Estebanez et al. 2012). Furthermore, recent work showed that the enhanced neurons in L2/3 are clustered above the edges of the L4 barrels (Estebanez et al. 2016). In our study, since the mice naturally whisked in a coherent fashion at a vertical bar, the stimulus we used is likely to be more similar to the global correlation condition. In any condition, the precise spatiotemporal pattern of multi-whisker touch likely has a profound influence on sensory integration. Similar to previous studies that investigated active sensation with a single whisker (Ferezou et al. 2007; Hentschke et al. 2006; Lee et al. 2008), our results have the advantage that they are drawn from volitionally whisking mice, and thus within the ethologically relevant range of multi-whisker contact patterns. However, this naturalistic approach prevented us from identifying the precise moments of multi-whisker touch, thereby obscuring the effects of multi-whisker integration on the fine temporal structure of spiking. Future studies, using technological advances that permit the imaging and quantification of multi-whisker contacts during exploration of objects with complex surface geometry (Hobbs et al. 2016), in combination with the physiological approaches here, could address how a spatial map in S1 facilitates the encoding of higher order stimulus features. Furthermore, processing stages downstream of S1 could integrate topographic information of scanned space with sensorimotor signals conveying whisking set point to construct an egocentric map of space.

MISCELLANEOUS

Acknowledgements

The authors acknowledge the GENIE Project, Janelia Farm Research Campus, and the Howard Hughes Medical Institute for the GCaMP6 viruses as well as Dan Feldman and members of the Adesnik and Feldman labs for comments on the manuscript. H.A. is a New York Stem Cell Foundation-Robertson Investigator. This work was supported by The New York Stem Cell Foundation. This work was supported by NINDS grant DP2NS087725-01 and Whitehall Foundation grant #2012-08-09.

Author Contributions

H.A. and S.P. conceptualized the study. H.A., S.P., and E.L. devised the methodology. E.R.-W. performed all thalamic recordings. G.T. recorded and analyzed all high-speed whisker tracking data. S.P. performed all barrel cortex electrophysiology experiments and analyzed all electrophysiology data. E.L. performed all two-photon calcium imaging experiments and analyzed all calcium imaging data. S.P., E.L., and H.A. wrote the paper. S.P. and E.L. contributed equally to this study. A copy of this study can be found at Pluta et al. 2017.

METHODS

Experimental Model and Subject Details

Wild-type adult ICR white (Charles River) mice between 6 and 10 weeks of age and of either gender were used for all experiments, except for those involving imaging cortical layer 4, for which the scnn1-tg3-Cre line (JAX), outcrossed to the ICR line for several generations, was used. All procedures were approved by the Animal Care and Use Committee of UC Berkeley. Both female and male animals were used and maintained on a 12:12 reversed light:dark cycle. For supplemental figure 2.6, we used a Thy1-GCaMP6s (4.3) mouse.

Preparation for *in vivo* electrophysiology

Anesthesia was induced with 5% isoflurane and then maintained at 1 – 3% during surgery. Respiratory rate and response to toe/tail pinching was monitored throughout surgery to ensure adequate anesthetic depth. 0.05 mg/kg of buprenorphine was administered for post-operative analgesia. After disinfecting the scalp with 70% alcohol and 5% iodine, the skin and fascia above the sensory cortices were removed with surgical instruments. Following application of Vetbond (3M) to the skull surface and wound margins, a custom stainless steel headplate was fixed to the skull with dental cement (Metabond). Two days after surgery, mice were habituated over increasing durations for 4 – 8 days to head-fixation on a free-spinning circular treadmill, until they freely ran at a fast and steady pace (>35 cm/s). Intrinsic optical imaging was performed to localize one or two barrel columns of interest (C1 – C3). In preparation for electrophysiology, mice were briefly (10 – 15 minutes) anesthetized with isoflurane, the skull over S1 was thinned with a dental drill (Foredom), and a small (<200 μm for a single shank) craniotomy was made with a 27 gauge needle. For mutli-shank experiments a long, thin craniotomy was opened over S1 in a similar fashion. The small size of the craniotomy minimized motion of the brain during electrode penetration and animal movement. For recordings from the cortex, a 16 or 32-channel linear silicon probe (NeuroNexus) was guided into the brain using a micromanipulator (Sutter Instruments) and a stereomicroscope (Leica) to the desired barrel column (C1 – C3) by aligning the intrinsic optical signal (Fig. S2.2) with superficial blood vessels. For multi-shank experiments, a Neuronexus Buzsak32 probe was used. The principal whisker was verified electrophysiologically by deflecting individual whiskers and listening to multiunit activity (MUA). There was an audibly clear difference in MUA between principal and surround whisker contact. For recordings of the thalamus, a 16-channel linear silicon probe (NeuroNexus) was guided into the brain at 1600 μm posterior and 2000 μm lateral from bregma. The electrode was lowered until strong whisker responses were detected, usually around 2700-2800 μm, indicating the border of the ventro-posterior medial nucleus. The electrode was lowered further until it reached a barreloid corresponding to C2 or B2, where that whisker caused the strongest response from deflection. In all cases, electrical contacts on the probe spanned the C1 – C3 or B1 – B3 barreloids, as verified by electrophysiology.

Preparation for *in vivo* two photon imaging

The surgery was as described above, but with the following modifications for transcranial imaging through a glass window. 2 mg/kg of dexamethasone were administered as an anti-

inflammatory. A 3 mm diameter craniotomy over the left primary somatosensory cortex was drilled, and a Nanoinject II nanoliter injector was used to inject 18.4 nL of AAV-GCaMP6s at ten to twenty sites within the craniotomy at an overall rate of 0.5 nL/s. AAV9-synapsin-GCaMP6s (UPenn Vector Core) was injected into wildtype ICR mice (Charles River) for L2/3 datasets, and AAV9-flexed-CAG-GCaMP6s (UPenn Vector Core) was injected into scnn1-tg3-Cre mice (JAX) for L4 datasets. After viral injection a window plug consisting of two 3mm diameter coverslips glued to the bottom of a single 5mm diameter coverslip using Norland Optial Adhesive #71 was placed over the craniotomy and sealed permanently using Orthojet. Mice were head-fixed on a freely spinning running wheel under a Nixon 16x-magnification water immersion objective and imaged with a Neurolabware two-photon resonant scanning microscope within a light tight box. Image acquisition was at 15.45 Hz with fields of view (FoVs) ranging from 600 μm by 650 μm to 1.25 mm by 1.15 mm. To obtain large fields of view in all cases, in some experiments four adjacent FoVs were imaged sequentially. Wide-field reflectance imaging with a white LED was used to illuminate the vasculature and center the FoV on the region the intrinsic signal identified as corresponding to the C2 barrel. For L2/3 imaging, imaging depth was 100 – 300 μm, and for L4 imaging, depth was 400 – 500 μm deep.

Tactile Stimulus presentation

During continuous two-photon imaging or electrophysiological recording, a modified 0.7mm Hex key (McMaster-Carr) was presented vertically at 8 locations along an axis perpendicular to whisking motion and ~1 cm away from the mouse's face. The pole was presented to the whiskers for 1.5 seconds during each trial using a stepper motor (Oriental Motor) to quickly move the pole in, hold the pole stationary for the entire stimulus period, and then move it back out. There was an interval of 3 - 4.5 seconds between trials for imaging to allow the evoked calcium response to return to baseline. At the beginning of each inter-trial interval the stepper motor and pole were translated to the next trial's horizontal position using a motorized linear stage (Zaber). Stimuli were randomized in batches such that no stimulus was presented more than twice in a row. After >15 repetitions of the stimulus batches, data collection was paused and all but the principal whisker (always C2 for imaging experiments) were trimmed such that only the remaining whisker could contact the vertical pole stimulus at any position. Data collection immediately recommenced and at least 16 new batches of stimuli were presented. After conclusion of the experiment, the vertical pole was presented at each of the stimulus positions, and the PWCZ positions were identified by high speed camera acquisition or by visual inspection using stereomicroscope. This was verified post-hoc by determining which stimulus positions evoked significant activity throughout the object presentation period after trimming the surround whiskers.

Two photon imaging analysis

Raw two photon movies were first corrected for brain motion using Scanbox's fourier transform-based sbxalign script, written in MATLAB, to correct for the 2D translation of individual frames. The mean of each motion-corrected video was used to translate and register the before and after trimming datasets to within a single pixel of each other. Regions of interest (ROIs) encompassing neurons were identified in a semi-automated manner using Scanbox's sbxsegmentflood (MATLAB, Mathworks) which computes and thresholds the pixel-wise cross-

correlation for all pixels within a 60 by 60 pixel window. If an ROI only appeared in one of the datasets via the semi-automated method, then the ROI was copied over to its relative location in the dataset in which it was not identified. The ROI's signal (R_i) was taken as the mean value across all pixels within and unique to that ROI (Fig. S2.2). This signal is assumed to be a mixture of the cell's actual fluorescence signal and a contaminating neuropil signal resulting from scattering producing off-target excitation, high illumination powers producing out of focus fluorescence, or unresolvable neurites passing through the microscope's point spread function. The neuropil signal (N_i) for each ROI was computed by averaging over an annulus of pixels surrounding the ROI but excluded pixels assigned to other ROIs as well as a smaller annulus of pixels that acted as a buffer in case any motion artifact was not perfectly accounted for (Fig. S2.2). This buffer annulus existed for all ROIs and was excluded from any neuropil calculation. As a result the max diameter of the neuropil annulus varied per ROI in order to ensure a similar number of usable pixels to average over. Each neuron's true fluorescence signal (F_i) was computed per ROI by the following equation:

$$F_i(t) = R_i(t) - k_i * N_i(t)$$

The amount of contamination (k_i) was assumed to be constant per ROI, but vary between ROIs as a result of local differences in expression and scattering. Each k_i was defined by assuming that the neuron's true fluorescence signal (F_i) can never be negative (i.e. $k_i * N_i(t) \leq R_i(t)$), and that there must be a maximal bound for contamination. The contamination coefficient per neuron was defined as follows:

$$k_i = \min\left(\frac{R_i(t)}{N_i(t)}\right); if\ k_i > .65, k_i = .65$$

The true signal was then converted into a trial-wise change in fluorescence ($\frac{f(t)-f_0}{f_0}$ or df/f) to capture the stimulus-evoked changes in neural activity while compensating for any fluctuations in baseline fluorescence. The baseline fluorescence (f_0) for a trial was taken to be the mean fluorescence over the one second prior to stimulation.

High-Speed Whisker Tracking

In a subset of experiments the whiskers were tracked at high speed (~500 frames per second). Previous data, confirmed here (Fig. S2.1), indicate a tight correlation between run-speed of the mouse and whisker set-point, which plateaus above 35 cm/s (Sofroniew et al. 2014). A high-speed camera (Basler, acA2000-340kc) was placed below the running wheel; the principal whisker was imaged from below using a mirror angled at 45 degrees. The base of the PW was painted with a thin layer of Titanium White (Liquitex) paint and illuminated from below using a bright red LED, providing contrast from the other whiskers. High-speed videos were acquired at 500 fps with a 100 µs exposure and were synchronized with neural data acquisition via external triggers. Videos were processed in MATLAB using custom tracking software. An ROI was placed over the sector that the painted whisker swept out, cropping out other reflective surfaces (e.g. mouse's nose) that would otherwise interfere with tracking. All frames were luminance-thresholded to create a binary image, and the center of the painted region was calculated; the

angle between the center of the painted region and a user defined position on the face was calculated for all frames. Angle traces were created from these measurements to calculate the whisker kinematic features in Figure S2.1: set-point (median angle of envelope), amplitude (half-width of envelope), speed (distance/time), and frequency (cycles/second). The image of the PWCZ and the AWCZ in Figure 2.1 was created from tracking a mouse with a single row of whiskers illuminated from the top. The whisker traces were manually traced for display purposes only. It was not possible to detect contacts between the painted whisker and the stimulus bar, since only the base of the whisker was painted to avoid adding substantial weight to this whisker or altering its curvature.

Spike Sorting

16-32 channels of electrodes were amplified (AM Systems), filtered (0.1-5 kHz) and digitized at 30 kHz (National Instruments) using custom acquisition software (MATLAB, Mathworks). Spike detection was performed using the UltraMegaSort2000 package in MATLAB (Hill et al. 2011) (Mathworks). After detection, spikes were automatically sorted into clusters of units. Units were then further sorted manually to meet inclusion criteria and prevent pseudo-replication. Quality metrics included analysis of spike amplitude, spike rate, auto- and cross-correlation, inter-spike interval, outlier removal, distance from threshold, and cortical depth of largest waveform. With the exception of a small subset of fast-spiking or bursting units, included units had no more 1% of their individual waveforms violating a refractory period of 2.5 ms. The surround whisker trimming data was collected from 8 mice for the L5 RS population and 8 mice for the thalamus population. The principal whisker trimming data was collected from 8 separate mice.

Spike Waveform classification

Fast-spiking units were separated from regular spiking units using a k-means cluster analysis of two waveform components. One component was the normalized difference between the two positive-going peaks. The other component was the trough-to-peak latency of the large negative-going deflection. Fast-spiking units were categorized by a larger 2nd positive-going peak (positive difference), and a short (less than 0.33ms) trough-to-peak latency, following previously established approaches. Units on the border between the classification as FS or RS was excluded from analysis. FS neurons were excluded from the paper.

Trial inclusion criteria and layer boundaries

In sorted units, firing rates were computed by counting spikes in the final 500 ms of stimulus presentation. This window was chosen because within 1000 ms of the bar entering the whisker field, neuronal firing rates and behavior reached steady-state. Trials containing stimulation periods where the animal's mean run speed during the stimulus period dropped below 1.3 standard deviations of it population mean were excluded, to ensure consistency in whisking behavior across trials. In addition, trials where the standard deviation of an animal's run speed was more than 0.8 standard deviations from the population mean were excluded. Trials where the animal was not moving, thresholded by the animal's run speed being below 3 cm/s,

were completely excluded from analysis. The depth of each unit was assigned based on the calculated depth of the electrode on the linear array that exhibited its largest waveform. Layer boundaries were confirmed post-hoc using current source density analysis (CSD, Fig. S2.2) and labeling of the electrode track with a dye. CSDs were calculated from the trial-averaged local field potential (0.5 – 300 Hz) measured at each electrode contact, as previously published. We estimated the layer 4/5 boundary as the base of the current sink corresponding to layer 4.

Analytical Metrics

A *Trimming Index* for each condition was computed as the difference between the mean evoked firing rates during post-trimming (T) and control (C) conditions, divided by the sum of their mean evoked firing rates:

$$Trimming\ Index = \frac{T - C}{T + C}$$

The *Spatial Preference* of a neuron was determined by calculating the center of mass (CM) on the absolute value of its spatial tuning curves. FR, the mean evoked firing rate (or delta F) at position, P, at stimulus locations 1 through n:

$$Spatial\ Preference\ (CM) = \frac{FR_1 * P_1 + \ FR_2 * P_2 + \ldots + FR_n * P_n}{FR_1 + FR_2 + \ldots + FR_n}$$

Statistically significant changes in spatial preference at the level of single units was computed using a standard permutation test. For each unit, a null distribution of change in spatial preference was created by randomly sampling values among both conditions 5000 times. Significance ($p < 0.05$) was observed if the experimental effect was beyond the 97.5 percentile or below the 2.5 percentile of the null (two-tailed) distribution.

The relationship between the center and surround of the horizontal receptive fields of neurons was calculated as the difference between the max evoked firing rate (or delta F) in the PWCZ and the max evoked firing rate in the AWCZ divided by their sum.

$$Cent{:}Surr\ Index = \frac{\max(abs(PWCZ)) - \max\left(abs(AWCZ)\right)}{\max(abs(PWCZ)) + \max\left(abs(AWCZ)\right)}$$

The spatial selectivity of neurons was calculated from the normed (Euclidean) vector of the peak normalized spatial tuning curves. This value was then divided by square root of *n* dimensions – 1 to restrict its range from 0 to 1. Larger values signify higher spatial selectivity (lower broadness). Raw spike rates were used.

$$Spatial\ Selectivity = \ 1 - \left(\frac{\frac{||x||}{\max(x)} - 1}{\sqrt{n} - 1} \right)$$

Map analysis

Within each dataset, the centroids of all significantly driven and tuned ROIs were whitened and projected onto 1800 axes spanning from 0 to pi. The centroids of the ROIs were whitened to minimize spurious correlations derived from the structure of the ROIs sampled. A linear regression was computed between the projected location of the ROIs and their preferred positions (calculated over the entire tuning curve) for each axis. The axis of best fit was determined to be the axis whose linear regression had the largest r^2 value. This axis of best fit was then transformed into cortical space via the inverse of the whitening transform. The center of the axis was located to the center of the spared whisker column (as identified above) allowing for data across mice to be aggregated.

A Pearson's correlation was computed for the significantly driven and tuned neurons between their projected locations on the axis of best fit and their preferred positions, both before and after trimming. A linear regression was performed to compute the slope of that correlation. The mean pairwise correlation in tuning over the PWCZ (Pearson's R) was computed as a function of their pairwise difference of their projections along the axis of best fit and binned within 20 μm bins. Cumulative distribution functions were created by binning the location of the neurons along the projection into 18 equally sized bins. Only the central 8 bins, which had more than 145 neurons each (the expected value if the distribution of ROIs along the axis were uniform), are shown.

Quantification and Statistical Analysis

Statistically significant differences between conditions were determined using standard parametric or nonparametric tests in MATLAB, including a 1-way ANOVA, student's t-test, rank sum, and a Wilcoxon sign-rank test. Tests for normality were performed with a Lilliefors test. Units were defined as tuned for space if their evoked spike rate changed as a function of object position, determined by a 1-way ANOVA. Analysis of spatial preference changes was restricted to neurons that were significantly tuned for the stimulus both before and after trimming. The number of neurons that significantly changed their response per position was defined as neurons whose pre- and post-trimming response distributions were significantly different via a rank sum test. All "n" values are referring to the number of cells present in an analysis except when explicitly stated that the n is referring to the number of mice used.

For electrophysiology experiments, unless stated otherwise, analyses were performed from evoked spike rates. The spontaneous firing rate of a neuron in the 500 ms window preceding stimulation was subtracted from its firing rate of the last 500 ms of active touch, on a trial by trial basis. Neurons in L5 and the thalamus were classified as touch-facilitated or touch-suppressed. Touch facilitated neurons had a positive mean evoked spike rate in the principal whisker contact zone (PWCZ), while touch-suppressed neurons had a negative mean evoked rate in the PWCZ.

For two-photon calcium imaging experiments, analyses were performed on trial-wise dF/F. Analysis was limited to ROIs that met several criteria: they must be significantly driven by at least one stimulus, be larger than 50 μm^2, and for Figs. 2.2 and 2.3 have been within the principle whisker column. A significant response for a position had to meet two criteria: have a mean df/f greater than .2, and pass a t-test between the evoked responses at that position and the measured df/f values during control trials. The Benjamini & Hochberg false discovery rate correction was used to correct for the multiple comparisons taken across the multiple stimuli. Outlier responses per stimulus position were identified by the median rule, where values further than 2.3 times the inter-quartile range from the median are determined to be outliers, and were

removed prior to any analysis. Neurons were identified to be within the spared principle whisker column or to be in a surrounding column by using a custom MATLAB (Mathworks) algorithm to segment the pixels that exhibited a significant response post-trimming (t-test between control trials and the mean of PWCZ stimulus trials) which is putatively localized to the spared column (Fig. S2.2). The neural response for a single trial was calculated as the average df/f during the last 500 ms of stimulation.

SUPPLEMENTARY FIGURES

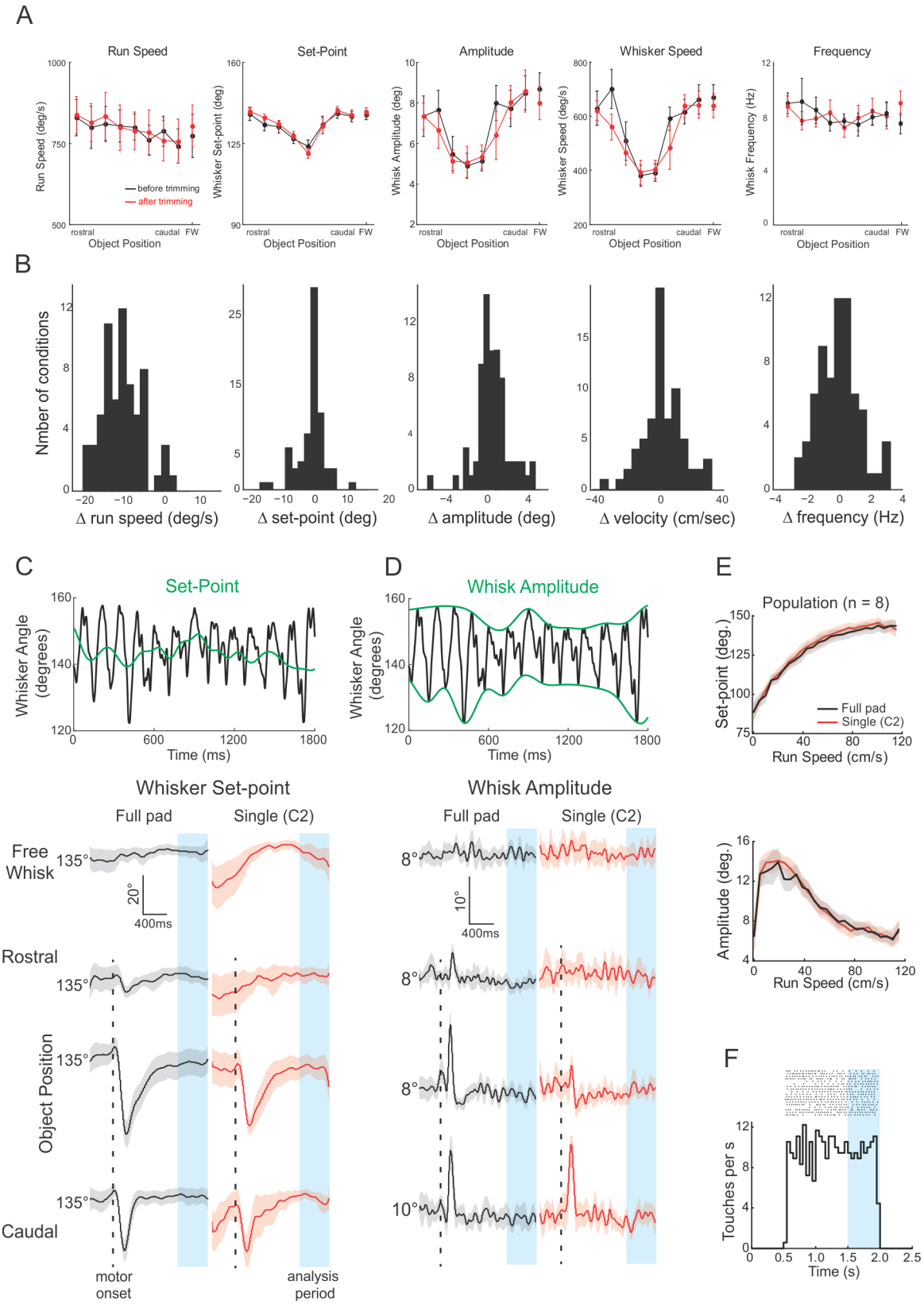

Supplemental Figure 2.1 Acute whisker trimming minimally impacts basic whisking kinematics

A) Plots from an example mouse of mean run speed, whisker set-point, amplitude, speed, and frequency for the C2 whisker against stimulus position before (black) and after (red) trimming all of the surrounding whiskers (mean ± 95% C.I.). FW: free whisking. B) Population histograms of change in the same kinematic variables as in A) (n = 8 mice, 9 conditions per mouse). For whisking kinematics, only a very slight, but significant change in amplitude was observed (0.93 ± 0.21 degrees, mean ± s.e.m), much smaller than the inter-stimulus spacing (10 - 15 degrees). C) Top: Example whisking trace with set-point (green line) overlaid. Whisker setpoint is the midpoint of the whisking envelope. Bottom: Average set-point of the tracked PW during free whisking and for three stimulus positions over the course of the trial. Shaded areas represent 95% confidence intervals. Cyan shaded area represents the analysis period. D) As in C) but for whisk amplitude. Whisk amplitude is defined as half the distance between the peak and trough of the whisking envelope. E) Mean (± s.e.m) whisker set-point (top) and amplitude (bottom) as a function of mouse run speed. Data are averaged across eight mice that were imaged once with their full whisker pad intact and then with only their C2 whisker intact. F) Top: raster plot of touches between the PW and the stimulus bar. Bottom: Average number of contacts per second the C2 whisker makes with the bar during a trial. Cyan shaded area indicates the analysis period.

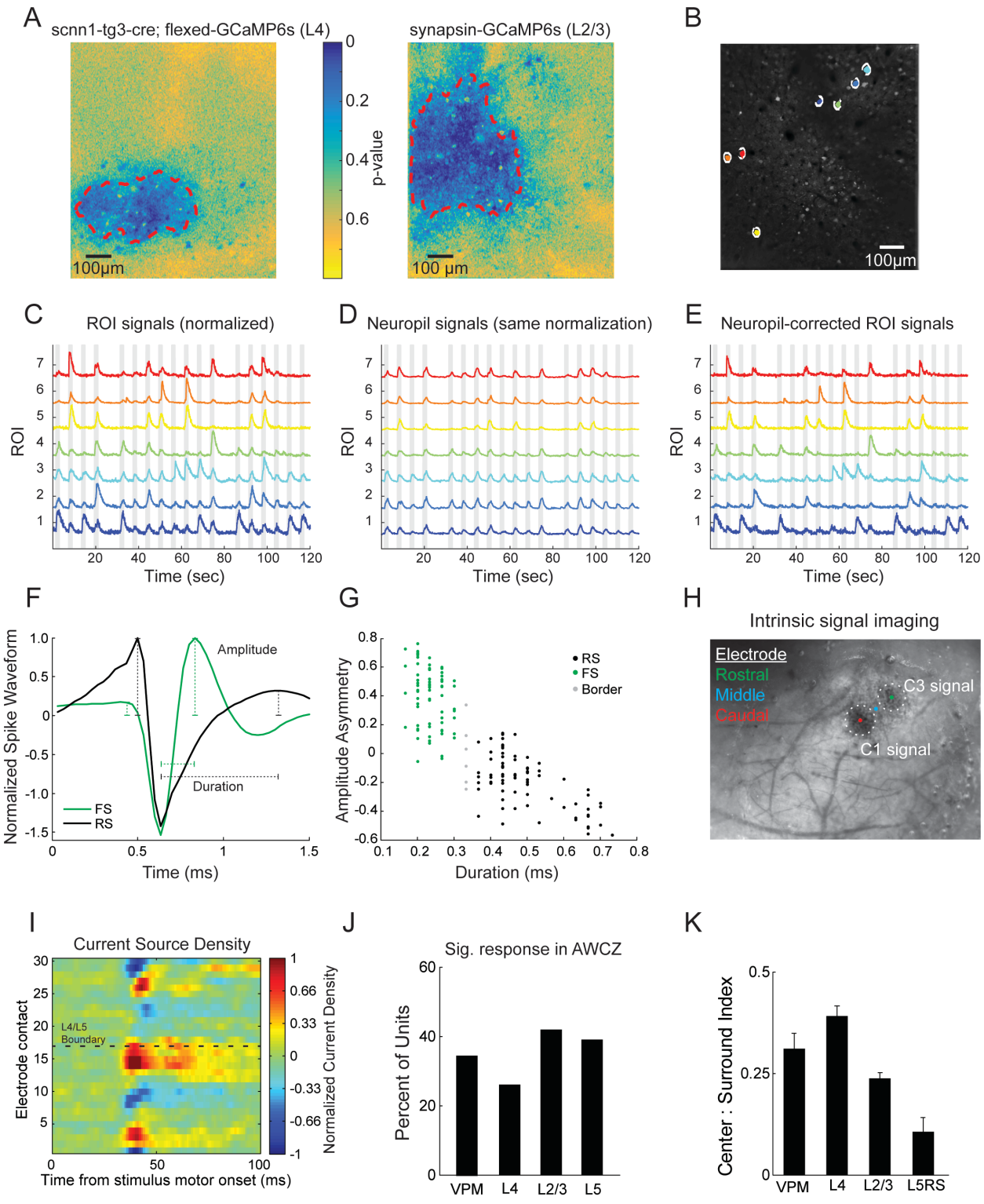
A
scnn1-tg3-cre; flexed-GCaMP6s (L4)
synapsin-GCaMP6s (L2/3)
p-value
0
0.2
0.4
0.6
100µm
100 µm
B
100µm
C
ROI signals (normalized)
D
Neuropil signals (same normalization)
E
Neuropil-corrected ROI signals
ROI
Time (sec)
F
Normalized Spike Waveform
Amplitude
Duration
FS
RS
Time (ms)
G
Amplitude Asymmetry
RS
FS
Border
Duration (ms)
H
Intrinsic signal imaging
Electrode
Rostral
Middle
Caudal
C3 signal
C1 signal
I
Current Source Density
Electrode contact
L4/L5
Boundary
Normalized Current Density
Time from stimulus motor onset (ms)
J
Sig. response in AWCZ
Percent of Units
VPM
L4
L2/3
L5
K
Center : Surround Index
VPM
L4
L2/3
L5RS

Supplemental Figure 2.2 Localization and unit identification methods and surround responses

A) Left: Example field of view (FoV) from L4 color coded by pixels that are significantly driven for PWCZ stimuli after trimming (computed via a t-test with control trials). An automated segmentation algorithm was applied to the images to produce the red dashed lines. ROIs whose centroids fall within or on the line are taken to be neurons located within the spared column. Right: same but for a FoV from L2/3. B) Mean FoV from one L2/3 mouse with 7 example ROIs and their corresponding neuropil ROIs overlaid. All pixels that are located within two or more ROIs are ignored from all ROIs. All pixels within any ROI are ignored from neuropil ROIs. C) Normalized fluorescence traces for the 7 ROIs from (B) captured during a series of stimulus presentations (gray bars). D) Fluorescence traces for the 7 neuropil ROIs from B) captured during the same time period as C) and normalized to the same value. E) Neuropil-corrected versions of the traces in C). F) Schematic of two example units, green: fast-spiking (FS), black, regular-spiking (RS), and criteria used for classification. G) Plot of amplitude asymmetry vs waveform duration for all L5 units in the study. Units are colored (green, FS, black, RS) according to cluster analysis. H) Example intrinsic optical signal overlaid on a picture of the cortical vasculature. Intrinsic signals were collected in anesthetized mice for the C1 and C3 whisker to identify the C row and location of the C2 whisker column. I) Example current source density from a laminar 32-channel multi-electrode array in the C2 column. The early sink (blue) in the middle layers correspond to L4. The dash line indicates the approximate L4/L5 boundary. Only units with their largest waveform on an electrode below this boundary were included in this study. J) Percent of units/cells in the VPM, L4, L2/3 and L5 that were significantly driven in the adjacent whisker contact zone (AWCZ) indicating they could be driven when only adjacent whiskers contact the stimulus. K) Center:Surround modulation index across VPM, L4, L2/3, and L5 showing a general trend towards a greater surround contribution across the conventional feed-forward circuit (mean ± s.e.m.).

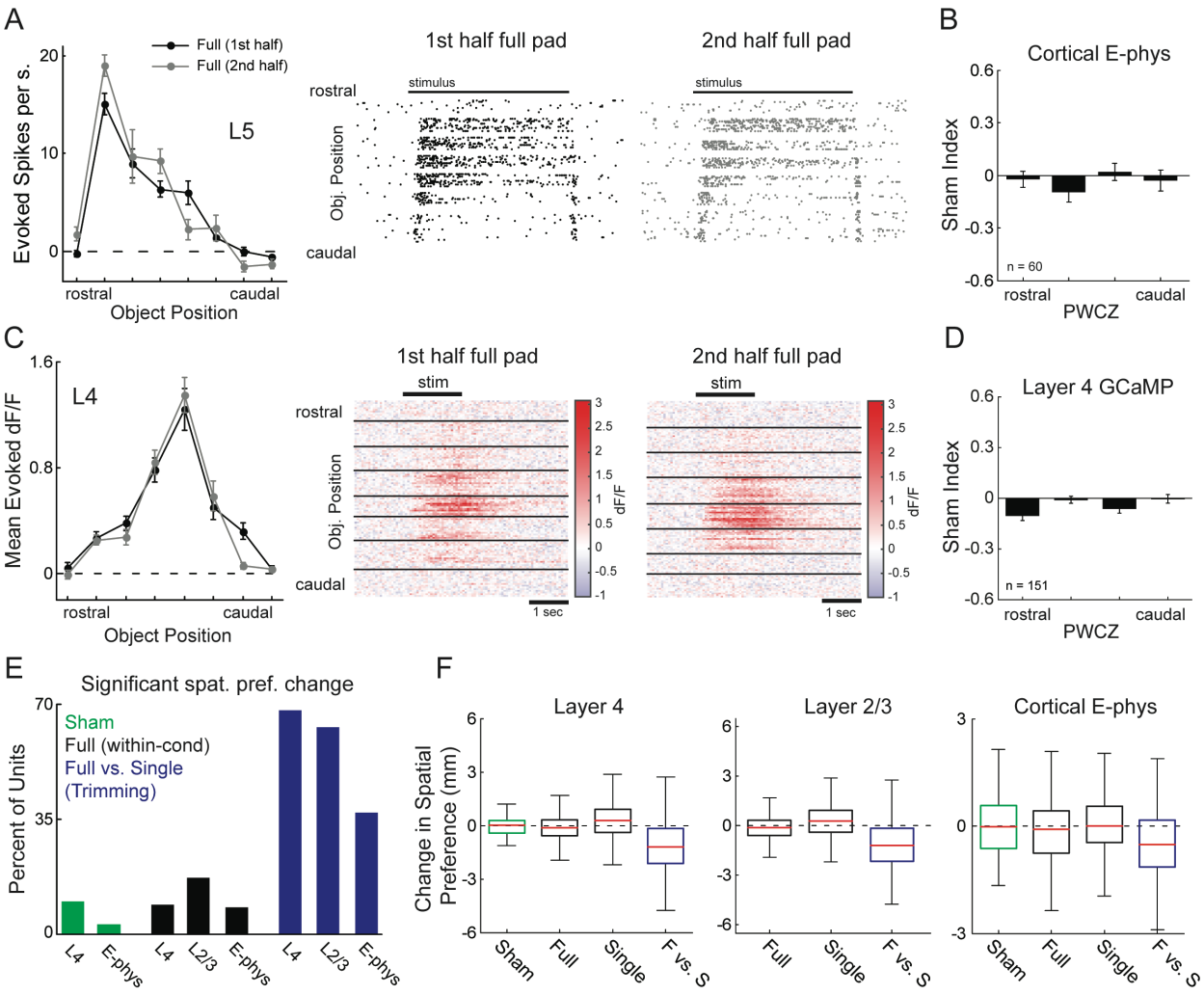

Supplemental Figure 2.3 Sham trimming and within-condition control tests show that spatial representations are stable over the recording duration.

A) Example spatial tuning functions (mean ± s.e.m) and raster plots of a unit before (black) and after (grey) the sham trim. Experimental time in each half is identical to the experiments in which the whiskers were actually trimmed. B) Sham indices (mean ± s.e.m) for data that were collected using electrophysiology (n = 60 units in 3 mice). C) & D) Same as A, B) except data was collected using two-photon GCaMP6s imaging (n = 151 ROIs in 1 mouse). E) Percent of individual units that displayed a significant shift in spatial preference using a permutation test with 5000 resamples (see methods). A small minority of units in the sham (green) and within-condition (black) data displayed a significant shift in spatial preference. In contrast, after trimming (blue bars), a large fraction of units displayed a significant shift in spatial preference. F) Boxplot illustrating the effect of sham trimming, within-condition consistency, and real trimming on the spatial preference of the neuronal populations. After sham trimming, no significant shift in the spatial preference of the population was observed (L4 GCaMP6s, n = 151, p = 0.3, paired t-test; E-phys, n = 28, p = 0.12, paired t-test).

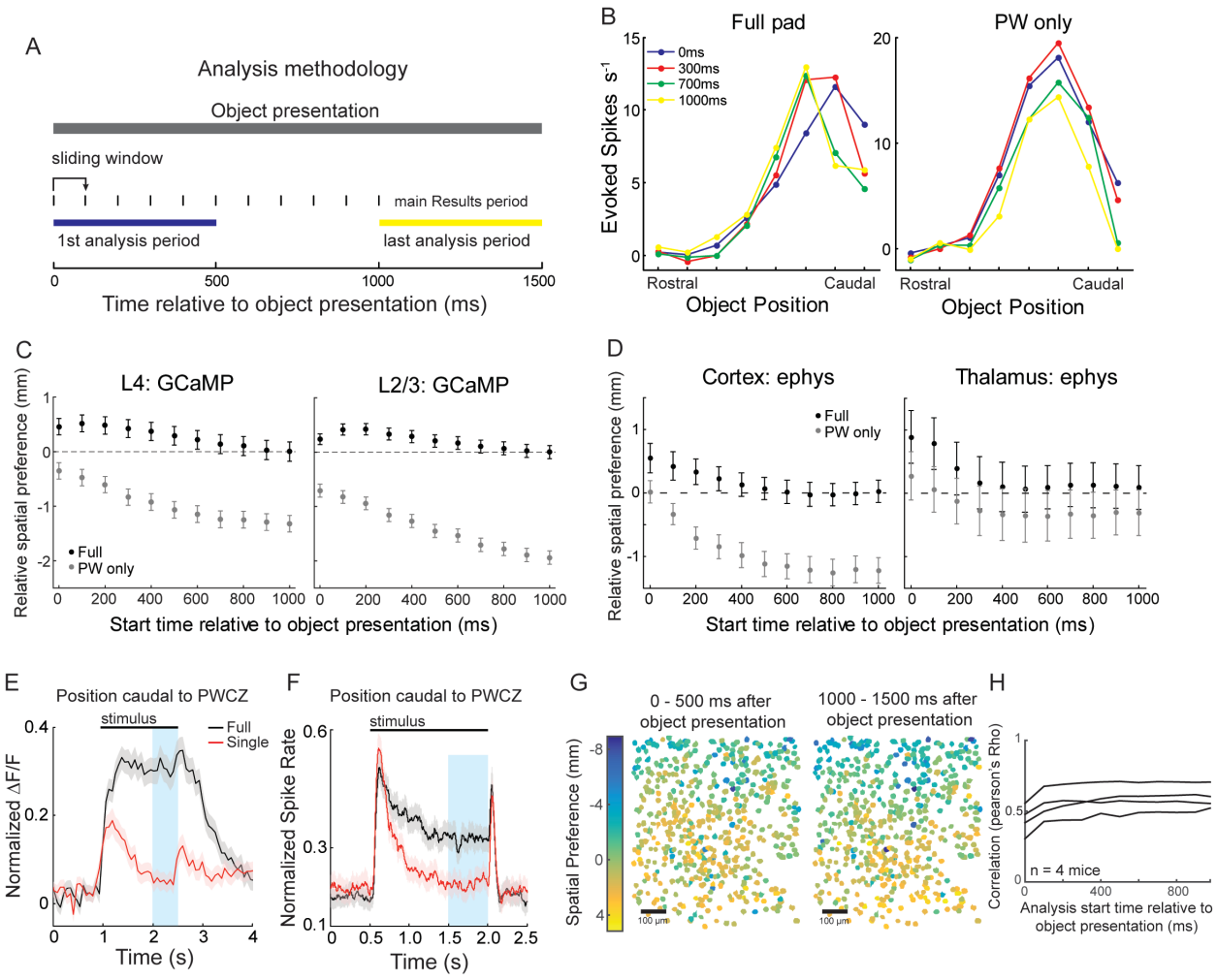

Supplemental Figure 2.4 Spatial preference stabilizes ~600 ms after stimulus onset

A) Diagram of the methodology used to determine the evolution of spatial preference over the time course of stimulus presentation. Eleven overlapping 500 ms windows were analyzed, starting 0 - 1000ms after object presentation. B) Example L5RS unit showing the slight progressive shift forward in spatial preference for the specified analysis start points. C) The evolution of spatial preference of the population using GCaMP6s imaging (mean ± 95% C.I.). Relative spatial preference is related to the analysis window used in the main Results section (starting 1000 ms after presentation). D) Same as C), except from data collected using electrophysiology in the cortex and the thalamus. E) Temporal dynamics of L4 population activity (n = 840 ROIs) for the stimulus position immediately caudal to the PWCZ. During the analysis period for the single whisker condition, activity returned to near baseline levels (mean ± 95% C.I.). F) Same as E, except for cortical electrophysiology population data (n = 190 units). During the analysis period for the single whisker condition, activity returned to a level indistinguishable from baseline. G) Maps of spatial preference in L2/3 that were calculated during the initial (0 - 500ms) and main Results (1000 - 1500) analysis periods. H) Pearson's correlation coefficient between the spatial preference and cortical location of the neurons along the axis of best fit across the analyzed time windows shown in A) for the 4 L2/3 mice in supplemental figure 7.

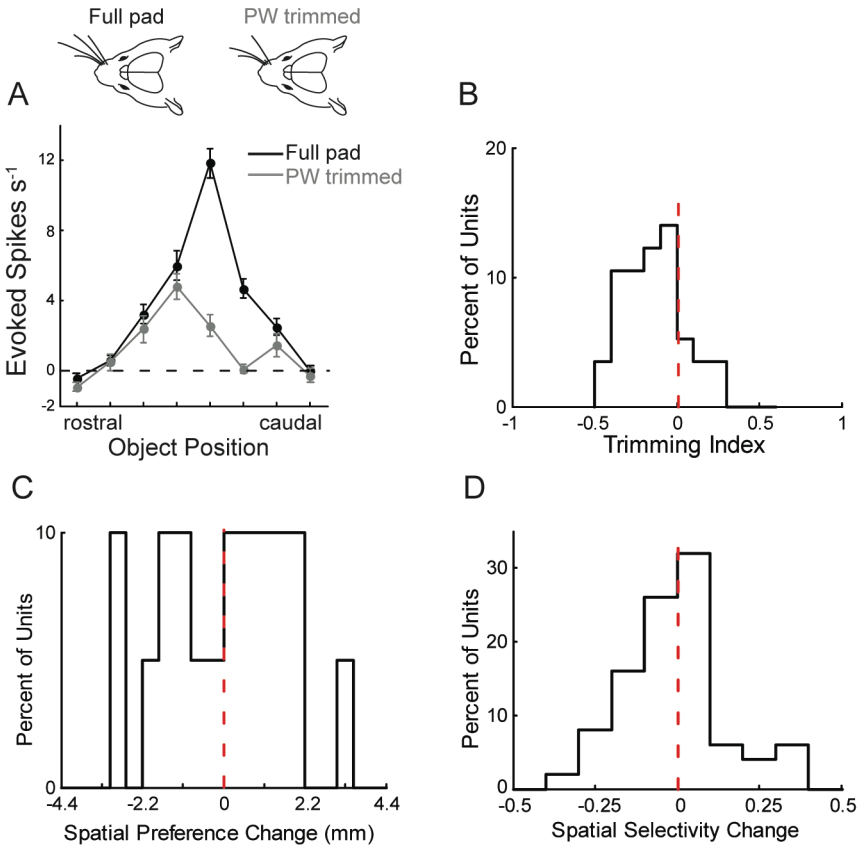

Supplemental Figure 2.5 Principal whisker contribution to spatial representations in L5 RS units facilitated by touch

A) An example spatial tuning curve (mean ± s.e.m.) of a L5 RS unit before (black) and after (grey) trimming the principal whisker. B) Histogram of the trimming index in touch-facilitated units (n = 36 units in 8 mice, $p < 0.001$, Wilcoxon. C) Histogram of the spatial preference change (n = 20 units, $p = 0.53$, Wilcoxon). D) Histogram of the spatial selectivity change (n = 50 units, $p = 0.003$, Wilcoxon).

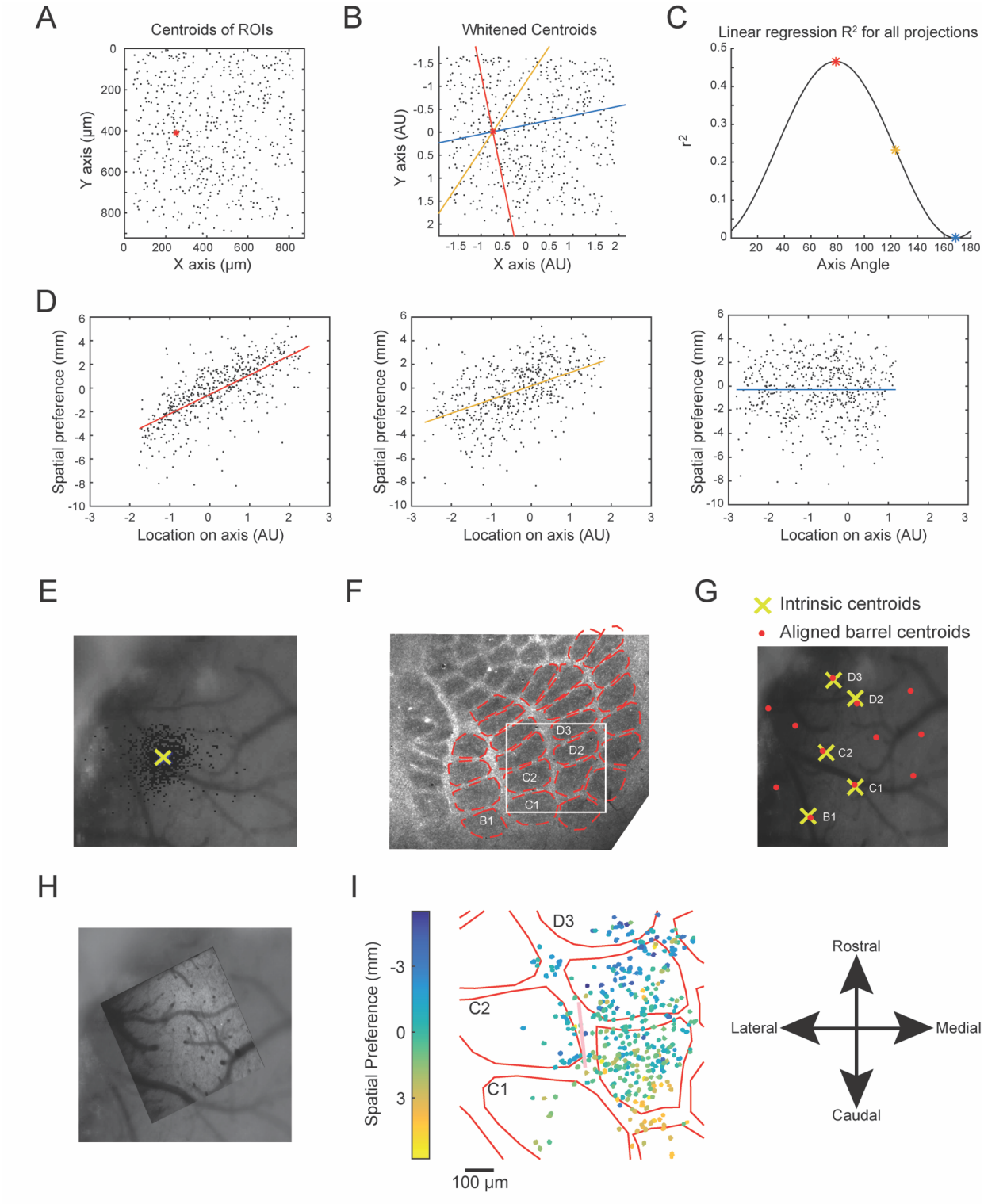
A
Centroids of ROIs
Y axis (µm)
X axis (µm)
B
Whitened Centroids
Y axis (AU)
X axis (AU)
C
Linear regression R² for all projections
r²
Axis Angle
D
Spatial preference (mm)
Location on axis (AU)
E
F
D3
D2
C2
C1
B1
G
Intrinsic centroids
Aligned barrel centroids
D3
D2
C2
C1
B1
H
I
Spatial Preference (mm)
D3
C2
C1
100 µm
Rostral
Lateral
Medial
Caudal

Supplemental Figure 2.6 Determining the map's axis and example map overlaid on underlying barrels

A) The centroids of all significantly driven and tuned ROIs in an example field of view. The center of the spared column (as identified in Fig. S2) is shown by the red asterisk. B) Same as in A) but the centroids have been whitened. Three example axes that were projected upon have been overlaid. C) The linear regression's r2 value between the neurons' preferred position and its projected location onto all 1800 axes tested. The r2 value of the example axes in B) are shown by corresponding asterisks of the same color. The red axis is the axis of best fit as the projection of the whitened ROI centroids produces the linear regression with the highest r^2 value. D) The spatial preference vs. the projected location of the given ROIs for the example axes in B), separated by their corresponding color. The linear regressions of the data are overlaid. E) Example thresholded intrinsic optical signal resulting from deflecting the C2 whisker registered to an image of the cranial window for a 4.3 Thy1-GCaMP6s mouse (JAX). The yellow x marks the center of the two-dimensional Gaussian fit to the intrinsic signal. F) Cytochrome oxidase staining of the barrels in tangential sections from same mouse as in E). G) The centroids of the Gaussian fits to the intrinsic optical signals for the stimulated whiskers are shown as yellow x's. The centroids of the barrels as determined from the histology were registered to the intrinsic signals via an affine transform and are overlaid in red. H) Image of the vasculature directly above the two-photon imaging field of view overlaid on the image of the cranial window. I) The outline of the underlying L4 barrels are overlaid on the L2/3 map of the same mouse.

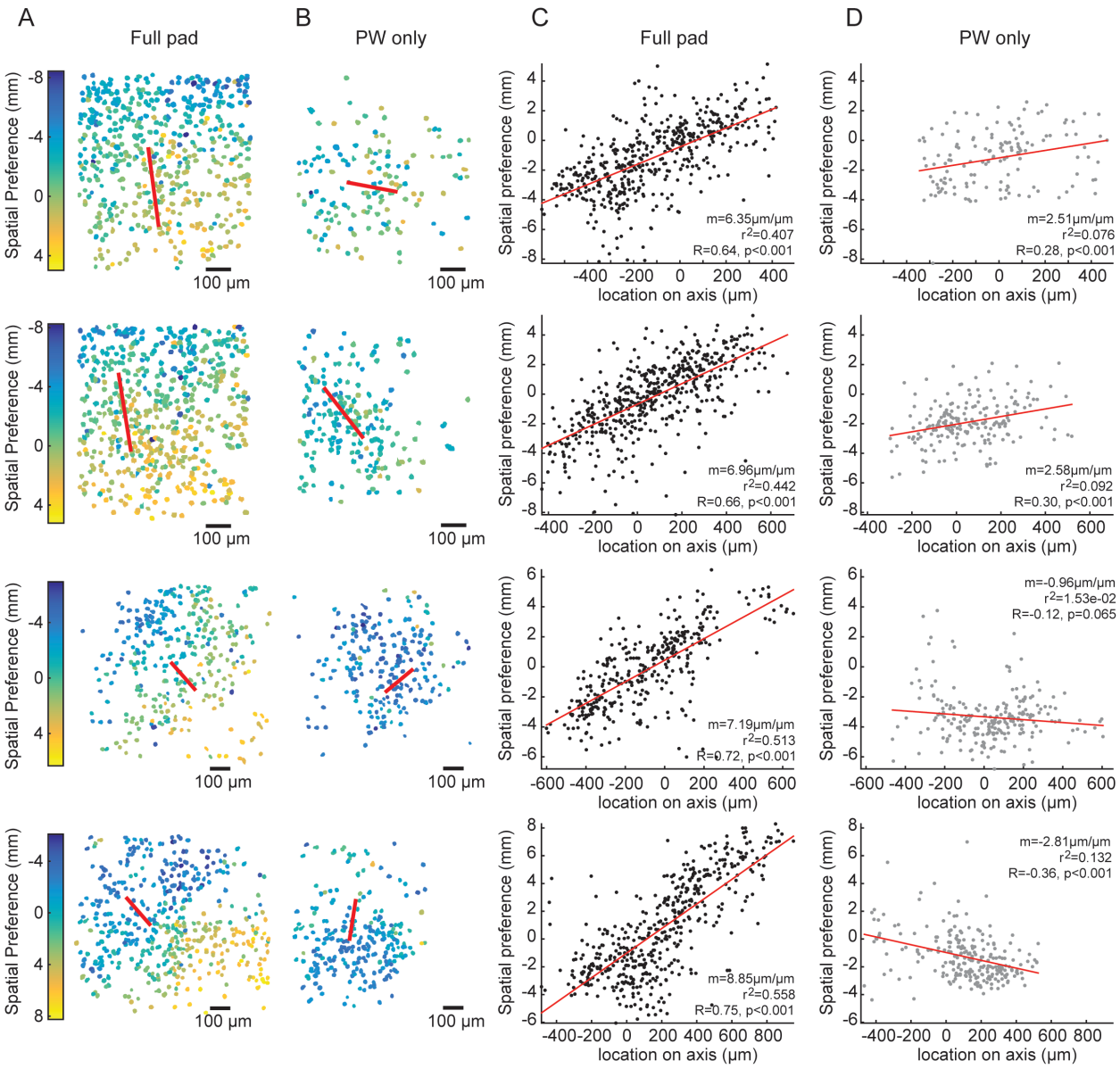

Supplemental Figure 2.7 Four L2/3 maps of scanned space

A) Fields of view (FoVs) from four L2/3 mice showing significantly driven and tuned ROIs colored by the center of mass of their pre-trimming tuning curve. The axis of best fit (see Methods & Fig. S9) between location on that axis and spatial preference is overlaid in red and centered on the spared column. B) Same FoVs as A) but for data acquired post-trimming. C) Scatter plots of spatial preference to location along the axis of best fit for the four FoVs and ROIs in A). A linear regression was performed and its slope (m) and coefficient of determination (r^2) are presented. A Pearson's correlation was also performed, and its correlation coefficient (R) and significance value (p) are also presented. D) Same analysis as C) but for the post-trimming data presented in B).

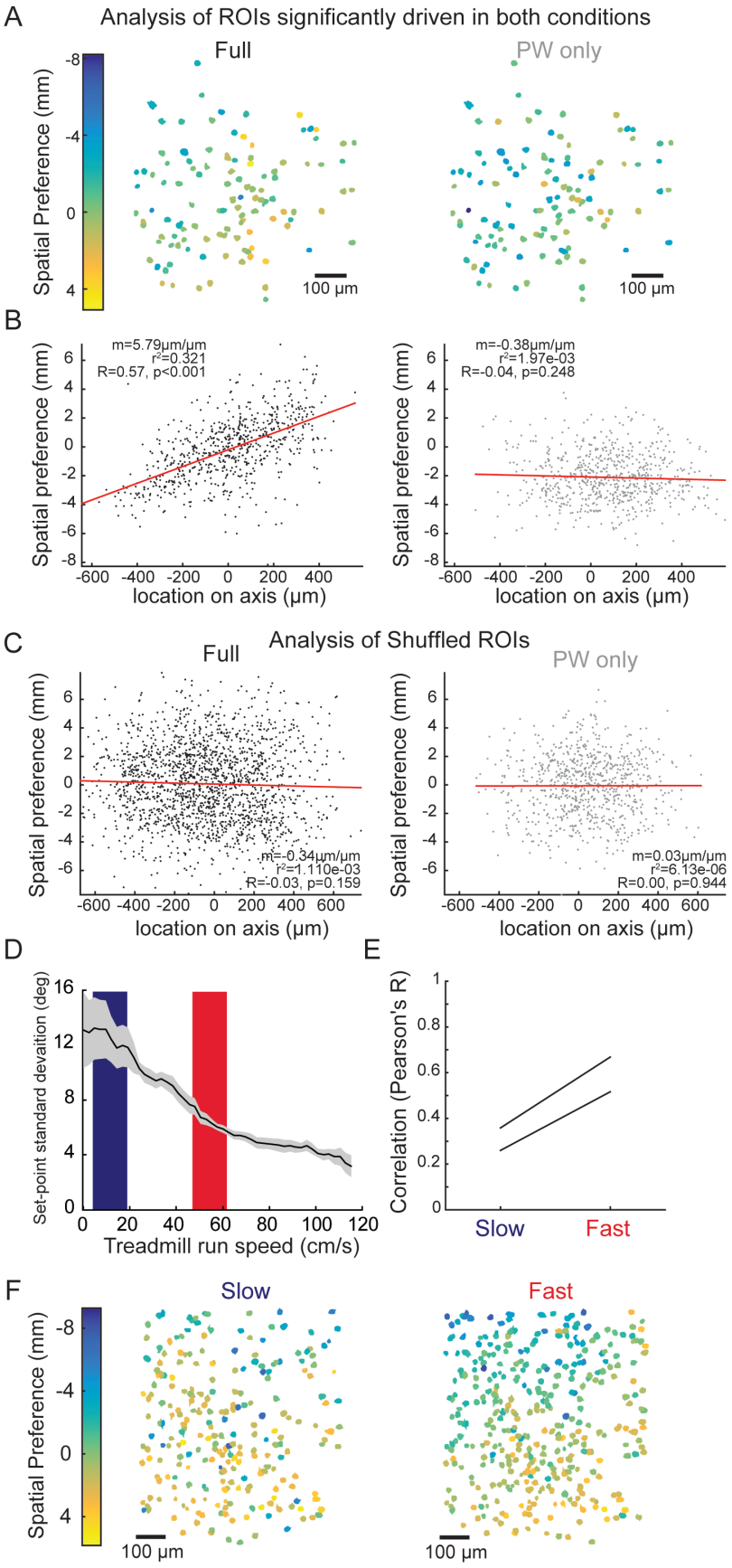

Supplemental Figure 2.8 L2/3 map produced via multi-whisker integration is not a result of sampling, chance, or behavioral variability

A) Example maps from mouse shown in Fig. 6, but now limited to only the ROIs that are significantly driven and tuned both before and after trimming. B) Scatter plot of preferred position to location along the axis of best fit before trimming for all ROIs significantly driven and tuned both before and after trimming across all 4 mice. Same analysis as D) but for data acquired after trimming. C) Same scatter plots as those presented in Fig. 6 but presented after randomly shuffling spatial preference across ROIs within each FoV. F) Same shuffle as in E) but for data after trimming. D) Plot of the standard deviation of whisker set-point as a function of run speed (mean ± s.e.m.). Note the standard deviation of the whisker set point decreases as the run speed increases. Trials from two different bins of run speed (blue: slow, and red: fast) were used in the subsequent analyses. E) The Pearson's correlation value calculated for the slow and fast run speed bins for two mice. Note the map correlation is higher at higher run speeds where the whisker set-point is less variable. F) Example maps generated for a single mouse when the trials are restricted to slower run speeds (left) and faster run speeds (right).

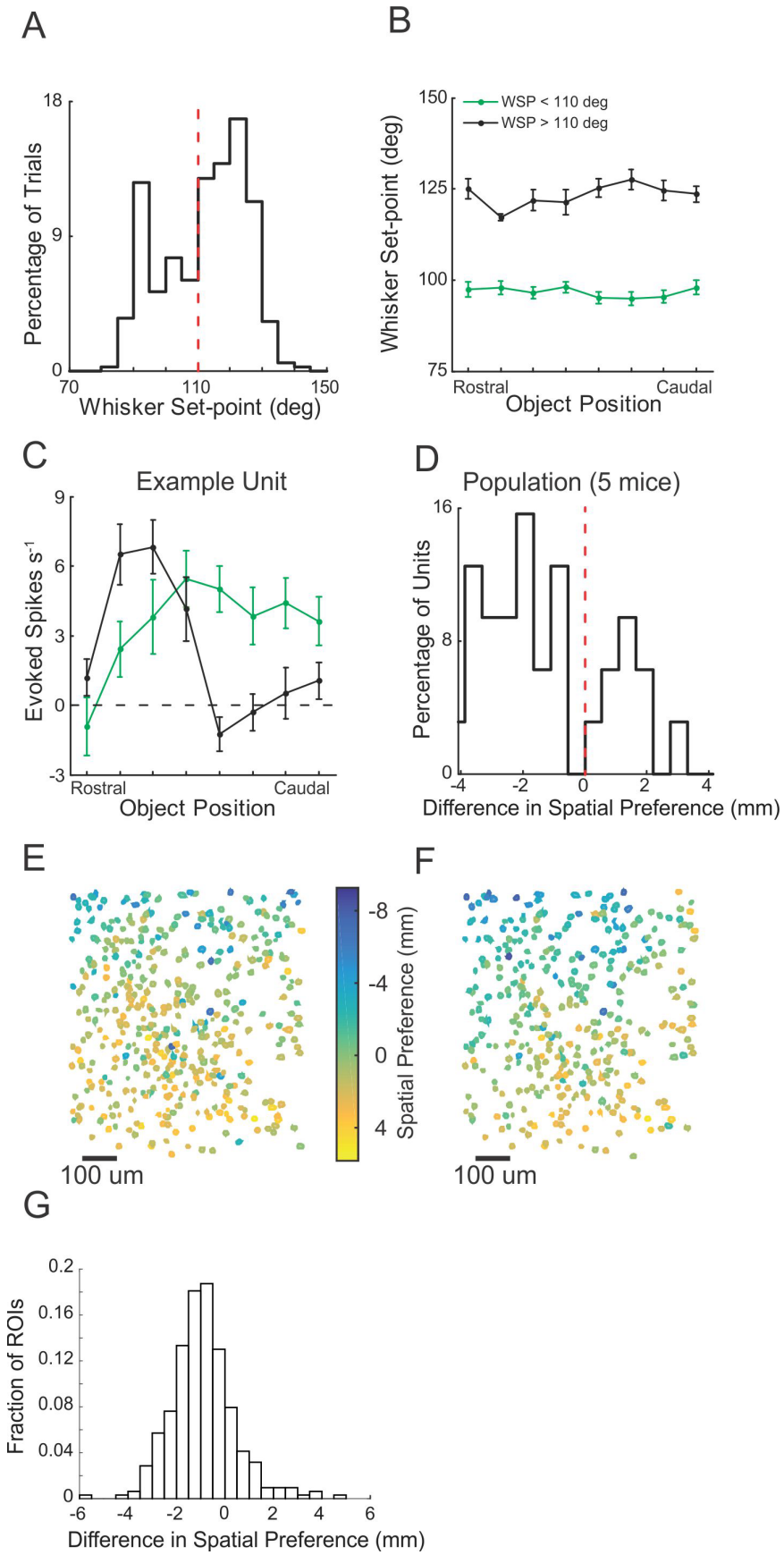

Supplemental Figure 2.9 The map of spatial preference in L2/3 depends on whisker set-point

A) Distribution of whisker set-points for an example mouse across all (n = 360) trials in an experiment. The trials were arbitrarily divided into two groups with a dividing line of 110 degrees. B) Mean (± s.e.m.) whisker set-point as a function of object position for the low and high whisker set-point group. C) Example spatial tuning curves from a unit in S1 created from trials less than 110 degrees (green) or greater than 110 degrees (black) (mean ± s.e.m.). D) The difference in each neuron's spatial preference between the two groups (protracted spatial preference minus retracted spatial preference). A negative value indicates that a neuron's spatial preference was more rostral for trials containing more protracted (> 110 deg.) whisker set-points. E) Example two photon map in L2/3 of spatial preference for slow running trials. F) As in E), but for faster running trials. G) As in D) but for the two photon imaging data (fast spatial preference minus slow spatial preference).

CHAPTER 3

THE LOGIC OF CORTICAL SUMMATION DURING ACTIVE SENSATION

FOREWORD

The next chapter involves unpublished work I completed during the second half of my doctoral research. This project worked to uncover how neurons in different cortical layers integrate information across whiskers during active sensation at the single whisker level. This involved developing a novel tactile display using pneumatic pistons that can stimulate an arbitrary combination of five whiskers during active whisking. I acquired all two-photon calcium imaging and high-speed whisker tracking data, and performed all the analyses. Dr. Scott Pluta performed electrophysiology recordings and spike sorting that is not presented here. Professor Hillel Adesnik oversaw and guided this work. After further revision, this work will be submitted for peer review, where it is sure to undergo even further revision.

Lyall, E. H., Pluta, S. R., & Adesnik, H. The logic of cortical summation during active sensation. *In preparation.*

SUMMARY

Cortical neurons could summate over sensory space to encode complex features of a stimulus. In most cases, however, sensory stimulation outside a cortical neuron's receptive field suppresses its firing rate divisively, controlling gain rather than generating higher order feature selectivity. We re-examined this question in awake animals involved in active sensation, hypothesizing that in more ethological conditions the logic of cortical summation might favor the synthesis of new coding properties. We took advantage of the discretized and active nature of the rodent whisker system to probe how somatosensory cortical neurons summate over sensory space using multiphoton imaging across the layers of the somatosensory cortex. During active sensation, the majority of barrel cortex neurons summed specific combinations of inputs supra-linearly to give rise to a sparse, but complete code of second order tactile stimuli. Input-specific supra-linear summation might generally support higher order feature coding in natural contexts, such as active sensation, and could contribute in non-sensory cortical areas to selective encoding of cognitive variables such as value.

INTRODUCTION

Primary sensory cortical neurons encode diverse features of sensory stimuli. By integrating inputs within their receptive fields, cortical neurons can extract local features of the sensory scene (Hubel & Wiesel 1959). By integrating inputs beyond their receptive fields, cortical neurons could extract more global sensory features, such as contour and shape, which may be critical for object identification. Local summation is exemplified by primary visual cortical neurons, which extract stimulus orientation by linearly summing specific combinations of spatially offset thalamocortical inputs within their receptive fields (Hubel & Wiesel 1962). Global summation, however, is typically found to be highly sub-linear: stimulation beyond the receptive field typically suppresses firing rates, often divisively (Adesnik & Scanziani 2010; Adesnik et al. 2012). Although divisive suppression can improve information coding and efficiency, supra-linear summation could represent a powerful means for cortical neurons to compute and selectively encode second order features of sensory stimuli.

Most studies of global summation have been conducted in anesthetized, paralyzed, or fixating animals. These experimental constraints are typically needed so that the spatial features of the sensory stimulus can be tightly controlled by eliminating volitional motion of the sensors. However, in many conditions sensation is active: we scan our eyes or our hands to identify and localize objects by sight or by touch. We asked whether in an active sensory system cortical neurons might summate specific sensory inputs supra-linearly in order to encode higher order features of the stimulus. We took advantage of the mouse whisker system, which is both discretized and naturally active, to probe this question in a condition that still provides tight experimental control. We developed a novel tactile stimulator for head-fixed, whisking mice, and used large-scale calcium imaging to probe how summation over discrete whisker/touch combinations might give rise to population codes of second order haptic features. We further imaged principal neurons across three layers of the barrel cortex to monitor how summation and feature selectivity evolved across the cortical axis. Many cortical neurons summated input from specific combinations of 2-4 whiskers highly supra-linearly. In individual neurons, supra-linear summation engendered high selectivity for specific combinations. Across neural populations, stimulus preference of second order features covered the entire presented stimulus space. These properties of the population code for haptic features were much less pronounced when the whiskers were stimulated passively in anesthetized animals. Thus, supra-linear summation during active sensation might be a general mechanism by which cortical neurons compute higher order stimulus features that contribute to haptic perception.

RESULTS

Quantifying multi-whisker integration during active sensation

We probed tactile coding in the mouse barrel cortex with two photon calcium imaging. To investigate the logic of summation over the whisker array during active sensation we developed a novel paradigm for reliably generating active touch between a user-defined set of whiskers and a corresponding set of pneumatic actuators. Awake mice were head-fixed on a rotary treadmill and habituated to run at a speed in which they moved their whiskers in a rhythmic and stereotyped fashion for many minutes at a time (Figure S2.1). A set of up to five pneumatically controlled pistons was presented to precise locations and in all 32 possible combinations, ensuring that on each trial the corresponding set of whiskers made repeated active touches with the presented set of pistons. Under these conditions we sampled excitatory neuron activity from cortical layers 2/3 (L2/3) and 4 (L4) with GCaMP6s (see Methods, Fig. 3.1A). On each trial the pistons entered the whisking field within one whisk cycle (~4 ms to target position from entering the whisking field). High speed imaging and slight trimming of the whiskers ensured that only one whisker made contact with each piston (Fig. 3.1A). Two example trials with corresponding video frame and whisker tracking is presented in Figure 3.1B. Looking at the bottom trial, only the C2, C1, and gamma whisker were targeted with pistons, and each whisker made 10 to 16 absolutely selective contacts with its respective piston (Fig. 3.1B). During this trial 66/588 neurons showed a dF/F increase greater than 0.2 (Fig. 3.1D)., the expected fluorescence change of GCaMP6s for one spike (Chen et al. 2013).

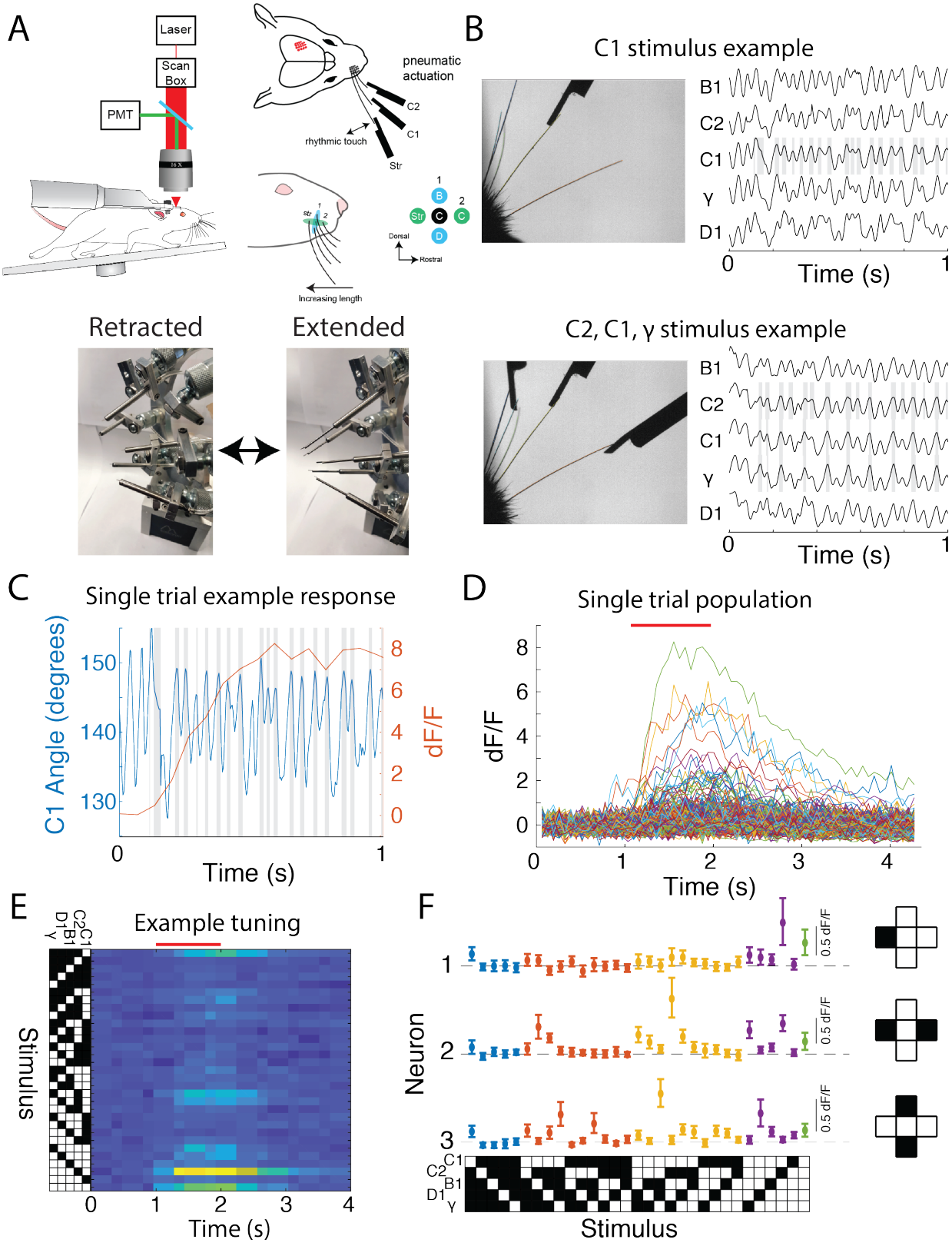
A
Laser
Scan Box
PMT
16 X
pneumatic actuation
C2
C1
rhythmic touch
Str
Dorsal
Rostral
Increasing length
B
C1 stimulus example
B1
C2
C1
γ
D1
0
1
Time (s)
Retracted
Extended
C2, C1, γ stimulus example
C
Single trial example response
C1 Angle (degrees)
dF/F
Time (s)
D
Single trial population
dF/F
Time (s)
E
Example tuning
Stimulus
Time (s)
F
Neuron
0.5 dF/F
Stimulus

Figure 0.1 Tactile display experimental setup
A) Top left: mouse is head-fixed under a two-photon microscope and over a circular treadmill. Top right: all but the C2, C1, B1, D1, and gamma whiskers are trimmed off. The remaining whisker lengths are trimmed in a staircase pattern such that each whisker only makes contact with one pneumatic piston, and contact occurs at the peak of the protraction cycle. Bottom: pictures of pneumatic piston with all pistons retracted and all pistons extended. B) Still frames from high speed whisker tracking and corresponding whisker angle traces for two example trials. Top: only the C1 whisker is stimulated. Bottom: the C2, C1, and gamma whiskers are stimulated. Touch events for each whisker is overlaid on the whisker angle traces as shaded boxes. C) The dF/F of the best responding neuron is overlaid with the C1 whisker angle trace and touch events shown in B top. D) dF/F traces of all 588 neurons recorded during the example trial presented in B top are overlaid. E) A raster plot of the average response to each stimulus for an example neuron. F) Left: three example tuning curves for the entire presented stimulus space. Right: diagram of preferred stimulus for each neuron.

Single whisker tuning is more clustered and selective in L4 than L2/3

We presented all 32 possible combinations of the five pistons to probe how barrel cortex neurons encoded first and second order tactile features. 43% of identified neurons showed a significant response to at least one of the 32 stimuli and will be referred to as driven neurons. When the pistons were presented individually to map the 'receptive field' of each neuron, 60% of driven neurons in L4 exhibited a significant response to just one whisker, 3% responded to 2 or more, and 37% did not respond any single whisker, although these neurons responded robustly to at least one multi-whisker combination (Fig. S3.1C). This compares to L2/3 where 45% of driven neurons were selective for one whisker, 10% were multi-whisker, and 45% were not driven by any single whisker.

To determine how well single-whisker neurons clustered, and therefore reflected the underlying barrel architecture, we performed a silhouette analysis in the layers where we performed calcium imaging (Fig. S3.2B; Methods). A silhouette value of 1 says a neuron is perfectly clustered, while a value of -1 says it is in the wrong cluster. A value of 0 is obtained when the cluster centers overlap. L4 neurons were significantly more clustered than L2/3 neurons as shown by L4 having a mean silhouette value of 0.10 ± 0.02 as compared to L2/3's -0.04 ± 0.01. This is consistent with anesthetized experiments that have shown L4 whisker selectivity to match the well-known whisker topography with passive stimulation (Brecht & Sakmann 2002). L2/3 neurons also exhibited topography, but with much greater hetereogeneity, also consistent with prior measurements, demonstrating that the basic topographic features of whisker representations in the barrel cortex did not differ between passive stimulation and active sensation (Clancy et al. 2015; but see Fig. S3.2C).

Many cortical neurons exhibit supralinear summation to at least one multi-whisker combination

In previous recordings from barrel cortex neurons in which whiskers were passively stimulated (and in analogous studies in the visual or auditory cortex), stimuli presented outside a neuron's receptive field typically suppressed the response to stimulation of the receptive field alone, a form of contextual modulation often termed 'surround suppression'. We observed a strikingly different type of modulation under our conditions. In 67% of driven L4 neurons and 84% of driven L2/3 neurons, at least one combination of pistons presented to surround whiskers potently summated supralinearly than what would be expected by the linear sum. In the first representative example neuron in Figure 3.1F, the neuron responds solely to the C1 stimulus with

respect to the single-whisker stimuli, but responds far more strongly when the C1, B1, D1, and gamma whiskers were all stimulated in combination. Contrary to the phenomenon of surround suppression, stimulation of whiskers beyond its receptive field (i.e., beyond the C1 whisker) facilitated, rather than suppressed the response to the principal whisker. Remarkably, this facilitated response was highly selective in that most other combinations of pistons had a weak or no effect on the neuron's activity, giving rise to a highly selective response for this specific four-whisker stimulus.

If many other neurons were to show similarly strong and selective responses for various combinations of whisker touches, with different neurons encoding all possible combinations, barrel cortex could contain a sparse, but complete code of second order tactile features. To answer this question we analyzed the stimulus tuning of 3897 imaged neurons in L2/3 and 2428 imaged in L4. Several additional representative examples of neurons exhibiting high selectivity for a specific multi-whisker stimulus and strong supra-linear summation are presented in Figure 3.2A. Across the population of responsive neurons in L2/3, 46% showed a maximal evoked response to a multi-whisker stimulus whose amplitude was strongly under-predicted by the linear sum of the responses to the individual whiskers (Fig. 3.2B). These data indicate that nearly half of barrel cortex neurons supra-linearly summate a specific subset of surround whisker touches to respond strongly and selectively to one or a small number of tactile features in whisker space. Across the population, neurons exhibiting a least one supra-linear response showed a slightly higher degree of stimulus selectivity (0.39 ± 0.00) compared to neurons that only showed linear or sub-linear summation (0.36 ± 0.01; Fig. 3.2D). The best stimulus response for each neuron always contained the principal whisker, when one was identified, demonstrating that it was required for the preferred supra-linear response.

Population of cortical neurons exhibit a sparse and complete code

We next probed whether barrel cortex neurons (within a 1.2 x 1.2 mm field of view) encoded all 32 possible piston combinations within the five piston stimulus set, thus covering the stimulus space, or if instead specific combinations were strongly over-represented. We found that across the population of imaged neurons all 26 multi-whisker stimuli were represented approximately evenly (Fig. 3.3). On average, each of the 26 stimuli was the preferred response for **3%** of the responsive neurons. This demonstrates that barrel cortex has the ability to encode all possible second order tactile stimuli in the five whisker space we probed. Comparing the stimulus selectivity and deviance from linear summation from each neuron side by side (data not shown) reveals that the population code for multi-whisker stimuli correlated well with supra-linear summation for the most preferred stimulus. This supports the idea that stimulus-specific supra-linear summation over surround whiskers helps promote a sparse and selective code for second order tactile features.

Since our observations of surround facilitation and supra-linear summation contrast markedly with prior studies using passive whisker deflection, we executed an analogous set of experiments in lightly anesthetized mice with passive whisker stimulation while imaging neurons in L2/3. We simulated active touch for each of the 32 whisker stimuli for non-whisking mice using a set of five piezo actuators. Under these conditions, 41% of neurons showed supralinear summation, as compared to the 84% of neurons when the mouse was awake. In nearly all cases (74% of all combination stimuli), surround whisker stimuli suppressed the response to stimulation of the PW alone.

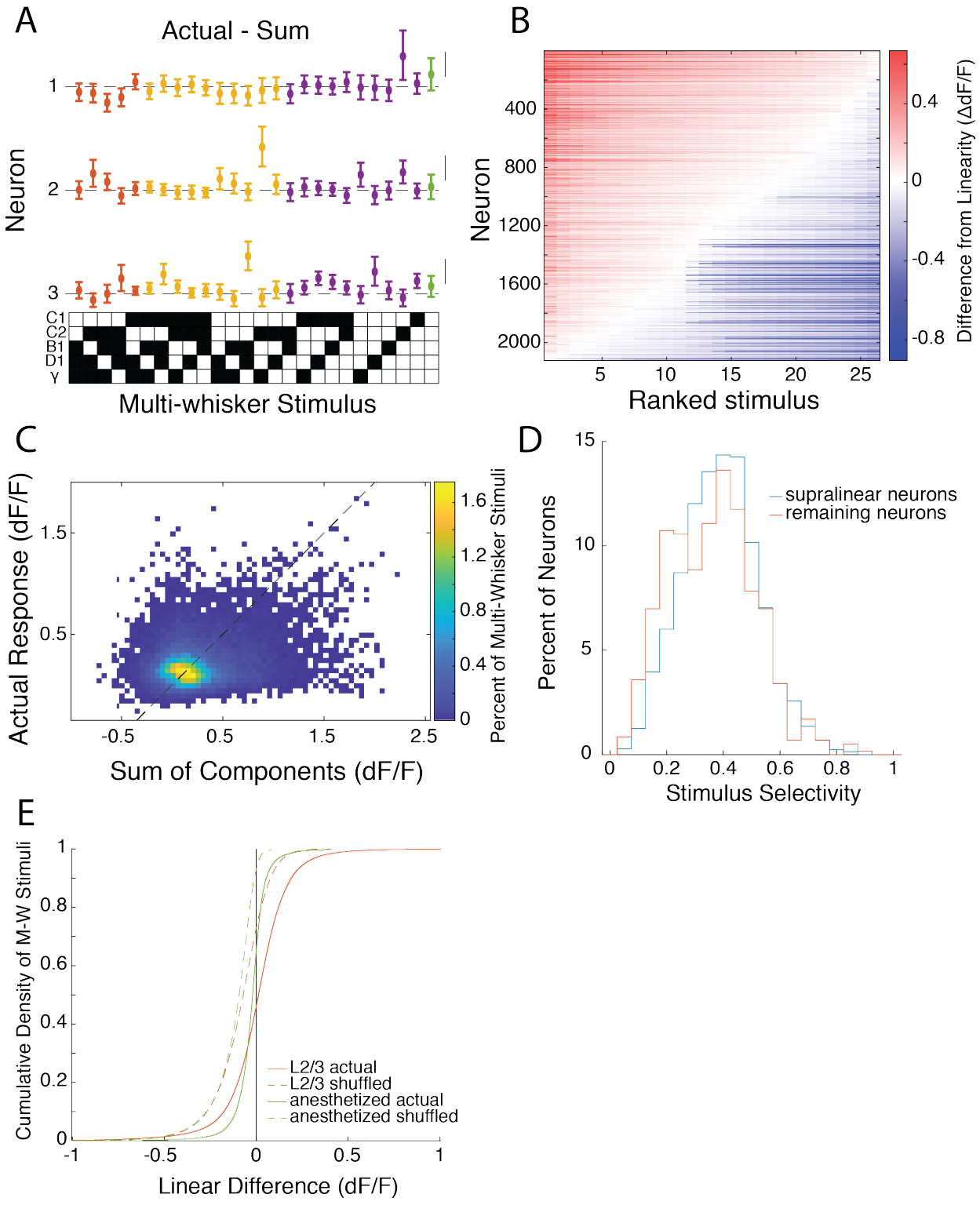

Figure 0.2 Many neurons summate specific whisker combinations supralinearly

A) The difference between the observed response and the sum of the component responses are shown for all multi-whisker stimuli for three example neurons. Error bars are bootstrapped 95% confidence intervals. B) The linear difference for all multi-whisker stimuli of all L2/3 neurons are shown. X axis is rank ordered, while Y axis is

ordered by the number of stimuli whose linear difference is positive. C) 2D histogram of the actual response vs the sum of the components for all significant stimulus combinations for all L2/3 neurons. D) Histograms of stimulus selectivity for neurons that significantly supralinearly summate at least one combination vs neurons that don't. E) Cumulative density plots for the linear difference of all multiwhisker combinations of all L2/3 neurons. Awake mice have more supralinear responses than anesthetized mice, though both exhibit some supralinearity greater than chance.

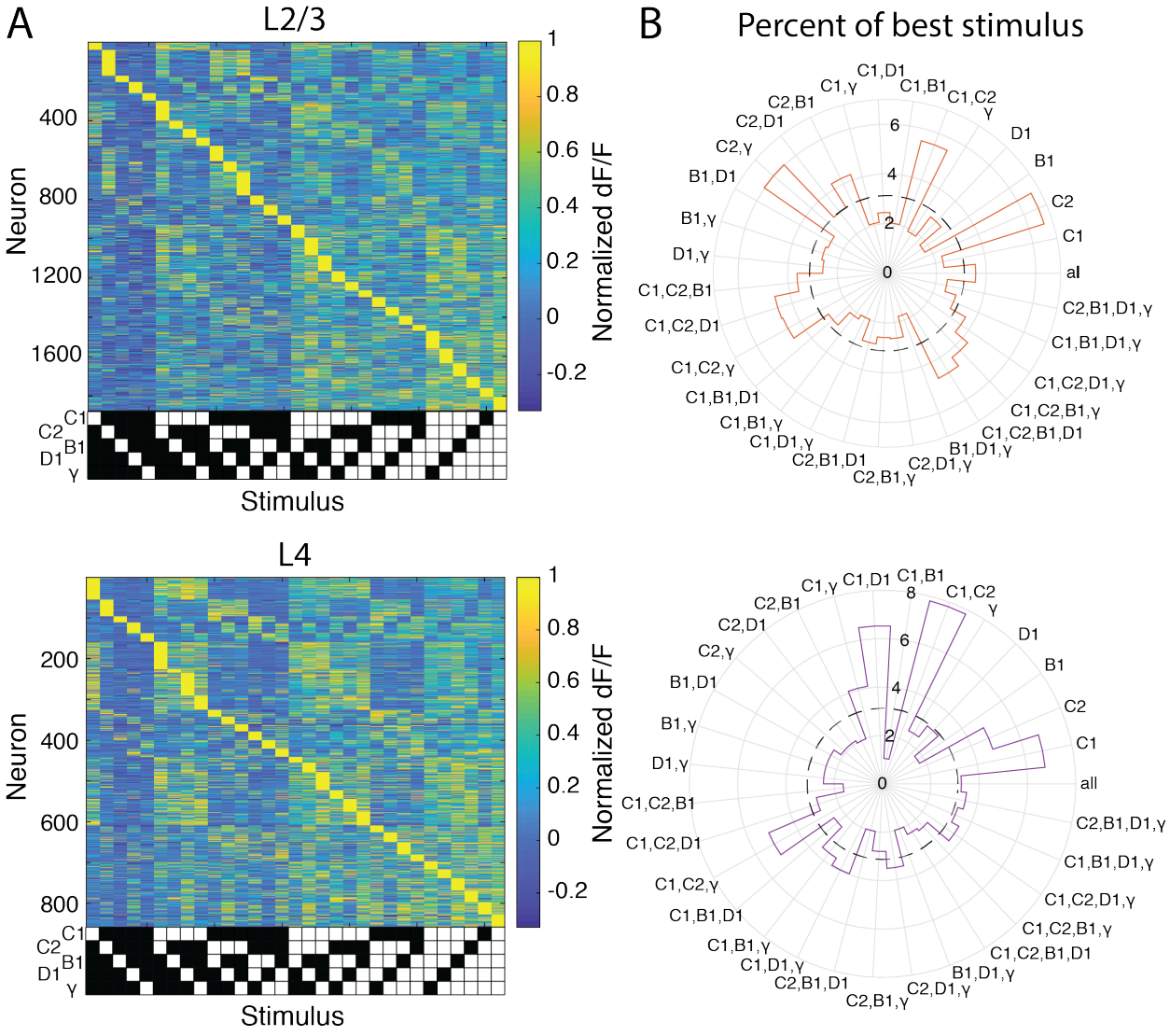

Figure 0.3 Population of neurons encode the entire stimulus space
Top: L2/3 data; Bottom: L4 data. A) Normalized tuning curves for all neurons, showing that every stimulus is encoded by the population. B) Radial histogram of the neurons' preferred stimulus. Dotted line is what would be expected for a uniform distribution.

DISCUSSION

Our data show that the logic of spatial summation during active sensation in the barrel cortex is strikingly different from that typically observed in the somatosensory, visual or auditory cortices during passive sensory stimulation. Unlike most prior studies, we found that barrel cortex neurons could be potently facilitated by surround whiskers. However, this facilitation was highly specific to just one or a small number of multi-whisker combinations, while most other combinations suppressed or had no impact on the response to the principal whisker. The net consequence was to generate highly selective responses for specific tactile 'features' composed of active touches with a specific set of surround whiskers. Importantly, a small, but relatively uniform fraction of the image neurons encoded each of all 27 multi-whisker stimuli.

This potent facilitation to stimulation of specific components of the receptive field surround contrasts with the widely observed phenomenon of surround suppression, a prominent form of divisive normalization. Instead, it supports the notion that individual somatosensory cortical neurons selectively encode higher order tactile features (that is, features that extend beyond their receptive fields). Our data further suggests that sparse, distributed ensembles of barrel cortex neurons might encode all possible second order tactile features in whisker space. These ensembles might be crucial for contour detection and shape perception. Our findings also raise the possibility that stimulus-specific supra-linear summation might be a more general feature of cortical sensory coding, or even cortical coding more generally, in active or ethological contexts.

However, there are two main caveats to this study. First, GCaMP6s's transformation function between spiking and dF/F may be nonlinear, as well as cell-type dependent (Khan et al. 2018). To address this one could use various computational techniques to account for any nonlinearity and estimate the underlying spiking or spike rates (Vogelstein et al. 2010; Friedrich et al. 2017). Even better, one could use two-photon targeted patch to measure the transformation between spiking and dF/F for the cell type being imaged and fit a recently developed biophysical model that is able to estimate spike times with high fidelity (Greenberg et al. 2018). Second, we did not show that the stimulus strength for a single whisker is consistent across the various stimulus conditions. To address this, one could track the whiskers within the high-speed whisker imaging videos and then calculate the distributions of bending force and touch events for each whisker across all stimuli. Should there be any consistent differences, one could fit a generalized linear model to the whisker kinematics to account for those sources of variance. Whisker tracking is time prohibitive to accomplish manually, but could be efficiently completed using a recently developed artificial neural network approach known as DeepLabCut (Mathis et al. 2018). These caveats will be addressed prior to submitting this work for peer review.

MISCELLANEOUS

Acknowledgements

The authors acknowledge the GENIE Project, Janelia Farm Research Campus, and the Howard Hughes Medical Institute for the GCaMP6 viruses as well as Dan Feldman and members of the Adesnik and Feldman labs for comments on the manuscript. H.A. is a New York Stem

Cell Foundation-Robertson Investigator. This work was supported by The New York Stem Cell Foundation.

Author Contributions

E.L., S.P., and H.A. conceptualized the study. S.P. acquired all multicellular electrophysiology data and performed all spike sorting. E.L. acquired all two-photon calcium imaging data and high-speed whisker tracking data, and performed all analyses of neural data. E.L. and H.A. wrote the paper.

METHODS

Experimental Model and Subject Details

All mice used were between 1.5 and 3 months of age. Wild-type adult ICR white mice (Charles River) were used for all electrophysiology experiments. Imaging experiments in L2/3 used CaMKII-tTA mice (JAX) crossed to tetO-GCaMP6s mice (JAX), and both lines had been outcrossed to the ICR line for several generations. Imaging experiments in L4 used scnn1-tg3-Cre mice (JAX), that had been outcrossed to the ICR line for several generations. All procedures were approved by the Animal Care and Use Committee of UC Berkeley. Both female and male animals were used and maintained on a 12:12 reversed light:dark cycle.

Preparation for *in vivo* two photon imaging

Anesthesia was induced with 5% isoflurane and then maintained at 1 – 3% during surgery. Respiratory rate and response to toe/tail pinching was monitored throughout surgery to ensure adequate anesthetic depth. 0.05 mg/kg of buprenorphine was administered for post-operative analgesia. After disinfecting the scalp with 70% alcohol and 5% iodine, the skin and fascia above the sensory cortices were removed with surgical instruments. Following application of Vetbond (3M) to the skull surface and wound margins, a custom stainless steel headplate was fixed to the skull with dental cement (Metabond). Two days after surgery, mice were habituated over increasing durations for 4 – 8 days to head-fixation on a free-spinning circular treadmill, until they freely ran at a fast and steady pace (>35 cm/s). Intrinsic optical imaging was performed to localize one or two barrel columns of interest (C1 – C3).

In scnn1-tg3-Cre mice (JAX) that reached running criterion, mice were again anesthetized and administered buprenorphine as described above. A dental drill (Foredom) was used to create a small bur hole 1.3 μm posterior and 3.5 μm lateral to bregma (marked previously with a sharpie during the headplate procedure). Then a Nanoinject II nanoliter injector was used to inject 300 nL of AAV9-flexed-CAG-GCaMP6s (UPenn Vector Core) at a depth of 350 μm and a rate of 0.5 nL/s. Post-injection, the needle was left in the brain for 5 minutes to allow the virus to absorb into the tissue.

In preparation for imaging, the mice were anesthetized and administered buprenorphine as described above, and administered 2 mg/kg of dexamethasone as an anti-inflammatory. The drug cocktail resulted in the isofluorane needing to be between 1 – 1.5% for this procedure. Respiratory rate and response to toe/tail pinching was monitored throughout surgery to ensure adequate anesthetic depth. A 3 mm diameter craniotomy over the left primary somatosensory

cortex was drilled. A window plug consisting of two 3mm diameter coverslips glued to the bottom of a single 5mm diameter coverslip using Norland Optial Adhesive #71 was placed over the craniotomy and sealed permanently using Orthojet. Mice were head-fixed on a freely spinning running wheel under a Nixon 16x-magnification water immersion objective and imaged with a Neurolabware two-photon resonant scanning microscope within a light tight box. Image acquisition was at 15.45 Hz with fields of view (FoVs) ranging from 800 μm by 1 mm to 1.2 mm by 1.2 mm. Wide-field reflectance imaging with a blue LED was used to illuminate the vasculature and center the FoV on the region the intrinsic signal identified as corresponding to the C2 barrel. For L2/3 imaging, imaging depth was 100 – 300 μm, and for L4 imaging, depth was 350 – 500 μm deep.

Tactile Stimulus presentation

A piece of aluminum was custom machined into a circle to hold 5 pneumatic pistons on ball joints at equally spaced positions. Prior to the experiment the mouse's whiskers were trimmed. The mouse was anesthetized with 5% isofluorane that was lowered to 2.5% when the mouse was fully induced. All but the C2, C1, B1, D1, and gamma whiskers were trimmed completely off, then the remaining whiskers were trimmed in a staircase like fashion as described in Figure 3.1A. The mouse was then moved to the experimental rig and head-fixed over a running wheel. Each piston was extended moved into place one-by-one such that the corresponding whisker contacted the piston at the peak of its protraction. A stereoscope and high-speed whisker tracking camera were used to verify contact was specific and repetitive.

During the experiment, continuous two-photon imaging or electrophysiological recording of S1 occurred while each of the piston combinations were presented sequentially to the mouse's whiskers in a pseudo-randomized fashion. Average running speed per trial was computed online, and if the mouse did not surpass a minimum threshold, the trial was repeated later in the experiment. The experiment finished once each stimulus was presented at least 20 times while the mouse was running.

Two photon imaging analysis

Raw two photon movies were first corrected for brain motion using Scanbox's fourier transform-based sbxalign script, written in MATLAB, to correct for the 2D translation of individual frames. The mean of each motion-corrected video was used to translate and register the before and after trimming datasets to within a single pixel of each other. Regions of interest (ROIs) encompassing neurons were identified in a semi-automated manner using Scanbox's sbxsegmentflood (MATLAB, Mathworks) which computes and thresholds the pixel-wise cross-correlation for all pixels within a 60 by 60 pixel window. If an ROI only appeared in one of the datasets via the semi-automated method, then the ROI was copied over to its relative location in the dataset in which it was not identified. The ROI's signal (R_i) was taken as the mean value across all pixels within and unique to that ROI (Fig. S2.2). This signal is assumed to be a mixture of the cell's actual fluorescence signal and a contaminating neuropil signal resulting from scattering producing off-target excitation, high illumination powers producing out of focus fluorescence, or unresolvable neurites passing through the microscope's point spread function. The neuropil signal (N_i) for each ROI was computed by averaging over an annulus of pixels surrounding the ROI but excluded pixels assigned to other ROIs as well as a smaller annulus of

pixels that acted as a buffer in case any motion artifact was not perfectly accounted for (Fig. S2.2). This buffer annulus existed for all ROIs and was excluded from any neuropil calculation. As a result the max diameter of the neuropil annulus varied per ROI in order to ensure a similar number of usable pixels to average over. Each neuron's true fluorescence signal (F_i) was computed per ROI by the following equation:

$$F_i(t) = R_i(t) - k_i * N_i(t)$$

The amount of contamination (k_i) was assumed to be constant per ROI, but vary between ROIs as a result of local differences in expression and scattering. Each k_i was defined by assuming that the neuron's true fluorescence signal (F_i) can never be negative (i.e. $k_i * N_i(t) \leq R_i(t)$), and that there must be a maximal bound for contamination. The contamination coefficient per neuron was defined as follows:

$$k_i = \min\left(\frac{R_i(t)}{N_i(t)}\right); if\ k_i > .65, k_i = .65$$

The true signal was then converted into a trial-wise change in fluorescence ($\frac{f(t)-f_0}{f_0}$ or df/f) to capture the stimulus-evoked changes in neural activity while compensating for any fluctuations in baseline fluorescence. The baseline fluorescence (f_0) for a trial was taken to be the mean fluorescence over the one second prior to stimulation.

High-Speed Whisker Tracking

In all imaging experiments the whiskers were tracked at high speed (~300 frames per second). Previous data, confirmed here (Fig. S2.1), indicate a tight correlation between run-speed of the mouse and whisker set-point, which plateaus above 35 cm/s (Sofroniew et al. 2014). A high-speed camera (FLIR Flea3) was placed below the running wheel; the five whiskers were imaged from below using a mirror angled at 45 degrees. The whiskers were illuminated in a trans-illumination fashion by a panel of near infrared LEDs covered with a piece of drawing paper acting as a diffuser. The illumination source was placed at a sufficient distance as to create a flat background of uniform intensity. High-speed videos were synchronized with neural data acquisition via external triggers. Videos were processed in MATLAB and Python using software from Clack et al. 2012 and custom tracking software.

Quantification and Statistical Analysis

Statistically significant differences between conditions were determined using standard parametric or nonparametric tests in MATLAB, including a 1-way ANOVA, student's t-test, rank sum, and a Wilcoxon sign-rank test. Tests for normality were performed with a Lilliefors test. Analyses were performed on trial-wise dF/F. Analysis was limited to ROIs that met two criteria: they must be significantly driven by at least one stimulus, and be larger than 50 μm^2. A significant response for a stimulus had to meet two criteria: have a mean dF/F greater than .2, and pass a t-test between the evoked responses at that position and the measured dF/F values during control trials. The Benjamini & Hochberg false discovery rate correction was used to

correct for the multiple comparisons taken across the multiple stimuli. Outlier responses per stimulus position were identified by the median rule, where values further than 2.3 times the inter-quartile range from the median are determined to be outliers, and were removed prior to any analysis. The neural response for a single trial was calculated as the average dF/F during the entire 1 second of stimulation.

A neuron was labeled as a single whisker neuron if it only exhibited a significant response to one of the five single whisker stimuli. It was labeled as a multi-whisker neuron if it responded to two or more of the five single whisker stimuli. Or it was labeled as a combination neuron if it wasn't significantly driven by any single whisker stimuli, but was driven by a multi-whisker stimulus.

Clustering analysis was restricted to single whisker neurons whose best single whisker response was greater than 0.2 dF/F larger than its second best single whisker response. Each neuron's location was taken as the centroid of its ROI. Each neuron was assigned to the whisker cluster it significantly responded to. A silhouette value for neuron i was computed as:

$$s(i) = \frac{b(i) - a(i)}{\max\{a(i), b(i)\}}$$

where $a(i)$ is the average distance between i and all other neurons within its cluster, and $b(i)$ is the smallest average distance between i and all other neurons in a cluster of which i is not a member. If i is perfectly clustered, then it will have a silhouette value of 1, if it's in the wrong cluster it will have a value of -1, and if the clusters overlap then it will have a value of 0.

SUPPLEMENTARY FIGURES

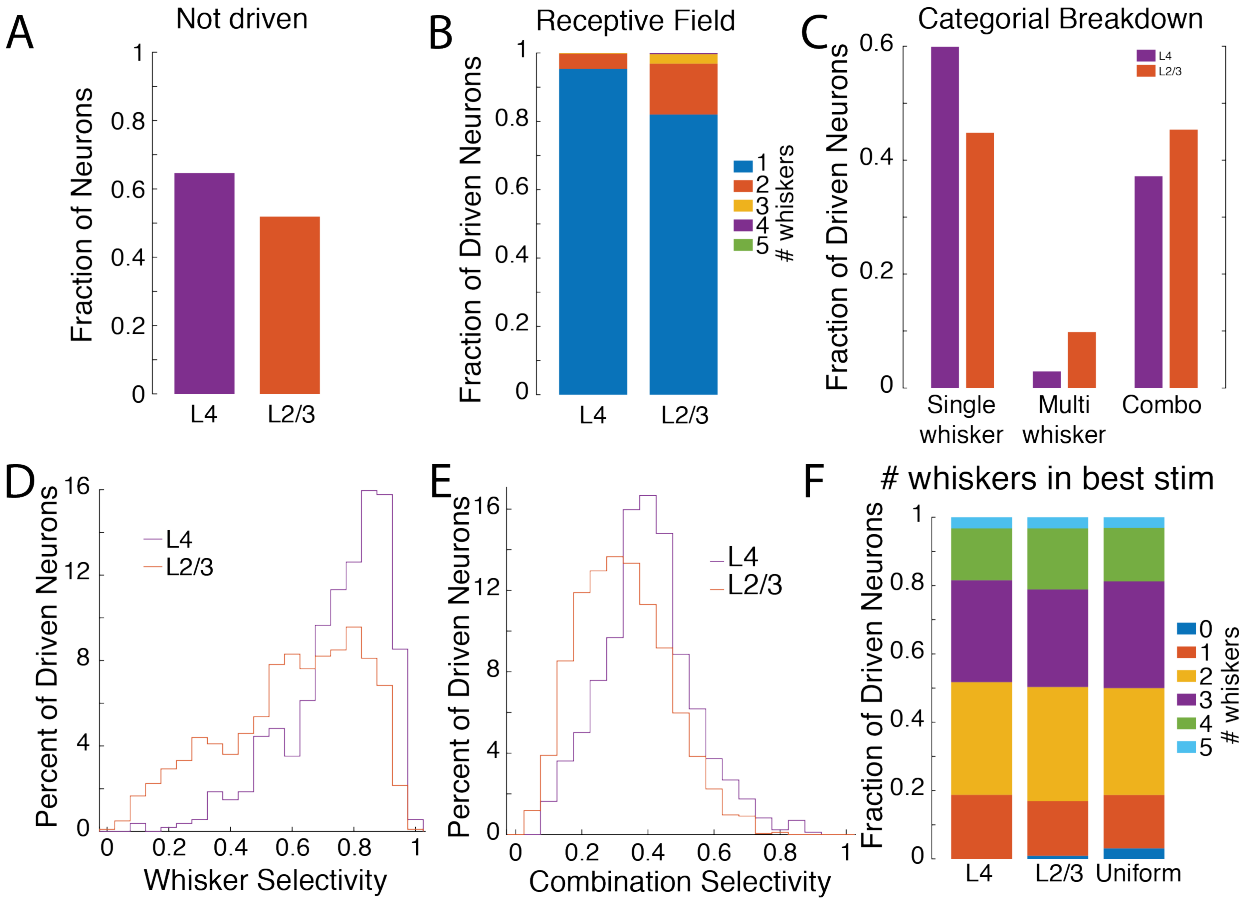

Supplemental Figure 3.1 L4 neurons are more selective than L2/3 neurons
A) Fraction of neurons not significantly driven by any stimulus in each of the layers. B) Fraction of neurons driven by single-whisker stimuli broken down by how many single whisker stimuli significantly drive them. C) Breakdown of driven neurons into how many neurons are driven by a single single-whisker stimulus, multiple single-whisker stimuli, or not driven by any single-whisker stimulus, but driven by at least one combination of whiskers being stimulated. D) Histogram of neurons' selectivity for single-whisker stimuli. L4 neurons are more whisker selective than L2/3 neurons. E) Histogram of neurons' selectivity for combination stimuli. Again, L4 neurons are more stimulus selective. F) Stacked bar chart of the number of whiskers in the preferred stimulus across the different layers. A uniform distribution where each stimulus is evenly represented is shown at right.

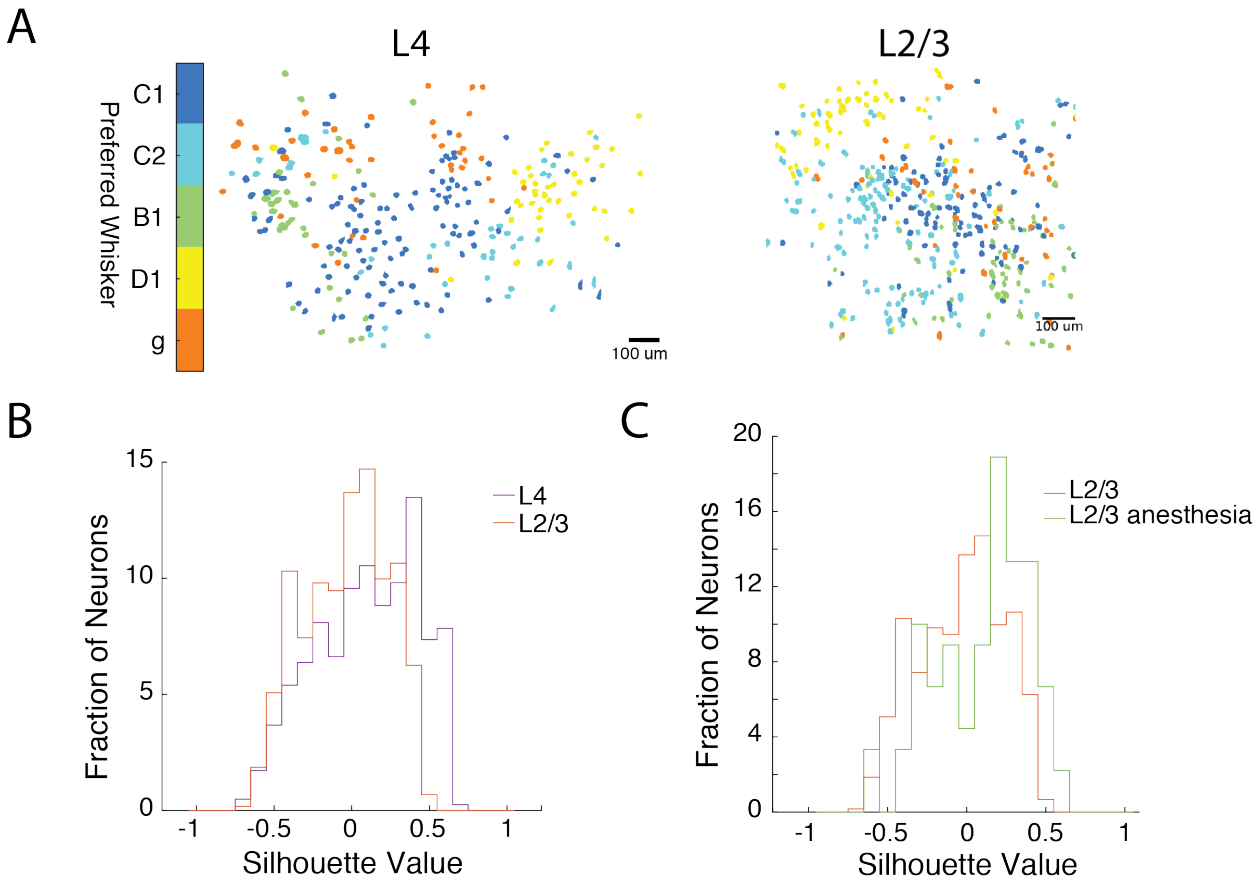

Supplemental Figure 3.2 L4 neurons are more clustered than L2/3 neurons
A) Example maps of preferred whisker for mouse imaged in L4 and a mouse imaged in L2/3. B) Histograms of silhouette values for all single-whisker neurons. L4 neurons were better clustered than L2/3 neurons, while L2/3 neurons had a mean of 0, meaning that the clusters overlapped. C) Same L2/3 histogram from B but now compared to the silhouette values of the single-whisker L2/3 neurons recorded during anesthesia. The anesthetized dataset clustered more than the awake dataset, but was the difference was not as significant as the L4 to L2/3 comparison.

CHAPTER 4

CONCLUSION

Novel findings in the mouse whisker system

In Chapter 2 we presented a vertical pole at several positions within the whisking field of an awake, running mouse and simultaneously recorded neural activity in four distinct brain areas. First we showed that anterior whiskers powerfully suppress the responses of L4 neurons in posterior barrels. Second we showed that this results in a powerful thalamocortical transformation where surround whiskers powerfully transform the representation of space in the cortex but not the thalamus. Third we showed that ultimately the mouse relies on the integration of information across whiskers to generate a map of space in L2/3. Fourth we showed that this map is referenced to the whiskers themselves and is not an allocentric map referenced to the environment.

In Chapter 3 we presented a pneumatic piston-based tactile display that we used to stimulate an arbitrary combination of five whiskers at the peak of the protraction of the mouse's whisk cycle. Here we showed that contrary to results in anesthetized mice, cortical neurons summate unique whisker combinations supralinearly, resulting in the population having slightly sharper tuning.

Measuring neural activity in ethological regimes is integral to understanding a circuit's function

Science revolves around the tradeoff of maintaining as natural a setting as possible while controlling as many experimental variables as possible. In the past, neuroscientists have dealt with this by either studying the neural representation of passive sensation, or that of active sensation in severely reduced preparations. To accomplish these studies the subjects were anesthetized, trained to fixate, or had part of their sensors removed. These studies have taught us a lot about how the brain encodes sensory stimuli, but the non-ethological conditions in which they were performed limits the scope and takeaways of the studies.

Our studies have benefitted from technological advances in head fixation in the rodent model (Dombeck et al. 2007). This granted us the ability to record activity from large numbers of neurons while the mouse ran and whisked. In doing so, this allowed us to discover multiple novel features of sensory processing during active sensation in the mouse whisker system. These findings would not have been possible if the mouse were in an unnatural brain state or trimmed preparation. This data further proves the importance of studying neural coding in the setting of naturalistic behaviors. Animals experience most sensation actively rather than passively, thus it is important that sensory circuits are studied in the context of active sensation.

However, head-fixation itself is not ethological. As technology continues to develop, researchers will be able to account for more experimental variability through non-invasive measurements, such as full body imaging and small, head-mounted recording devices. The goal is that one day this will allow researchers to quantify the exact sensory stimuli being experienced by a naturally roaming mouse while it interacts with other mice and its environment (Meyer et al. 2018). However, these measurements are currently out of reach at the resolution necessary to properly perform such experiments.

Solving the brain will require a holistic approach

The brain processes both active sensation and passive sensation using the same circuits. Studies of passive sensation have taught us a tremendous amount about how the brain works. Additionally, many studies are not possible in an active sensing paradigm. Therefore, it is important that studies of neural coding during passive sensation continue to take place and evolve alongside studies of neural coding during active sensation. Only with a holistic approach combining both lines of inquiry, as well as *ex vivo* studies of neuronal connectivity, identity, and electrophysiology, will we solve the circuitry of the mammalian brain and begin to truly understand its mechanisms and function.

Future Directions

My studies added a few more pieces to the puzzle of understanding how the brain processes and represents active touch, however the puzzle is far from complete. To further advance these studies there are few things that can be done. First, the dimensionality of the stimulus should be increased. The stimuli presented in this study are relatively low dimensional, meaning they capture a very small amount of the statistics of the natural tactile scenes experienced by mice in nature. To combat this, one can adapt the tactile display such that the pistons move along the whisk axis (i.e. rostral-caudal axis), allowing it to produce arbitrary surface shapes. As well, more pistons can be added such that it can stimulate a larger number of whisker combinations. To deal with the unnaturalness of the surface being a thin sheet (i.e. the whiskers can slip past each piston), the pistons can be presented from the front of the mouse, pushing each whisker in a posterior direction as it shoots out. The tradeoff of increasing the dimensionality of the stimulus is that the experimental time exponentially increases. Therefore, such a study would probably require being performed longitudinally over days if not months, as well as presented in a continuous fashion utilizing a spike-triggered, rather than a stimulus-triggered, type of approach.

Beyond increasing the stimulus dimensionality, one would probably want to examine how different cell types differentially encode the stimulus space. This would most effectively be accomplished by combining *in vivo* imaging of all neurons with post hoc Fluorescent *In Situ* Hybridization sequencing (FISHseq) of neurons in the imaged field of view(s). Based on previous research studying orientation and direction tuning in V1 (e.g. Runyan & Sur 2013), my prediction would be that PV and SST neurons exhibit tuning similar to a local average of nearby neurons, and would exhibit much less cell to cell variance compared to that of the excitatory neuron population.

Once the picture is more complete, and both the neural activity and behavioral kinematics are being tracked at high temporal fidelity, then the last major step would be to build an encoding model predicting each neuron in the circuit's spikes relative to the stimulus and the mouse's measured behavioral state. Neuron to neuron interactions within such a model could then be tested and iterated by suppressing or activating single cells using optogenetics and holography (Mardinly et al. 2018).

BIBLIOGRAPHY

Adesnik, H. et al., 2012. A neural circuit for spatial summation in visual cortex. *Nature*, 490(7419), pp.226–31. Available at: http://www.ncbi.nlm.nih.gov/pubmed/23060193 [Accessed January 30, 2013].

Adesnik, H. & Scanziani, M., 2010. Lateral competition for cortical space by layer-specific horizontal circuits. *Nature*, 464(7292), pp.1155–60. Available at: http://dx.doi.org/10.1038/nature08935 [Accessed January 29, 2013].

Andermann, M.L. & Moore, C.I., 2006. A somatotopic map of vibrissa motion direction within a barrel column. *Nature neuroscience*, 9(4), pp.543–51. Available at: http://www.ncbi.nlm.nih.gov/pubmed/16547511 [Accessed April 29, 2014].

Andersen, R.A., Essick, G.K. & Siegel, R.M., 1985. Encoding of spatial location by posterior parietal neurons. *Science (New York, N.Y.)*, 230(4724), pp.456–8. Available at: http://www.ncbi.nlm.nih.gov/pubmed/4048942 [Accessed June 22, 2018].

Armstrong-James, M., Fox, K. & Das-Gupta, A., 1992. Flow of excitation within rat barrel cortex on striking a single vibrissa. *Journal of neurophysiology*, 68(4), pp.1345–58. Available at: http://www.ncbi.nlm.nih.gov/pubmed/1432088 [Accessed June 9, 2018].

Bagdasarian, K. et al., 2013. Pre-neuronal morphological processing of object location by individual whiskers. *Nature neuroscience*, 16(5), pp.622–31. Available at: http://www.ncbi.nlm.nih.gov/pubmed/23563582 [Accessed January 22, 2014].

Bandyopadhyay, S., Shamma, S.A. & Kanold, P.O., 2010. Dichotomy of functional organization in the mouse auditory cortex. *Nature Neuroscience*, 13(3), pp.361–368. Available at: http://www.nature.com/articles/nn.2490 [Accessed June 9, 2018].

Bender, K.J. et al., 2006. Synaptic basis for whisker deprivation-induced synaptic depression in rat somatosensory cortex. *The Journal of neuroscience : the official journal of the Society for Neuroscience*, 26(16), pp.4155–65. Available at: http://www.pubmedcentral.nih.gov/articlerender.fcgi?artid=3070309&tool=pmcentrez&rendertype=abstract [Accessed March 22, 2014].

Bender, K.J., Rangel, J. & Feldman, D.E., 2003. Development of columnar topography in the excitatory layer 4 to layer 2/3 projection in rat barrel cortex. *The Journal of neuroscience : the official journal of the Society for Neuroscience*, 23(25), pp.8759–8770.

Berg-Johnsen, J. & Langmoen, I.A., 1992. The effect of isoflurane on excitatory synaptic transmission in the rat hippocampus. *Acta Anaesthesiologica Scandinavica*, 36(4), pp.350–355.

Boloori, A.-R. & Stanley, G.B., 2006. The Dynamics of Spatiotemporal Response Integration in the Somatosensory Cortex of the Vibrissa System. *Journal of Neuroscience*, 26(14), pp.3767–3782. Available at: https://www.scopus.com/inward/record.uri?eid=2-s2.0-33645645265&partnerID=40&md5=20cb8acb5eeb8d8304b9ec0adf6db7bb.

Brecht, M., 2007. Barrel cortex and whisker-mediated behaviors. *Current opinion in neurobiology*, 17(4), pp.408–16. Available at: http://www.ncbi.nlm.nih.gov/pubmed/17702566 [Accessed September 24, 2013].

Brecht, M., Preilowski, B. & Merzenich, M.M., 1997. Functional architecture of the mystacial vibrissae. *Behavioural brain research*, 84(1–2), pp.81–97. Available at: http://www.ncbi.nlm.nih.gov/pubmed/9079775.

Brecht, M., Roth, A. & Sakmann, B., 2003. Dynamic Receptive Fields of Reconstructed Pyramidal Cells in Layers 3 and 2 of Rat Somatosensory Barrel Cortex. *The Journal of*

Physiology, 553(1), pp.243–265. Available at: http://doi.wiley.com/10.1113/jphysiol.2003.044222.
Brecht, M. & Sakmann, B., 2002. Dynamic representation of whisker deflection by synaptic potentials in spiny stellate and pyramidal cells in the barrels and septa of layer 4 rat somatosensory cortex. *The Journal of physiology*, 543(Pt 1), pp.49–70.
Brown, A.W. & Waite, P.M., 1974. Responses in the rat thalamus to whisker movements produced by motor nerve stimulation. *The Journal of physiology*, 238(2), pp.387–401. Available at: http://www.ncbi.nlm.nih.gov/pubmed/4840852 [Accessed June 9, 2018].
Brumberg, J.C., Pinto, D.J. & Simons, D.J., 1999. Cortical columnar processing in the rat whisker-to-barrel system. *Journal of neurophysiology*, 82(4), pp.1808–1817. Available at: http://eutils.ncbi.nlm.nih.gov/entrez/eutils/elink.fcgi?dbfrom=pubmed&id=10515970&retmode=ref&cmd=prlinks%5Cnpapers2://publication/uuid/A180D1AB-873B-44CB-8B09-D0E17B1555B6.
Brumberg, J.C., Pinto, D.J. & Simons, D.J., 1996. Spatial gradients and inhibitory summation in the rat whisker barrel system. *Journal of neurophysiology*, 76(1), pp.130–40. Available at: http://www.ncbi.nlm.nih.gov/pubmed/8836214.
Cariani, P., 2000. Anesthesia, Neural Information Processing, and Conscious Awareness. *Consciousness and Cognition*, 9(3), pp.387–395.
Castro-Alamancos, M. a & Oldford, E., 2002. Cortical sensory suppression during arousal is due to the activity-dependent depression of thalamocortical synapses. *The Journal of Physiology*, 541(1), pp.319–331. Available at: http://www.jphysiol.org/cgi/doi/10.1113/jphysiol.2002.016857 [Accessed April 7, 2014].
Castro-Alamancos, M.A., 2004a. Absence of Rapid Sensory Adaptation in Neocortex during Information Processing States. *Neuron*, 41(3), pp.455–464.
Castro-Alamancos, M.A., 2004b. Dynamics of sensory thalamocortical synaptic networks during information processing states. *Progress in Neurobiology*, 74(4), pp.213–247.
Castro-Alamancos, M.A. & Bezdudnaya, T., 2015. Modulation of artificial whisking related signals in barrel cortex. *Journal of neurophysiology*, 113(5), pp.1287–301. Available at: http://jn.physiology.org/content/113/5/1287.abstract.
Chapman, C.E. & Ageranioti-Belanger, S.A., 1991. Discharge properties of neurones in the hand area of primary somatosensory cortex in monkeys in relation to the performance of an active tactile discrimination task. *Experimental Brain Research*, 87(2), pp.319–339. Available at: http://link.springer.com/10.1007/BF00231849 [Accessed June 22, 2018].
Chen-Bee, C.H. et al., 2012. Whisker array functional representation in rat barrel cortex: transcendence of one-to-one topography and its underlying mechanism. *Frontiers in neural circuits*, 6, p.93. Available at: http://www.ncbi.nlm.nih.gov/pubmed/23205005 [Accessed June 9, 2018].
Chen, T.-W. et al., 2013. Ultrasensitive fluorescent proteins for imaging neuronal activity. *Nature*, 499(7458), pp.295–300. Available at: http://www.ncbi.nlm.nih.gov/pubmed/23868258 [Accessed August 6, 2013].
Civillico, E.F. & Contreras, D., 2006. Integration of Evoked Responses in Supragranular Cortex Studied With Optical Recordings In Vivo. *Journal of Neurophysiology*, 96(1), pp.336–351. Available at: http://www.physiology.org/doi/10.1152/jn.00128.2006 [Accessed June 22, 2018].
Clack, N.G. et al., 2012. Automated tracking of whiskers in videos of head fixed rodents. *PLoS computational biology*, 8(7), p.e1002591. Available at:

http://www.pubmedcentral.nih.gov/articlerender.fcgi?artid=3390361&tool=pmcentrez&rendertype=abstract [Accessed December 24, 2013].
Clancy, K.B. et al., 2015. Structure of a Single Whisker Representation in Layer 2 of Mouse Somatosensory Cortex. *Journal of Neuroscience*, 35(9), pp.3946–3958. Available at: http://www.jneurosci.org/cgi/doi/10.1523/JNEUROSCI.3887-14.2015.
Constantinople, C.M. & Bruno, R.M., 2011. Effects and mechanisms of wakefulness on local cortical networks. *Neuron*, 69(6), pp.1061–1068. Available at: http://dx.doi.org/10.1016/j.neuron.2011.02.040.
Crochet, S. et al., 2011. Synaptic mechanisms underlying sparse coding of active touch. *Neuron*, 69(6), pp.1160–75. Available at: http://www.ncbi.nlm.nih.gov/pubmed/21435560 [Accessed October 23, 2013].
Curtis, J.C. & Kleinfeld, D., 2009. Phase-to-rate transformations encode touch in cortical neurons of a scanning sensorimotor system. *Nature neuroscience*, 12(4), pp.492–501. Available at: http://www.pubmedcentral.nih.gov/articlerender.fcgi?artid=2863011&tool=pmcentrez&rendertype=abstract [Accessed April 29, 2014].
Diamond, M.E. et al., 2008. "Where" and "what" in the whisker sensorimotor system. *Nature reviews. Neuroscience*, 9(8), pp.601–12. Available at: http://www.ncbi.nlm.nih.gov/pubmed/18641667 [Accessed August 8, 2013].
Dombeck, D. a et al., 2007. Imaging large-scale neural activity with cellular resolution in awake, mobile mice. *Neuron*, 56(1), pp.43–57. Available at: http://www.pubmedcentral.nih.gov/articlerender.fcgi?artid=2268027&tool=pmcentrez&rendertype=abstract [Accessed February 10, 2013].
Drew, P.J. & Feldman, D.E., 2007. Representation of moving wavefronts of whisker deflection in rat somatosensory cortex. *Journal of neurophysiology*, 98(3), pp.1566–80. Available at: http://www.ncbi.nlm.nih.gov/pubmed/17567777 [Accessed March 21, 2014].
Ego-Stengel, V. et al., 2005. Spatiotemporal characteristics of neuronal sensory integration in the barrel cortex of the rat. *Journal of neurophysiology*, 93(3), pp.1450–67. Available at: http://www.ncbi.nlm.nih.gov/pubmed/15496491 [Accessed May 2, 2014].
Estebanez, L. et al., 2016. A radial map of multi-whisker correlation selectivity in the rat barrel cortex. *Nature Communications*, 7, p.13528. Available at: http://www.nature.com/doifinder/10.1038/ncomms13528.
Estebanez, L. et al., 2012. Correlated input reveals coexisting coding schemes in a sensory cortex. *Nature neuroscience*, 15(12), pp.1691–9. Available at: http://www.ncbi.nlm.nih.gov/pubmed/23160042 [Accessed September 24, 2013].
Fanselow, E.E. & Nicolelis, M.A., 1999. Behavioral modulation of tactile responses in the rat somatosensory system. *The Journal of neuroscience : the official journal of the Society for Neuroscience*, 19(17), pp.7603–7616. Available at: http://www.ncbi.nlm.nih.gov/pubmed/10460266.
Feldman, D.E. & Brecht, M., 2005. Map Plasticity in Somatosensory Cortex. *Science*, 310(November), pp.810–815.
Feldmeyer, D. et al., 2013. Barrel cortex function. *Progress in neurobiology*, 103, pp.3–27. Available at: http://www.ncbi.nlm.nih.gov/pubmed/23195880 [Accessed August 1, 2013].
Ferezou, I. et al., 2007. Spatiotemporal Dynamics of Cortical Sensorimotor Integration in Behaving Mice. *Neuron*, 56(5), pp.907–923.
Fox, K., 2002. Anatomical pathways and molecular mechanisms for plasticity in the barrel

cortex. *Neuroscience*, 111(4), pp.799–814. Available at: https://www-sciencedirect-com.libproxy.berkeley.edu/science/article/pii/S0306452202000271 [Accessed June 9, 2018].
Friedrich, J. et al., 2017. Fast online deconvolution of calcium imaging data. *PLOS Computational Biology*, 13(3), p.e1005423. Available at: http://dx.plos.org/10.1371/journal.pcbi.1005423.
Ganmor, E., Katz, Y. & Lampl, I., 2010. Intensity-dependent adaptation of cortical and thalamic neurons is controlled by brainstem circuits of the sensory pathway. *Neuron*, 66(2), pp.273–286. Available at: http://dx.doi.org/10.1016/j.neuron.2010.03.032.
Ghazanfar, a a & Nicolelis, M. a, 1999. Spatiotemporal properties of layer V neurons of the rat primary somatosensory cortex. *Cerebral cortex (New York, N.Y. : 1991)*, 9(4), pp.348–61. Available at: http://www.ncbi.nlm.nih.gov/pubmed/10426414.
Gibson, J.J., 1962. Observations of active touch. *Psychological review*, 69(6), pp.477–491.
Glazewski, S. & Fox, K., 1996. Time course of experience-dependent synaptic potentiation and depression in barrel cortex of adolescent rats. *Journal of neurophysiology*, 75(4), pp.1714–29. Available at: http://www.ncbi.nlm.nih.gov/pubmed/8727408 [Accessed June 9, 2018].
Goldin, M.A. et al., 2018. Rich spatio-temporal stimulus dynamics unveil sensory specialization in cortical area S2. *Nature Communications*, 9(1), p.4053. Available at: http://www.nature.com/articles/s41467-018-06585-4.
Goldreich, D., Kyriazi, H.T. & Simons, D.J., 1999. Functional Independence of Layer IV Barrels in Rodent Somatosensory Cortex. *Journal of Neurophysiology*, 82(3), pp.1311–1316. Available at: http://www.physiology.org/doi/10.1152/jn.1999.82.3.1311 [Accessed June 9, 2018].
Greenberg, D.S. et al., 2018. Accurate action potential inference from a calcium sensor protein through biophysical modeling. *bioRxiv*. Available at: https://www.biorxiv.org/content/early/2018/11/29/479055.
Greenberg, D.S., Houweling, A.R. & Kerr, J.N.D., 2008. Population imaging of ongoing neuronal activity in the visual cortex of awake rats. *Nature Neuroscience*, 11(7), pp.749–751. Available at: http://www.nature.com/articles/nn.2140 [Accessed June 22, 2018].
Hartline, H., Wagner, H. & Ratliff, F., 1956. Inhibition in the eye of Limulus. *The Journal of general …*, 39(5). Available at: http://jgp.rupress.org/content/39/5/651.abstract [Accessed November 25, 2014].
Hartline, H.K., 1938. the Response of Single Optic Nerve Fibers of the Vertebrate Eye To Illumination of the Retina. *American Journal of Physiology-Legacy Content*, 121(2), pp.400–415. Available at: http://www.physiology.org/doi/10.1152/ajplegacy.1938.121.2.400.
Hartmann, M.J.Z., 2011. A night in the life of a rat: vibrissal mechanics and tactile exploration. *Annals of the New York Academy of Sciences*, 1225(1), pp.110–118. Available at: http://doi.wiley.com/10.1111/j.1749-6632.2011.06007.x [Accessed June 9, 2018].
Hemelt, M.E. et al., 2010. Consistency of angular tuning in the rat vibrissa system. *Journal of neurophysiology*, 104(6), pp.3105–12. Available at: http://www.pubmedcentral.nih.gov/articlerender.fcgi?artid=3007639&tool=pmcentrez&rendertype=abstract [Accessed May 7, 2014].
Hentschke, H., Haiss, F. & Schwarz, C., 2006. Central signals rapidly switch tactile processing in rat barrel cortex during whisker movements. *Cerebral Cortex*, 16(8), pp.1142–1156.
Higley, M.J. & Contreras, D., 2003. Nonlinear integration of sensory responses in the rat barrel

cortex: an intracellular study in vivo. *The Journal of neuroscience : the official journal of the Society for Neuroscience*, 23(32), pp.10190–200. Available at: http://www.ncbi.nlm.nih.gov/pubmed/14614077 [Accessed June 9, 2018].
Hill, D.N. et al., 2011. Primary motor cortex reports efferent control of vibrissa motion on multiple timescales. *Neuron*, 72(2), pp.344–56. Available at: http://www.pubmedcentral.nih.gov/articlerender.fcgi?artid=3717360&tool=pmcentrez&rendertype=abstract [Accessed September 19, 2013].
Hirata, A. & Castro-Alamancos, M.A., 2008. Cortical Transformation of Wide-Field (Multiwhisker) Sensory Responses. *Journal of Neurophysiology*, 100(1), pp.358–370. Available at: http://jn.physiology.org/cgi/doi/10.1152/jn.90538.2008 [Accessed May 4, 2014].
Hires, S.A. et al., 2015. Low-noise encoding of active touch by layer 4 in the somatosensory cortex. *eLife*, 4, pp.1–18. Available at: http://elifesciences.org/lookup/doi/10.7554/eLife.06619.
Hobbs, J.A., Towal, R.B. & Hartmann, M.J.Z., 2016. Spatiotemporal Patterns of Contact Across the Rat Vibrissal Array During Exploratory Behavior. *Frontiers in Behavioral Neuroscience*, 9(January), pp.1–18. Available at: http://journal.frontiersin.org/article/10.3389/fnbeh.2015.00356.
Horton, N.G. et al., 2013. In vivo three-photon microscopy of subcortical structures within an intact mouse brain. *Nature Photonics*, 7(March), pp.205–209. Available at: http://dx.doi.org/10.1038/nphoton.2012.336.
Hubel, D. & Wiesel, T., 1962. Receptive fields, binocular interaction and functional architecture in the cat's visual cortex. *The Journal of physiology*, pp.106–154. Available at: http://www.ncbi.nlm.nih.gov/pmc/articles/PMC1359523/ [Accessed November 20, 2014].
Hubel, D. & Wiesel, T., 1959. Receptive fields of single neurones in the cat's striate cortex. *The Journal of physiology*, pp.574–591. Available at: http://www.ncbi.nlm.nih.gov/pmc/articles/PMC1363130/ [Accessed November 20, 2014].
Isett, B.R. et al., 2018. Slip-Based Coding of Local Shape and Texture in Mouse S1. *Neuron*, pp.1–16. Available at: http://linkinghub.elsevier.com/retrieve/pii/S0896627317311686.
Jacob, V. et al., 2008. Emergent properties of tactile scenes selectively activate barrel cortex neurons. *Neuron*, 60(6), pp.1112–25. Available at: http://www.ncbi.nlm.nih.gov/pubmed/19109915 [Accessed September 24, 2013].
Jadhav, S.P. & Feldman, D.E., 2010. Texture coding in the whisker system. *Current opinion in neurobiology*, 20(3), pp.313–8. Available at: http://www.ncbi.nlm.nih.gov/pubmed/20299205 [Accessed October 22, 2013].
Jadhav, S.P., Wolfe, J. & Feldman, D.E., 2009. Sparse temporal coding of elementary tactile features during active whisker sensation. *Nature neuroscience*, 12(6), pp.792–800. Available at: http://www.ncbi.nlm.nih.gov/pubmed/19430473 [Accessed October 22, 2013].
Jung, J.C. et al., 2004. In Vivo Mammalian Brain Imaging Using One- and Two-Photon Fluorescence Microendoscopy. *Journal of Neurophysiology*, 92(5), pp.3121–3133. Available at: http://www.physiology.org/doi/10.1152/jn.00234.2004 [Accessed November 25, 2018].
Kelly, M.K. et al., 1999. Sensory loss by selected whisker removal produces immediate disinhibition in the somatosensory cortex of behaving rats. *The Journal of neuroscience : the official journal of the Society for Neuroscience*, 19(20), pp.9117–9125.
Khan, A.G. et al., 2018. Distinct learning-induced changes in stimulus selectivity and

interactions of GABAergic interneuron classes in visual cortex. *Nature Neuroscience*. Available at: http://dx.doi.org/10.1038/s41593-018-0143-z.
Kleinfeld, D., Ahissar, E. & Diamond, M.E., 2006. Active sensation: insights from the rodent vibrissa sensorimotor system. *Current opinion in neurobiology*, 16(4), pp.435–44. Available at: http://www.ncbi.nlm.nih.gov/pubmed/16837190 [Accessed November 7, 2013].
Knudsen, E.I., Lac, S. & Esterly, S.D., 1987. Computational Maps in the Brain. *Annual Review of Neuroscience*, 10(1), pp.41–65. Available at: http://www.annualreviews.org/doi/10.1146/annurev.ne.10.030187.000353 [Accessed June 9, 2018].
Knutsen, P.M., Biess, A. & Ahissar, E., 2008. Vibrissal kinematics in 3D: tight coupling of azimuth, elevation, and torsion across different whisking modes. *Neuron*, 59(1), pp.35–42. Available at: http://www.ncbi.nlm.nih.gov/pubmed/18614027 [Accessed March 14, 2014].
Knutsen, P.M., Pietr, M. & Ahissar, E., 2006. Haptic Object Localization in the Vibrissal System: Behavior and Performance. *Journal of Neuroscience*, 26(33), pp.8451–8464. Available at: http://www.jneurosci.org/content/jneuro/26/33/8451.full.pdf [Accessed June 9, 2018].
Kremer, Y. et al., 2011. Late emergence of the vibrissa direction selectivity map in the rat barrel cortex. *The Journal of neuroscience : the official journal of the Society for Neuroscience*, 31(29), pp.10689–700. Available at: http://www.ncbi.nlm.nih.gov/pubmed/21775612 [Accessed August 13, 2013].
Krupa, D.J. et al., 2001. Behavioral properties of the trigeminal somatosensory system in rats performing whisker-dependent tactile discriminations. *The Journal of neuroscience : the official journal of the Society for Neuroscience*, 21(15), pp.5752–5763.
Kuffler, S., 1953. Discharge patterns and functional organization of mammalian retina. *J Neurophysiol*. Available at: http://jn.physiology.org/content/jn/16/1/37.full.pdf [Accessed November 23, 2014].
Kwegyir-Afful, E.E. et al., 2005. The role of thalamic inputs in surround receptive fields of barrel neurons. *The Journal of neuroscience : the official journal of the Society for Neuroscience*, 25(25), pp.5926–34. Available at: http://www.pubmedcentral.nih.gov/articlerender.fcgi?artid=1317101&tool=pmcentrez&rendertype=abstract [Accessed May 2, 2014].
Lamme, V.A.F., Zipser, K. & Spekreijse, H., 1998. Figure-ground activity in primary visual cortex is suppressed by anesthesia. *Proceedings of the National Academy of Sciences*, 95(6), pp.3263–3268. Available at: http://www.pnas.org/cgi/doi/10.1073/pnas.95.6.3263.
Lee, S. et al., 2013. A disinhibitory circuit mediates motor integration in the somatosensory cortex. *Nature neuroscience*, 16(11), pp.1662–70. Available at: http://www.ncbi.nlm.nih.gov/pubmed/24097044 [Accessed November 7, 2013].
Lee, S., Carvell, G.E. & Simons, D.J., 2008. Motor modulation of afferent somatosensory circuits. *Nature neuroscience*, 11(12), pp.1430–8. Available at: http://www.pubmedcentral.nih.gov/articlerender.fcgi?artid=2597103&tool=pmcentrez&rendertype=abstract [Accessed September 18, 2013].
Luczak, A. & Barthó, P., 2012. Consistent sequential activity across diverse forms of UP states under ketamine anesthesia. *European Journal of Neuroscience*, 36(6), pp.2830–2838.
Madisen, L. et al., 2010. A robust and high-throughput Cre reporting and characterization system for the whole mouse brain. *Nature Neuroscience*, 13(1), pp.133–140. Available at: http://www.nature.com/articles/nn.2467 [Accessed June 9, 2018].

Major, G. & Tank, D., 2004. Persistent neural activity: Prevalence and mechanisms. *Current Opinion in Neurobiology*, 14(6), pp.675–684.
Mardinly, A.R. et al., 2018. Precise multimodal optical control of neural ensemble activity. *Nature Neuroscience*, 21(6), pp.881–893. Available at: http://www.nature.com/articles/s41593-018-0139-8.
Mathis, A. et al., 2018. DeepLabCut: markerless pose estimation of user-defined body parts with deep learning. *Nature Neuroscience*, p.1. Available at: http://www.nature.com/articles/s41593-018-0209-y.
Meyer, A.F. et al., 2018. A Head-Mounted Camera System Integrates Detailed Behavioral Monitoring with Multichannel Electrophysiology in Freely Moving Mice. *Neuron*, 100(1), p.46–60.e7. Available at: https://doi.org/10.1016/j.neuron.2018.09.020.
Mirabella, G., Battiston, S. & Diamond, M.E., 2001. Integration of multiple-whisker inputs in rat somatosensory cortex. *Cerebral cortex (New York, N.Y. : 1991)*, 11(2), pp.164–70. Available at: http://www.ncbi.nlm.nih.gov/pubmed/11208671.
Moore, C.I. & Nelson, S.B., 1992. Spatio-Temporal Subthreshold Receptive Fields in the Vibrissa Representation of Rat Primary Somatosensory Cortex. *J. Neurophysiol. Chapin Chapin and Lin Simons Carvell*, 80(6), pp.2882–2892. Available at: http://www.physiology.org/doi/10.1152/jn.1998.80.6.2882 [Accessed June 9, 2018].
Moore, C.I., Nelson, S.B. & Sur, M., 1999. Dynamics of neuronal processing in rat somatosensory cortex. *Trends in Neurosciences*, 22(11), pp.513–520.
Naka, A. et al., 2018. Complementary networks of cortical somatostatin interneurons enforce layer specific control.
Niell, C.M. & Stryker, M.P., 2010. Modulation of visual responses by behavioral state in mouse visual cortex. *Neuron*, 65(4), pp.472–9. Available at: http://www.pubmedcentral.nih.gov/articlerender.fcgi?artid=3184003&tool=pmcentrez&rendertype=abstract [Accessed October 18, 2013].
O'Connor, D.H., Peron, S.P., et al., 2010. Neural activity in barrel cortex underlying vibrissa-based object localization in mice. *Neuron*, 67(6), pp.1048–61. Available at: http://www.ncbi.nlm.nih.gov/pubmed/20869600 [Accessed February 5, 2013].
O'Connor, D.H. et al., 2013. Neural coding during active somatosensation revealed using illusory touch. *Nature neuroscience*, 16(7), pp.958–65. Available at: http://www.ncbi.nlm.nih.gov/pubmed/23727820 [Accessed August 1, 2013].
O'Connor, D.H., Clack, N.G., et al., 2010. Vibrissa-based object localization in head-fixed mice. *The Journal of neuroscience : the official journal of the Society for Neuroscience*, 30(5), pp.1947–67. Available at: http://www.ncbi.nlm.nih.gov/pubmed/20130203 [Accessed March 21, 2014].
Oberlaender, M., Ramirez, A. & Bruno, R.M., 2012. Sensory experience restructures thalamocortical axons during adulthood. *Neuron*, 74(4), pp.648–55. Available at: http://www.ncbi.nlm.nih.gov/pubmed/22632723 [Accessed June 9, 2018].
Ohki, K. et al., 2005. Functional imaging with cellular resolution reveals precise micro-architecture in visual cortex. *Nature*, 433(7026), pp.597–603. Available at: http://www.ncbi.nlm.nih.gov/pubmed/15660108.
Peron, S.P. et al., 2015. A Cellular Resolution Map of Barrel Cortex Activity during Tactile Behavior. *Neuron*, 86(3), pp.1–17. Available at: http://dx.doi.org/10.1016/j.neuron.2015.03.027.
Petersen, C.C.H., 2007. The functional organization of the barrel cortex. *Neuron*, 56(2), pp.339–

55. Available at: http://www.ncbi.nlm.nih.gov/pubmed/17964250 [Accessed January 21, 2014].
Petersen, R.S., Panzeri, S. & Diamond, M.E., 2001. Population Coding of Stimulus Location in Rat Somatosensory Cortex. *Neuron*, 32(3), pp.503–514. Available at: https://www.sciencedirect.com/science/article/pii/S0896627301004810 [Accessed June 9, 2018].
Pluta, S. et al., 2015. A direct translaminar inhibitory circuit tunes cortical output. *Nature Neuroscience*, (September). Available at: http://www.nature.com/doifinder/10.1038/nn.4123.
Pluta, S.R. et al., 2017. Surround Integration Organizes a Spatial Map during Active Sensation. *Neuron*, 94(6), p.1220–1233.e5. Available at: http://linkinghub.elsevier.com/retrieve/pii/S0896627317303525.
Poulet, J.F. a & Petersen, C.C.H., 2008. Internal brain state regulates membrane potential synchrony in barrel cortex of behaving mice. *Nature*, 454(7206), pp.881–5. Available at: http://www.ncbi.nlm.nih.gov/pubmed/18633351 [Accessed January 26, 2014].
Ramirez, A. et al., 2014. Spatiotemporal receptive fields of barrel cortex revealed by reverse correlation of synaptic input. *Nature Neuroscience*, (April), pp.1–13. Available at: http://www.nature.com/doifinder/10.1038/nn.3720 [Accessed May 19, 2014].
Reimer, J. et al., 2014. Pupil Fluctuations Track Fast Switching of Cortical States during Quiet Wakefulness. *Neuron*, 84(2), pp.355–362. Available at: http://linkinghub.elsevier.com/retrieve/pii/S0896627314008915.
Ringach, D.L. et al., 2016. Spatial clustering of tuning in mouse primary visual cortex. *Nature Communications*, 7, p.12270. Available at: http://www.nature.com/doifinder/10.1038/ncomms12270.
Rothschild, G., Nelken, I. & Mizrahi, A., 2010. Functional organization and population dynamics in the mouse primary auditory cortex. *Nature Neuroscience*, 13(3), pp.353–360. Available at: http://www.nature.com/articles/nn.2484 [Accessed June 9, 2018].
Runyan, C. a & Sur, M., 2013. Response selectivity is correlated to dendritic structure in parvalbumin-expressing inhibitory neurons in visual cortex. *The Journal of neuroscience : the official journal of the Society for Neuroscience*, 33(28), pp.11724–33. Available at: http://www.ncbi.nlm.nih.gov/pubmed/23843539 [Accessed October 24, 2013].
Sato, T.R. et al., 2007. The functional microarchitecture of the mouse barrel cortex. *PLoS biology*, 5(7), p.e189. Available at: http://www.pubmedcentral.nih.gov/articlerender.fcgi?artid=1914403&tool=pmcentrez&rendertype=abstract [Accessed November 28, 2014].
Schubert, D., Kötter, R. & Staiger, J.F., 2007. Mapping functional connectivity in barrel-related columns reveals layer- and cell type-specific microcircuits. *Brain structure & function*, 212(2), pp.107–19. Available at: http://www.ncbi.nlm.nih.gov/pubmed/17717691 [Accessed August 1, 2013].
Severson, K.S. et al., 2017. Active Touch and Self-Motion Encoding by Merkel Cell-Associated Afferents. *Neuron*, 94(3), p.666–676.e9. Available at: http://dx.doi.org/10.1016/j.neuron.2017.03.045.
Sherrington, C.S., 1906. Observations on the scratch-reflex in the spinal dog. *The Journal of physiology*, 34(1–2), pp.1–50. Available at: http://www.ncbi.nlm.nih.gov/pubmed/16992835.
Shimegi, S. et al., 2000. Physiological and anatomical organization of multiwhisker response

interactions in the barrel cortex of rats. *The Journal of neuroscience : the official journal of the Society for Neuroscience*, 20(16), pp.6241–8. Available at: http://www.ncbi.nlm.nih.gov/pubmed/10934274 [Accessed June 9, 2018].
Shuler, M.G., Krupa, D.J. & Nicolelis, M. a, 2001. Bilateral integration of whisker information in the primary somatosensory cortex of rats. *The Journal of neuroscience : the official journal of the Society for Neuroscience*, 21(14), pp.5251–61. Available at: http://www.ncbi.nlm.nih.gov/pubmed/11438600.
Simons, D.J., 1978. Response properties of vibrissa units in rat SI somatosensory neocortex. *Journal of neurophysiology*, 41(3), pp.798–820. Available at: http://www.ncbi.nlm.nih.gov/pubmed/660231.
Simons, D.J. & Carvell, G.E., 1989. Thalamocortical response transformation in the rat vibrissa/barrel system. *Journal of neurophysiology*, 61(2), pp.311–30. Available at: http://www.ncbi.nlm.nih.gov/pubmed/2918357.
Smith, S.L. & Häusser, M., 2010. Parallel processing of visual space by neighboring neurons in mouse visual cortex. *Nature neuroscience*, 13(9), pp.1144–9. Available at: http://www.pubmedcentral.nih.gov/articlerender.fcgi?artid=2999824&tool=pmcentrez&rendertype=abstract [Accessed March 19, 2014].
Sofroniew, N.J. et al., 2016. A large field of view two-photon mesoscope with subcellular resolution for in vivo imaging. *eLife*, 5, pp.1–20. Available at: http://biorxiv.org/content/early/2016/05/28/055947.abstract.
Sofroniew, N.J. et al., 2014. Natural Whisker-Guided Behavior by Head-Fixed Mice in Tactile Virtual Reality. *Journal of Neuroscience*, 34(29), pp.9537–9550.
Sofroniew, N.J. et al., 2015. Neural coding in barrel cortex during whisker-guided locomotion. *eLife*, 4(September 2013), pp.1–36. Available at: http://elifesciences.org/lookup/doi/10.7554/eLife.12559.
Stirman, J.N. et al., 2016. Wide field-of-view, multi-region, two-photon imaging of neuronal activity in the mammalian brain. *Nature Biotechnology*. Available at: http://www.nature.com/doifinder/10.1038/nbt.3594.
Szwed, M., Bagdasarian, K. & Ahissar, E., 2003. Encoding of vibrissal active touch. *Neuron*, 40(3), pp.621–630.
Timofeeva, E. et al., 2004. Synthesis of Multiwhisker-Receptive Fields in Subcortical Stations of the Vibrissa System. *Journal of Neurophysiology*, 91(4), pp.1510–1515. Available at: http://www.physiology.org/doi/10.1152/jn.01109.2003 [Accessed June 9, 2018].
Tsai, P.S. et al., 2015. Ultra-large field-of-view two-photon microscopy. *Optics Express*, 23(11), p.13833. Available at: https://www.osapublishing.org/oe/abstract.cfm?uri=oe-23-11-13833.
Vinck, M. et al., 2015. Arousal and Locomotion Make Distinct Contributions to Cortical Activity Patterns and Visual Encoding. *Neuron*, pp.1–15. Available at: http://linkinghub.elsevier.com/retrieve/pii/S0896627315002524.
Vogelstein, J.T. et al., 2010. Fast nonnegative deconvolution for spike train inference from population calcium imaging. *Journal of neurophysiology*, 104(6), pp.3691–3704.
Waiblinger, C. et al., 2018. Primary Tactile Thalamus Spiking Reflects Cognitive Signals. *The Journal of Neuroscience*, 38(21), pp.4870–4885. Available at: http://www.jneurosci.org/lookup/doi/10.1523/JNEUROSCI.2403-17.2018.
Wallach, A., Bagdasarian, K. & Ahissar, E., 2016. On-going computation of whisking phase by mechanoreceptors revealed by a closed-loop interface. , (October 2015), pp.1–16.
Wen, J.A., DeBlois, M.C. & Barth, A.L., 2013. Initiation, labile, and stabilization phases of

experience-dependent plasticity at neocortical synapses. *The Journal of neuroscience : the official journal of the Society for Neuroscience*, 33(19), pp.8483–93. Available at: http://www.ncbi.nlm.nih.gov/pubmed/23658185 [Accessed June 9, 2018].

Whitmire, C.J., Liew, Y.J. & Stanley, G.B., 2018. Thalamic state influences timing and feature selectivity in the thalamocortical circuit. *bioRxiv*, p.439778. Available at: https://www.biorxiv.org/content/early/2018/10/10/439778.

Whitmire, C.J. & Stanley, G.B., 2016. Rapid Sensory Adaptation Redux: A Circuit Perspective. *Neuron*, 92(2), pp.298–315. Available at: http://dx.doi.org/10.1016/j.neuron.2016.09.046.

Wolfe, J. et al., 2008. Texture coding in the rat whisker system: slip-stick versus differential resonance. *PLoS biology*, 6(8), p.e215. Available at: http://www.pubmedcentral.nih.gov/articlerender.fcgi?artid=2525689&tool=pmcentrez&rendertype=abstract [Accessed April 7, 2014].

Woolsey, T. a & van der Loos, H., 1970. The Structural Organization of Layer IV in the Somatosensory Region (S1) of Mouse Cerebral Cortex. *Brain research*, 17, pp.205–242.

Yang, A.E.T. & Hartmann, M.J.Z., 2016. Whisking Kinematics Enables Object Localization in Head-Centered Coordinates Based on Tactile Information from a Single Vibrissa. *Frontiers in Behavioral Neuroscience*, 10(July), pp.1–15. Available at: http://journal.frontiersin.org/article/10.3389/fnbeh.2016.00145.

Yarbus, A.L., 1967. *Eye Movements and Vision*, New York, New York, USA: Plenum Press.

Yu, C. et al., 2015. Coding of object location in the vibrissal thalamocortical system. *Cerebral cortex (New York, N.Y. : 1991)*, 25(3), pp.563–577. Available at: http://www.ncbi.nlm.nih.gov/pubmed/24062318 [Accessed March 14, 2014].

Yu, J. et al., 2016. Layer 4 fast-spiking interneurons filter thalamocortical signals during active somatosensation. *Nature Neuroscience*, (October), pp.1–14. Available at: http://www.nature.com/doifinder/10.1038/nn.4412.

Zheng, H.J. V., Wang, Q. & Stanley, G.B., 2015. Adaptive shaping of cortical response selectivity in the vibrissa pathway. *Journal of Neurophysiology*, 113(10), pp.3850–3865. Available at: http://jn.physiology.org/lookup/doi/10.1152/jn.00978.2014.

Zhu, J.J. & Connors, B.W., 1999. Intrinsic Firing Patterns and Whisker-Evoked Synaptic Responses of Neurons in the Rat Barrel Cortex. *Journal of Neurophysiology*, 81(3), pp.1171–1183. Available at: http://www.physiology.org/doi/10.1152/jn.1999.81.3.1171 [Accessed June 9, 2018].